DOE/SF/70030-T28

Attachment to Letter No.
XL-611-00025

ANALYSIS OF THE DYNAMIC RESPONSE OF A DOUBLE RUPTURE DISC ASSEMBLY TO SIMULATED SODIUM-WATER REACTION PRESSURE PULSES

AT03-76SF70030

by

J. R. Leonard

Advanced Reactor Systems Department
General Electric Company
Sunnyvale, California

March 1980

Prepared for

U. S. Department of Energy
Under Contract No. ~~DE-AT03-76SF70030~~
Work Package AF15 10 05, WPT No. SG037

DISCLAIMER

ABSTRACT

A series of double rupture disc experiments were conducted in 1979 by SRI International under the direction of the General Electric Company to evaluate the dynamic response characteristics of this pressure relief apparatus. The tests were performed in a facility with water simmulating sodium and rising pressure pulses respresentative of the pressure increase resulting from a water/steam leak from a steam generator into sodium in the intermediate heat transport system of a breeder reactor power plant. Maximum source pressures ranged in magnitude from 50 psi to 800 psi. Dynamic response characteristics of each of the two rupture discs were similar to those observed in larger scale sodium-water experiments conducted in the Series I and Series II Large Leak Test Program at the Energy Technology Engineering Center.

The SRI double rupture disc dynamic behavior was found to be consistent and amendable to modelling in the TRANSWRAP II computer code. A series of correlations which represent rupture disc buckling parameters were developed for use in the TRANSWRAP II code. The semi-empirical modeling of the rupture discs in the TRANSWRAP II code showed very good agreement with the experimental results. The recommended TRANSWRAP II rupture disc model should provide realistic estimates of double rupture disc response over a wide range of source pressures and rupture disc diameters.

ACKNOWLEGEMENTS

The contributions of many individuals have been essential to the accomplishment of the objectives of this analysis. Prominent among these are as follows: J. Norvell of GE for various modifications to TRANSWRAP required for adequate representation of double rupture disc behavior, data processing, and assistance in operating the TRANSWRAP II code; D. Caglistro and T. Desmond of SRI for their concientious execution of the experimental phase of the program; A. Florence of SRI for his perceptive analysis of the data obtained from this experiment and articulate documentation of the results; and J. Fairbairn, R. Meyer, J. Norvell, and J. Sane for discussions at GE regarding prior experience in this area.

TABLE OF CONTENTS

1.0	INTRODUCTION	1
2.0	SUMMARY	2
3.0	DISCUSSION	3
	3.1 Description of the Experiment	3
	3.2 Comparison with TRANSWRAP II	3
	3.3 Scale Effects	5
4.0	CONCLUSIONS	15
5.0	REFERENCES	16
	Appendix A, TRANSWRAP Input Data	62
	Appendix B, Comparison plots for supplemental SRI Tests	73

1.0 INTRODUCTION

A series of experiments have been conducted at the Poulter Laboratory, which is operated by SRI International, to evaluate various aspects of pressure pulse propagation and rupture disc behavior in scaled assemblies representative of the Clinch River Breeder Reactor Plant double rupture disc assembly. Pressure pulses in the water system were generated by exploding a charge in a gas filled chamber causing a rapid pressure rise that propagates to the liquid in the piping system. In the initial experiments, the pulse closely simulated the shape and amplitude of the pressure rise in the IHTS following a design basis leak (DBL) and subsequent sodium/water reaction. Results of these early tests carried out in 1976-1978 are documented in Reference 1 and the corresponding evaluation of these results, using the TRANSWRAP II code at GE, is discussed in Reference 2. Recently, in 1979, a supplemental experiment (Reference 4) was performed to study the behavior of a double rupture disc assembly, prototypic in scale of the Clinch River assembly, for source pulses that cover a larger range of pressures.

Since the primary objective of this test was to isolate the buckling characteristics of the rupture discs, the SRI test rig consisted simply of the pulse generator, a 60 ft section of 2-½ inch ID stainless steel pipe, and the rupture disc assembly as shown in Figure 1.1a. The pulse generator was designed to provide maximum source pressures ranging from 50 to 800 psi with a rapid rise time (1-3 ms) and very long decay time in order to provide a sufficient period for response of both discs. Source pressure characteristics employed in this experiment are illustrated in Fig 1.1b. The latest version of the TRANSWRAP code, Reference 3, which incorporates the SWAAM elastic rupture disc model, (Reference 5) was used to evaluate the test results. Results of that evaluation along with an assessment of scale effects are discussed herein. A detailed discussion of the experiment and test data is presented in Reference 4.

2.0 SUMMARY

Initially, tests were conducted to establish the static rating of the rupture disc, establish pulse shape, and evaluate acoustic effects and pulse attenuation in the test apparatus. Following this work, a total of 24 tests were conducted to evaluate the effect of source pressures representative of a range of different steam generator leak sizes in the Clinch River IHTS system on double rupture disc performance. Source pressures ranged from 50 to 800 psi and closely followed the characteristic depicted in Figure 1.1b. Behavior of the rupture discs was found to be quite similar to that observed in the Series I Large Leak Test Program. The SRI experiments and data analysis are presented in Reference 4. Four tests representing source pressures of 200, 400, 600, and 800 psi were selected from this reference for emphasis in comparison with TRANSWRAP. Other comparisons which demonstrate repeatability are included in Appendix B.

The parameters which characterize the finite time required for buckling and tearing of the rupture disc were first identified in Series I of the Large Leak Test Program experiments and are discussed in Reference 3. Similar characteristics were observed in the 1/7 scale SRI experiment, Reference 4. Using "as measured" values for these parameters as input to the TRANSWRAP code, good agreement was obtained between the analytical model and experimental data. In the current analysis, correlations were developed which indicate that the trends observed in the SRI experiment are a valid representation of the those to be expected for large scale plant systems. Good agreement was also achieved when comparisons of the SRI experiment and larger scale sodium systems were analyzed using these correlations in conjunction with the TRANSWRAP analysis. This supports the basis for design calculations performed using the dynamic rupture disc model in the TRANSWRAP II code.

3.0 DISCUSSION

3.1 Description of the Experiment

The objective of the experiment was to evaluate the dynamic behavior of double rupture disc assemblies when subjected to source pressure pulses in the range from 50 to 800 psi. To this end, four types of tests were conducted: (1) pulse shaping tests to provide a smooth pulse with rapid rise time (1-3 ms), (2) static rupture disc tests to determine the "as installed" static rating of the discs, (3) rigid end plug tests to verify that the acoustic behavior of the basic piping system follows expected trends and to assess the degree of attenuation effects, and (4) double rupture disc tests to study the response characteristics of this configuration to a pressure pulse. Details of the experiment are discussed in Reference 4. A brief summary of that description is presented in the following paragraphs.

The test apparatus is illustrated schematically in Figure 1.1a The primary components are the pulse generator, a 60 ft straight pipe section, and the double rupture disc assembly. The pulse generator consists of a gas filled chamber which contains the charge, an orifice plate to diffuse the expanding gas following detonation and to provide some attenuation of the shock system in the chamber, and a piston which provides the mechanism for energy transfer from the expanding gas in the chamber to the liquid in the pipe. The shape of the pressure pulse in the liquid is primarily a function of the magnitude of the charge and the configuration of the orifice plate. A schematic of the pulse generator, taken from Reference 4, is presented in Figure 3.1.1 Initial tests were conducted to provide a pressure pulse with the characteristic shown in Figure 1.1.b. The general nature of the pulse generated is illustrated later in Figure 3.2.1, and closely approximates the desired shape.

The stainless steel piping section is 60 feet in length and 2 ½ inches in diameter (ID) with wall thickness of 0.12 in. Liquid water contained in the pipe was used to represent the sodium in an actual system. Four pressure transducers were mounted in the pipe wall at locations 10, 20, 40, and 60 feet from the pulse generator to monitor transmitted and reflected pressures. The transducer closest

to the rupture disc assembly (i.e., 60 feet from the pulse generator) was omitted for tests involving the rigid end plate.

The rigid end plug and double rupture disc assemblies are shown in Figure 3.1.2 (also taken from Reference 4). The double rupture disc assembly is composed of Inconel rupture discs rated from the manufacturer at 310 psi, and inlet and outlet flanges which contain pressure transducers to monitor the upstream pressure, P5, and cavity pressure P7. Also, the assembly contains cutter blades spaced 120 degrees apart and welded into the outlet flange with electrical circuitry to the disc to indicate time of contact, and a spacer ring to provide the same spacing between the discs and a 1/7 scale prototype design. Static tests with a single disc in place established that the actual static rating of the discs in this installation is in the neighborhood of 250-260 psi. The shape of the spherical cap on the aluminum rigid end plug is identical to that of the rupture discs.

Typical results of a double rupture disc test with a source pressure pulse of approximately 400 psi are shown in Figure 3.1.3. The source pressure is derived from the transducer closest to the pulse generator, P2. The data for P5, directly upstream of the first disc, indicates that a rapid collapse of the disc occurs at 14.6 ms. The disc buckles until it encounters the obstruction provided by the cutter blade structure; the electrical switch recorded contact with the cutter blade at 15.2 ms. The pressure upstream of the disc recovers and holds at a value which is approximately 2/3 of the reflected pressure wave as the disc collapses around the cutter blade structure and is penetrated by the cutter. Once tearing of the disc is initiated the upstream pressure decreases rapidly to a value somewhat above the cavity pressure. The initial cavity pressure was 15 psia. As the cavity fills, the upstream pressure and the cavity pressure tend to equalize and simultaneously recover to approximately 225 psi where the second disc ruptures following the same characteristic as the first disc. The lower-than-static-rated pressure which causes buckling of the second disc indicates that the disc may have been weakened locally by the impingement loading of the liquid as it enters the cavity and impacts the second disc.

The good repeatability of data trends achieved between tests with similar pulse shapes and magnitudes is demonstrated in Figures 3.1.4 through 3.1.8 Note, however, that irregular jet impingement effects may slightly influence the response of the system following rupture of the first disc.

The dynamic buckling characteristics displayed in Fig 3.1.4 are very similar to those observed in the LLTR Series 1 and 2 Test as identified in Volume 2 of Reference 3. As a result of these observations, buckling characteristics are currently represented by the following parameters(see the sketch in Fig 3.1.9 :). (a) rise time, Δt_R, which is the time between the initial drop in upstream pressure and the time required for recovery to the hold pressure, (b) hold pressure, P_H, which is the recovery pressure level reached before the disc tears, (c) hold time, Δt_H, which is the time interval between initial buckling and initial tearing of the disc, and (d) tearing time, Δt_t, which is the time required to tear the disc to its final open area. These parameters are investigated more thoroughly in Section 3.3 of this report.

Tests conducted with a rigid end plug indicated that slight attenuation of transmitted and reflected waves was experienced as represented by the data from a typical test in Figure 3.1.10 through 3.1.12. The measured acoustic velocity of 4440 ft/sec (Reference 4) is in excellent agreement with the theoretical value of 4400 ft/sec for this installation. These results demonstrate that the acoustic properties of the experiment were not significantly influenced by secondary factors such as pipe deformation, or fluid/structure interaction. As shown in Figure 3.1.10, the pulse is reinforced at the downstream end because the velocity of the reflected wave is opposite in direction to the particle velocity at this point. This compression wave is reflected back to the source and is followed by a rarefaction which appears at the source after approximately 55 milliseconds.

3.2 Comparison of Data with Predicted Response by the TRANSWRAP II Code.

Four tests representing maximum source pressure levels of 200, 400, 600, and 800 psi were selected for comparison with the analytical prediction produced by TRANSWRAP II calculations, and represent the source pressure

range of interest. Other comparisons are presented in Appendix B to demonstrate repeatability. In the nomenclature of Reference 4, these are RD150-1, RD400-3, RD600-4, and RD800-1. Pressure pulses near the source as represented by P2 are shown in Figures A1 through A3 of Appendix A. Included in these figures is the source pressure at the pulse generator that is thought to be representative of the nearly constant pulse issuing from a reservoir that would produce the transmitted and reflected waves measured in the experiment. These source pressures were used to generate the pressure vs time table required for the input-bubble pressure option in TRANSWRAP II, and are summarized in Figure 3.2.1.

Buckling parameters Δt_R, Δt_H, Δt_t, and P_H representative of these tests were measured directly from the rupture disc upstream pressure records for P5 as illustrated in Figures A5 through A8 in Appendix A. The relative open area for the disc, $\overline{A}$, was determined from an average line drawn through the measurements recorded in Reference 4 (Figure 3.10 of Reference 4). The nominal rather than the tabulated areas in Reference 4 were used because of the uncertainty in measuring actual flow area from the axially projected area from a photograph. Estimated values of the rupture disc parameters for the four tests are summarized in Table 3.2.1 below.

Table 3.2.1

Test	Δt_R	Δt_H	Δt_t	P_H	$\overline{A}$
RD150-1	0.004	0.0001	0.010	180	.12
RD400-3	0.003	0.0001	0.004	200	.23
RD600-4	0.002	0.0001	0.003	230	.35
RD800-1	0.001	0.0001	0.002	250	.47

The TRANSWRAP model used to represent the test apparatus is illustrated in Figure 3.2.2. An input data listing, exclusive of the source pressure and rupture disc parameters which vary from test to test, is included as Table A1 in Appendix A. Source pressure and rupture disc data input for each test are listed separately in Table A2.

The rigid end plug data for tests RP200-1 and RP800-3 were employed to verify that the method of deriving the source pulse shape from the pressure record for P2 provides an adequate boundary condition for the acoustic response of the fluid to the pulse transmitted by the piston in the pulse generator. Results of the comparison between the pressure data for P2, P3, and P4 for test RP800-3 and the TRANSWRAP II prediction using the source pulse shown in figure 3.2.3 are presented in Figures 3.2.3 through 3.2.5. The agreement is good throughout the piping system. The incident pulse impacts the disc, reinforces, and is reflected back through the pipe as a compression wave which theoretically disappears at the source. Since the particle velocity at the source is opposite in direction to the reflected wave velocity, a rarefaction appears which is seen at all locations as it is transmitted to the plug and back again. This trend is well represented by classical hydraulic wave theory, and the TRANSWRAP II representation of these acoustic effects is considered more than adequate. Although not presented herein, a similar result was obtained at the 200 psi source pressure level.

Before presenting a comparison between computed and experimental results, a brief discussion of the dynamic double rupture disc model embodied within TRANSWRAP is appropriate. The TRANSWRAP II code currently includes: 1) rupture disc buckling parameters as defined above which are input by the user and provide a boundary condition for the pressure at the disc which dominates the calculation until tearing of the disc is complete, and 2) the SWAAM elastic dynamic rupture disc model (Reference 5) which includes a cavity model between the two rupture discs and reflects the delay time between rupture of the first and second discs. The cavity model is based upon the hypothesis that, after the upstream disc begins to tear, the flow of liquid into the cavity compresses the gas in the cavity isentropically until the upstream and cavity pressures are approximately equal signifying that the cavity has been nearly filled with liquid. Once this occurs, the cavity pressure, which at this time is equivalent to the pressure upstream of the second rupture disc, responds to transport of the available energy

in the fluid adjacent to the disc in the same manner that the pressure upstream of the first rupture disc responds during its buckling transient. Rupture of the second disc is based upon the TRANSWRAP/SWAAM analysis of this pressure rise exclusive of the effect of liquid impingement on the second disc which leads to conservative predictions of the delay time between rupture of the first and second disc.

The SWAAM dynamic rupture disc model currently employed in the TRANSWRAP II code is based upon a finite element representation of the axisymmetric elastic deformation of a membrane in the shape of a spherical cap which is subjected to a uniform pressure pulse. Several experiments, including static conditions such as reported in Reference 6, have shown that, because of non-uniformities in the thickness and other material properties of the disc, the buckling characteristics are non-axisymmetric which significantly influences its dynamic response. Studies conducted at GE and elsewhere indicate that non-uniform buckling is equivalent to a loss of strength of an axisymmetric disc under dynamic conditions.

In order to simulate this effect in the TRANSWRAP model and match the dynamic rupture pressures measured in the SRI experiment, a series of TRANSWRAP runs were made using a nominal pulse shape with 3 ms rise time and peak magnitude of 400 psi over a range of rupture disc thickness from 0.004 inches to the manufactured thickness of 0.010 inches. Results are shown in Figure 3.2.6. The data in Figure 3.10 of Reference 3 indicate that for these conditions the dynamic rupture pressure for the first disc is approximately 330 psi which corresponds to an effective thickness in Fig 3.2.6 of 0.0059 inches. The ratio between effective and manufactured thickness was found to be similar to that used in analyses of the LLTR test results (eg. Reference 3), so the effective thickness of 0.0059 inches was used for subsequent analysis of the SRI test results.

Comparison plots between TRANSWRAP predictions using the semi-empirical parameters discussed above and the experimental records are presented for source pressure levels of 200, 400, 600 and 800 psi in Figures 3.2.7 through 3.2.26. An examination of these figures reveals that the agreement between predicted and measured pressures is very good.

At low source pressure levels ($< P_{rated}$ as represented by Figures 3.2.7 to 3.2.11) the first disc buckles and ruptures in response to interaction with the incident source pulse as shown in Figure 3.2.10. A compression wave is reflected from the disc to the source followed quickly by a rarefaction wave resulting from the local depressurization at the disc as it buckles, which produces, in effect, a characertistic of wave reflection from a free surface. The compression wave which reflects back to the source is well represented by the TRANSWRAP calculation, but the calculated pressure level near the source (ie. at station P2) is underpredicted by approximately 15% relative to the experimental measurement at this station. Several TRANSWRAP model modifications were attempted in order to properly represent this characteristic, but in each case excessively conservative trends were predicted later in the transient. Therefore, the orifice representation of disc rupture currently employed in TRANSWRAP is considered to be most representative of the experiment. Because the reflected compression pulse is of such short duration, the resulting underprediction of energy transport to the piping system is considered to be insignificant.

The use of measured buckling parameters to establish a boundary condition for the pressure just upstream of the disc adequately represents the reflected waves in the pipe following rupture of the first disc. The pressure spikes indicated in Figure 3.2.7 may be the result of the reaction of the piston to the incident rarefaction wave as noted in Reference 4. This effect could not be represented in the analytical model. When the disc tears and the cavity between discs is filled, the second disc responds to the available energy in the fluid adjacent to the rupture disc assembly. The pulse, which is simply a reapplication of the source pressure in this case, reinforces and causes rupture of the second disc.

Similar trends are evident for higher source pressures, but the effect of compression waves reflected from the rupture disc assembly just prior to rupture of the first disc is negligable as illustrated in Figure 3.2.12, 3.2.17, and 3.2.22. Excellent agreement between predicted and measured trends is indicated at each of the monitored pressure stations along the pipe. Pressure recovery to the upstream hold pressure and

rupture of the first disc occurs more quickly as the energy level of the pulse is increased. Also, the open area of the disc increases in proportion to energy input from the source so the cavity fills more rapidly as the source pressure increases for a fixed rise time. The second disc is able to respond to the available energy in the fluid near the disc after the cavity is filled which explains the decreasing time delay between rupture of the first and second discs as the energy level of the pulse increases. Note that the TRANSWRAP II calculation represents this trend very well. In the case where the disc appears to have been weakened as a result of fluid impingement (Test RD400-3 as indicated in Figures 3.2.15 and 3.2.16), the TRANSWRAP calculation results in a slightly conservative rupture pressure but the calculation of rupture time remains accurate.

Comparison plots for the data from other tests received from SRI are presented in Appendix B and demonstrate the repeatability both of the experimental data and, in most cases, of the accuracy of the calculation. These results significantly contribute to the confidence level placed upon double rupture disc modeling in the TRANSWRAP code.

3.3 Scale Effects

The current state of the art in calculating rupture disc performance is based on the SWAAM dynamic rupture disk model with several input parameters based on test data. This approach has been successful in predicting the system pressure response for the SRI small scale tests and the more prototypical Series I and Series II Large Leak Tests. The purpose of this section is to develop semi-empirical relationship between small and large scale rupture disc parameters.

The parameters of primary importance insofar as the behavior of the double rupture disc assembly is concerned and resultant energy transfer back to the piping system are the total time between initiation of the buckling process and the time at which the disc begins to tear, and the open area of the disc after tearing of the disc is completed.

The data that are currently available for rupture disc assemblies prototypic of the current CRBR design were reviewed in order to ascertain the degree of consistancy which would provide the basis for semi-empirical predictions of these parameters. These data were obtained from References 1,3, and 4 along with the recent LLTR Series II test A2. The total time before the disc begins to tear after initial buckling, Δt_H , is shown for Series 1 of the LLTR tests in Appendix II of Reference 3, Volume II. Attempts to plot the small scale data within this framework, which only represents the level of the pulse exclusive of the rate of energy transport to the fluid and subsequently transmitted to the rupture disc, were unsuccessful. A similar result was experienced when rupture disc open area correlations were attempted.

Therefore, other more fundamental parameters representing the rate of energy transport were considered. They are based upon the hypothesis that the rate of energy transport to the rupture disc assembly from the fluid is proportional to the rate of energy transport to the fluid from the source. For a closed system without heat addition, the rate of energy increase in the fluid can be represented as:

$$\frac{d}{dt}(E) = -\frac{d}{dt}(W) = -\frac{d}{dt}(p\,\Delta V)$$

For the compression of a nearly incompressible fluid this becomes:

$$\frac{dE}{dt} = -\frac{d}{dt}\left([-y\,p\,V_o]\right)$$

$$= 2y\,V_o\,p\,\frac{dp}{dt} \qquad (1)$$

where:

y = fluid compressibility

V_o = initial system volume = $\pi\, d_p^2\, \ell_p/4$

p = pressure in the fluid

d_p = rupture disc/pipe diameter

ℓ_p = distance from the source to the rupture disc

While this is not totally representative of the physical process which occurs following pulse generation, it is believed that the parameters reflected by Eq (1) may dominate the rate of energy transport from the fluid to the disc, which, in turn, dominates buckling characertistics of the disc. Thus, some grouping of these parameters might be expected to represent trends in the test results and be used as a scaling factor. Since the recovery pressure level at the disc for most of the experiments conducted to date are similar, the pressure term in this relationship was ommitted from further consideration although later studies may show some dependance upon source and/or reflected pressure pulses. Also, the distance from the source to the disc simply represents propagation effects rather than the rate of energy exchange to the disc so this parameter was also considered to be ineffectual for representing buckling characteristics of the first disc when subject to source energy rates in the range of interest. The latter interpretation applies only to the rate of energy transfer to the disc and not to phenomena experienced thereafter. This leaves fluid compressibility, disc cross sectional area, and rate of pressure rise upstream of the disc as parameters which might be expected to dominate the rate of energy transfer from the fluid to the disc.

Based upon the assumption that the total time from initial buckling and inception of disc rupture is primarily a function of the rate of pressure increase upstream of the disc, the plot shown in Figure 3.3.1 was constructed. Considerable data scatter is indicated which is attributed in part to uncertainty in reading values for these parameters from available graphs. However, a definite trend is indicated which correlates all of the data, regardless of scale effects, and the uncertainty is no larger than that shown in Figure A-II-15 of Reference 3, Vol. II.

The results in Figure 3.3.1 prompted an attempt to correllate other rupture disc parameters in the same manner. This effort was partially successful. Recovery time was found to directly correllate within $\pm$ 10 ms as shown in Figure 3.3.2. However, in order to attain this same uncertainty level for the tearing time of the disc it was found necessary to introduce the thickness of the disc into the correllation. This could probably be justified upon the basis of structural compliance and/or other physical properties of the disc, but the introduction of parameters of this nature would overly complicate the correllation. Results are shown in Figure 3.3.3. As would be expected, the data scatter is substantial but the trend is also evident in each of these figures. It is worthy of note that the trends indicate that high energy pulses, such as would be expected from a DBL, lead to very rapid buckling and tearing times which results in a very short delay time between rupture of the first and second discs as discussed in the previous section.

Attempts to correlate the open area of the upstream disc with the rate of pressure rise upstream of the disc were unsuccessful. However, a reasonable representation was achieved when the other influential terms in Eq (1) were included. As noted earlier these are the fluid compressibility and cross section area of the disc. Combining these to form the parameter $K_p \frac{dp}{dt}$, where $K_p = y\, d_p^2/144$, yields the result shown in Figure 3.3.5. This figure also contains significant uncertainty due to reading these parameters from graphical and photographic records, but the trend is clear; increasing energy level of the pulse is

directly reflected by an increase in open area of the upstream rupture disc which leads to rapid filling time in the cavity between the first and second rupture discs (note that the correlation presupposes that the disc ruptures since the curve does not pass through the origin). The recovery pressure was found to be a function only of the reflected pulse from the disc and seems to be relatively independant of the energy input to the disc. This result is shown in Figure 3.3.4.

The correlations in Figures 3.3.1 through 3.3.5 can be used directly as the basis for providing rupture disc data required for TRANSWRAP calculations of various rupture disc configurations. Further work would be expected to to reduce the uncertainty level of the correlations possibly through some dimensionless grouping of these variables;so further study in this area is warranted. As additional data becomes available from the LLTR Series II experiment and possibly from other sources the uncertainty level of the correlations will become more clearly defined.

The utility of the correlations developed in this section was evaluated by performing a TRANSWRAP calculation for the geometry employed in LLTR Test A2. The rate of rise of the pulse was estimated from preliminary pressure data measured in the test and was used to estimate rupture disc parameters from Figures 3.3.1 through 3.3.5. Results are shown in Figures 3.3.6. The calculated delay time agrees quite well with the measured value of 60 milliseconds. This agreement shows that the correlations developed from the SRI and Series I data and the double rupture disc model provide a good prediction of full scale double rupture disc behavior. Based upon this result it is recommended that finalized forms of these correlations be used in conjunction with TRANSWRAP to perform design calculations for large plant systems.

4.0 CONCULSIONS

Evaluation of the SRI double rupture disc experiment has led to the following conclusions regarding double rupture disc behavior:

1) Measured rupture disc parameters (ie, hold time, recovery time, tearing time, hold pressure, and open area) in the small scale test reflect the same characteristics as noted in the LLTR Series I experiment

2) Behavior of the double rupture disc assembly and system pressure response is well represented by the TRANSWRAP II calculation as shown by the very good agreement between predicted and measured pressures.

3) Scale and pulse shape effects can be represented on a consistent basis through the use of semi-empirical correlations which are based on the rate of energy transport from the pulse to the rupture disc.

4) Good agreement was obtained between measured and predicted double rupture disc characteristics when the correlations developed in this program were applied to preliminary data from the full scale LLTR Series II test A2. This adds confidence to the use of the correlations for prediction of double rupture disc pressure relief performance in large plant systems.

5.0 REFERENCES

1) D. Ploeger, "Simulation Experiments for a Large Leak Sodium Water Reaction Analysis", SRI Project PYD-6272, Vols I to IV, 1977-1978.

2) C. F. Wolfe, "TRANSWRAP II Analysis of the Stanford Research Institute IHTS/Relief System Simulation Tests" GEFR-00444 VC 79a, April, 1979

3) J. O. Sane et. al., "Evaluation of Sodium-Water Reaction Tests No. 1 through 6 Data and Comparison with TRANSWRAP Analyses Series I Large Leak Test Program, Vols I and II, GEFR 00420, V2, September, 1979

4) D. Cagliostro, T. Desmond, and A. Florence, "Response of Rupture Discs to Sodium-Water Reaction Pulses", SRI Project PYD-1110, February, 1980

5) Y. W. Shin, et al, "SWAAM I: A Computer Code System for Large Scale Sodium-Water Reaction Analysis in LMFBR Secondary Systems" (Draft), ANL 79- , November, 1979

6) R. G. Reynolds, "Development Status of Sodium-Water Reaction Pressure Relief Rupture Disc for the CRBRP", GEFR-00361 UC-79A, July 1978.

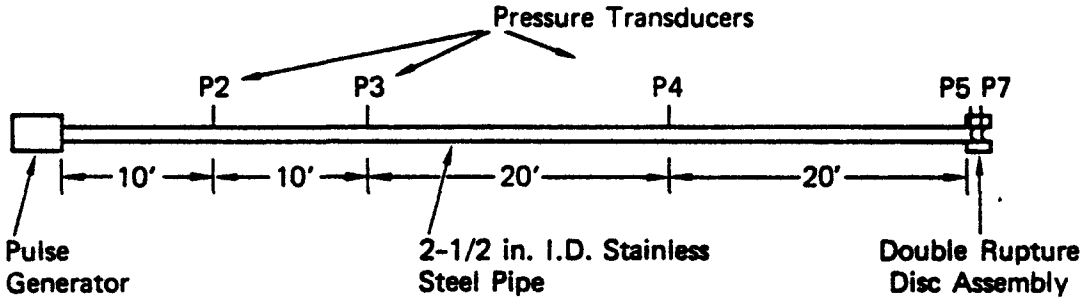

(a) Experimental Apparatus

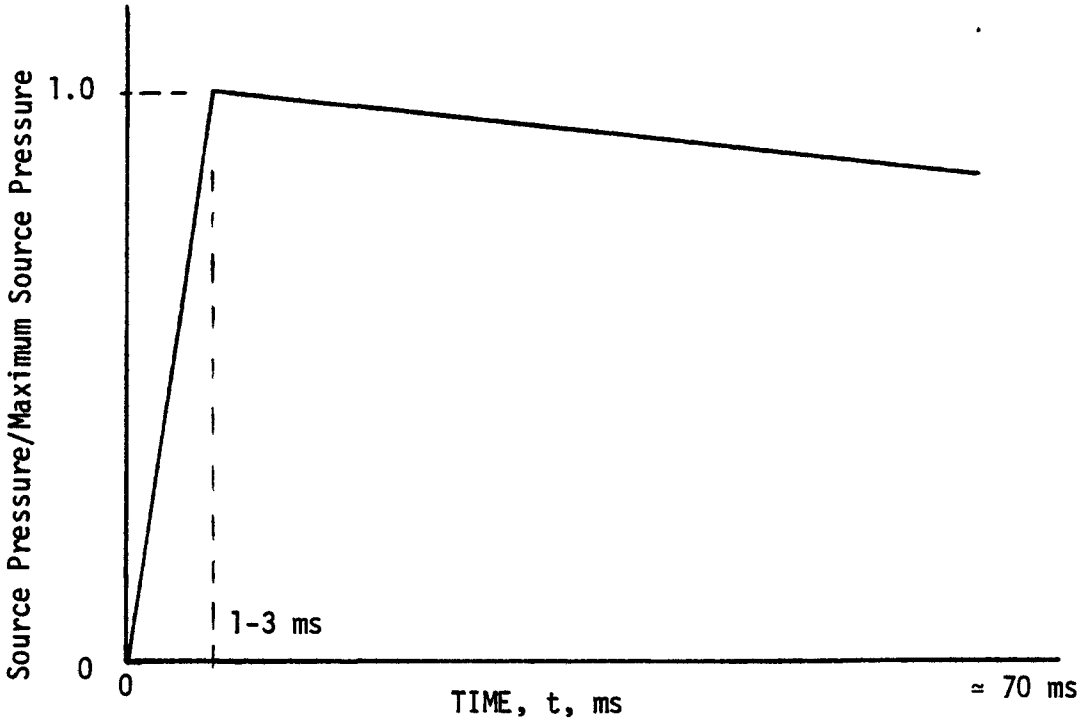

(b) Design Pulse

FIGURE 1.1, SRI TEST APPARATUS AND DESIGN PULSE SHAPE

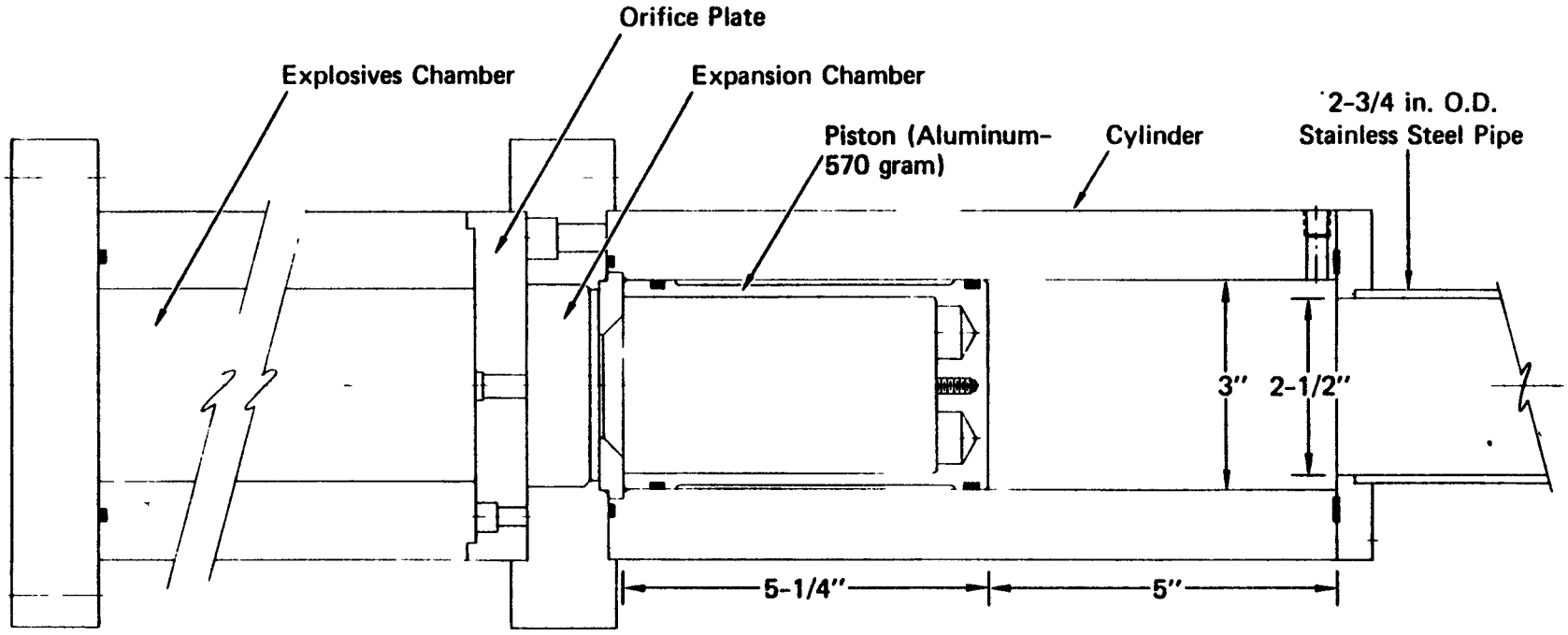

FIGURE 3.1.1 PULSE GENERATOR

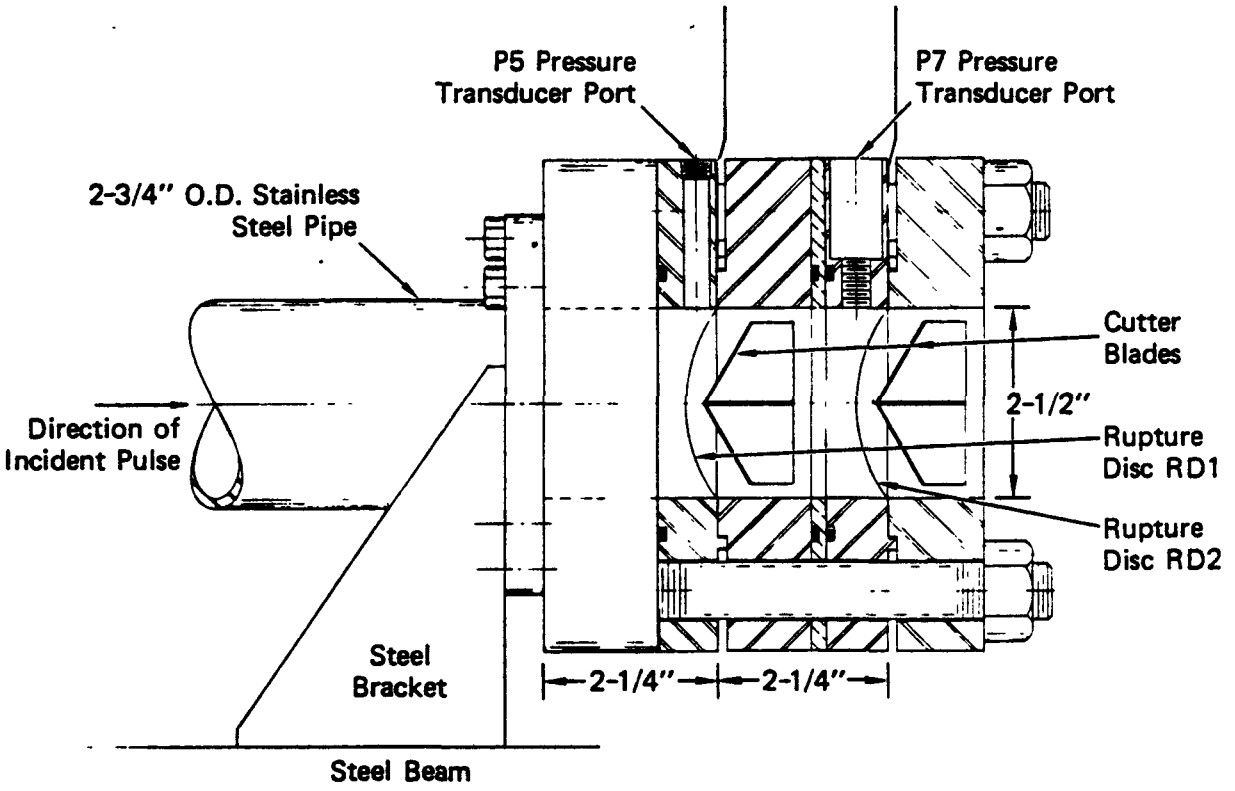

(a) DOUBLE RUPTURE DISC ASSEMBLY

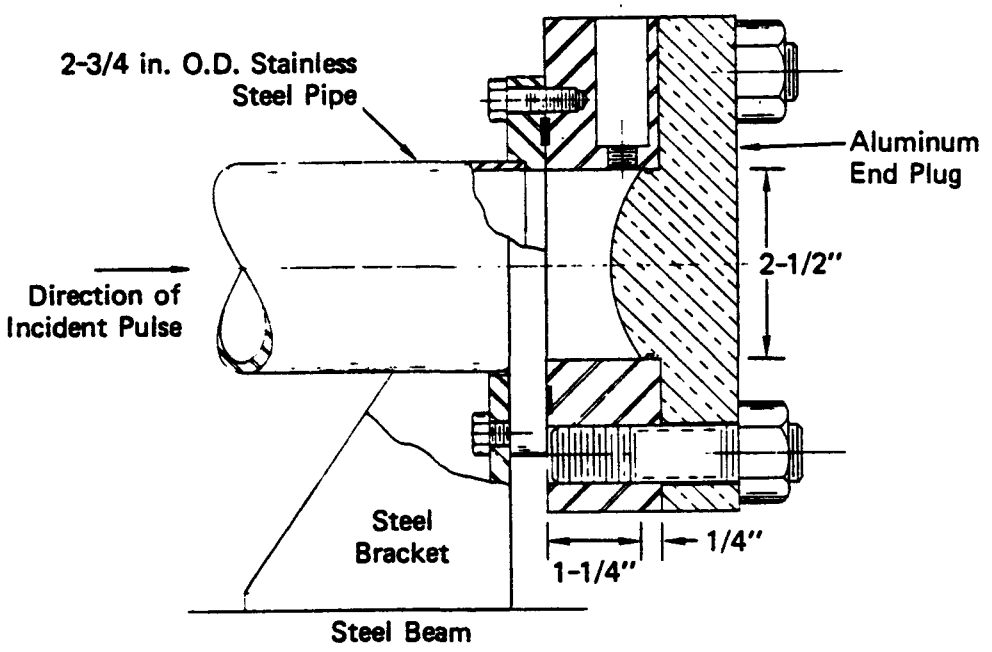

(b) RIGID END-PLUG ASSEMBLY

FIGURE 3.1.2 DOUBLE RUPTURE DISC AND END PLUG ASSEMBLIES

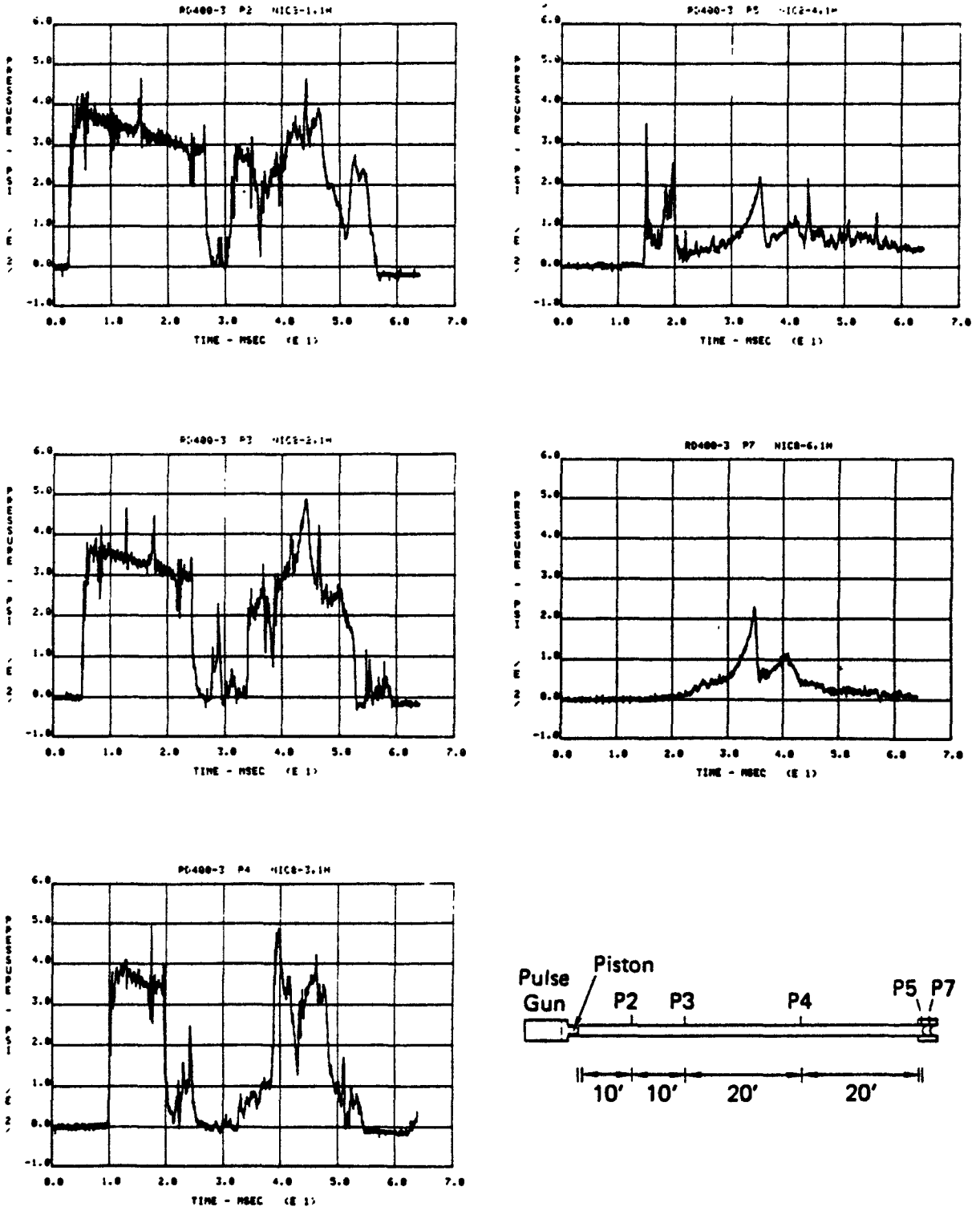

FIGURE 3.1.3 RD-400-3 PRESSURE RECORDS

PL 2

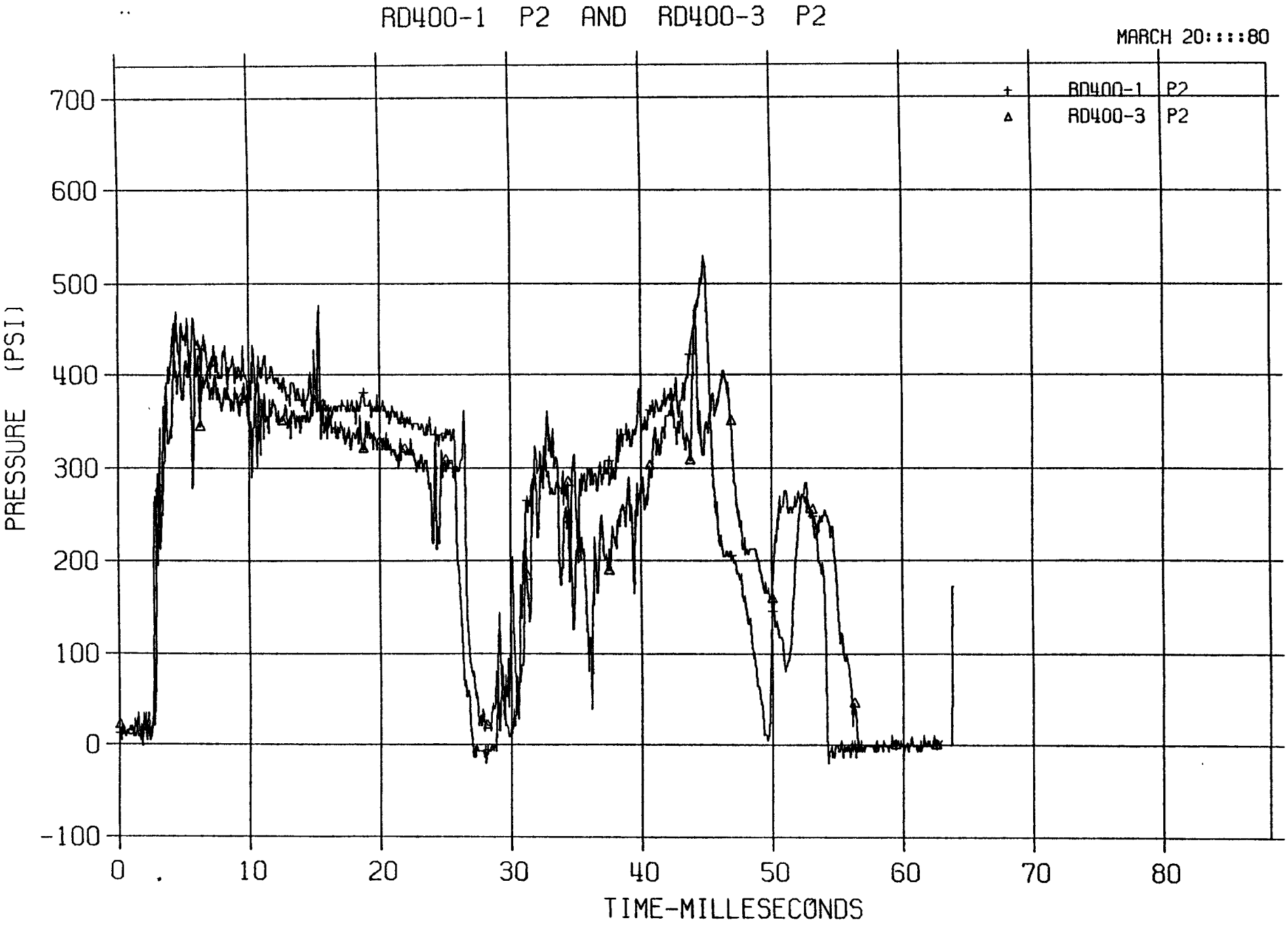

PL 1

FIGURE 3.1.4, DATA COMPARISON BETWEEN SRI TESTS RD400-1 AND RD400-3.

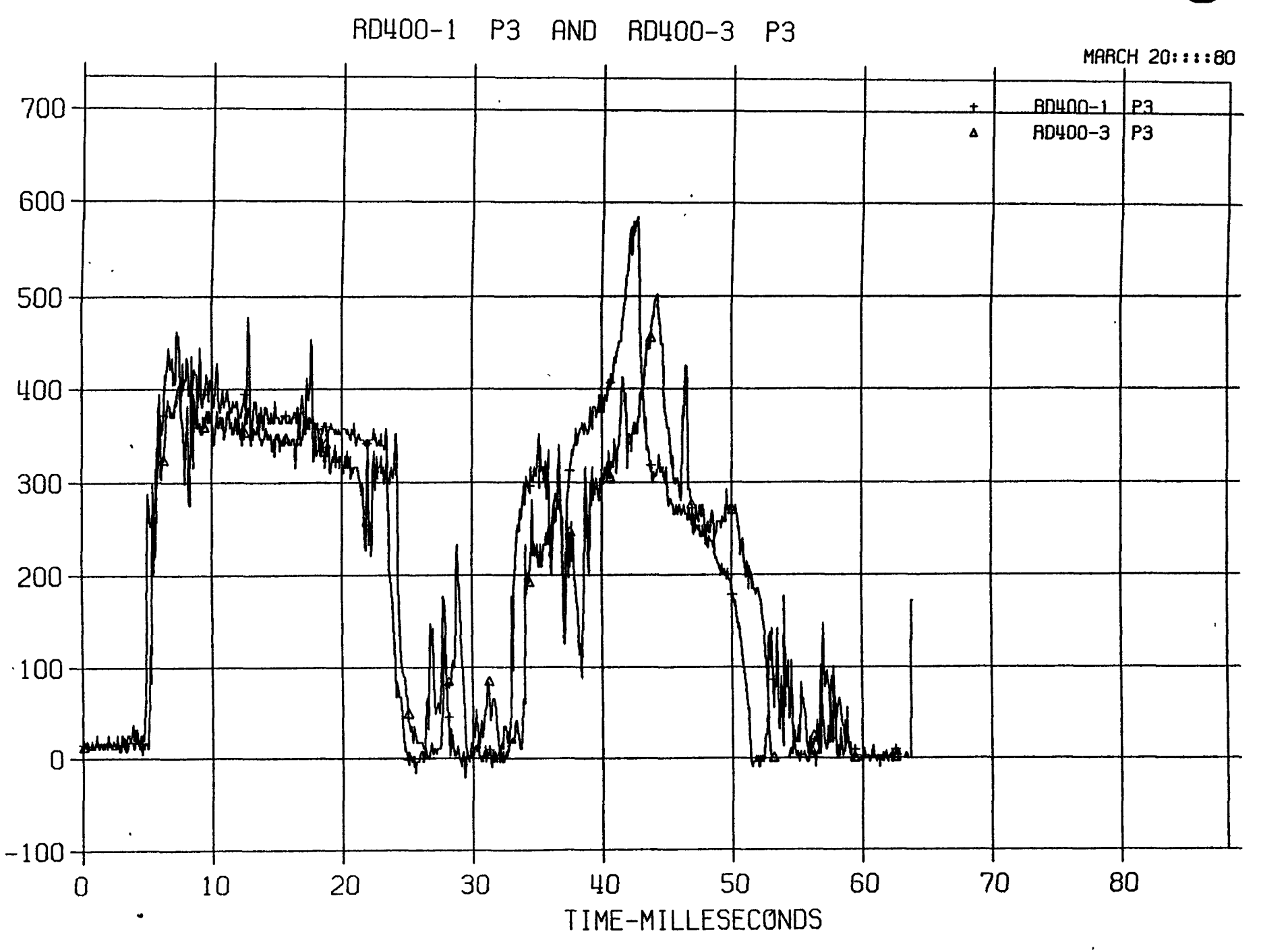

FIGURE 3.1.5, DATA COMPARISON BETWEEN SRI TESTS RD400-1 AND RD400-3.

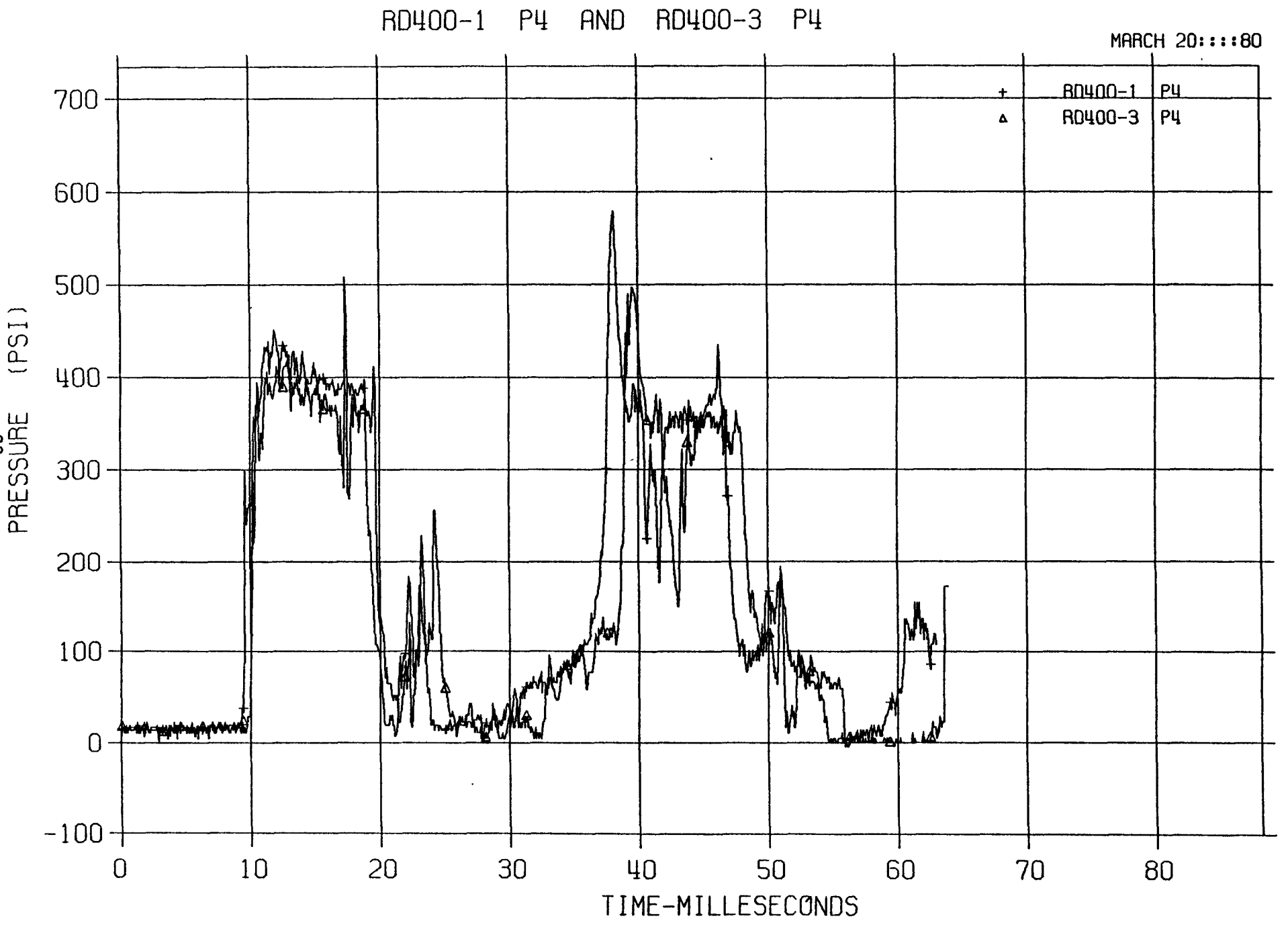

FIGURE 3.1.6, DATA COMPARISON BETWEEN SRI TESTS RD400-1 AND RD400-3.

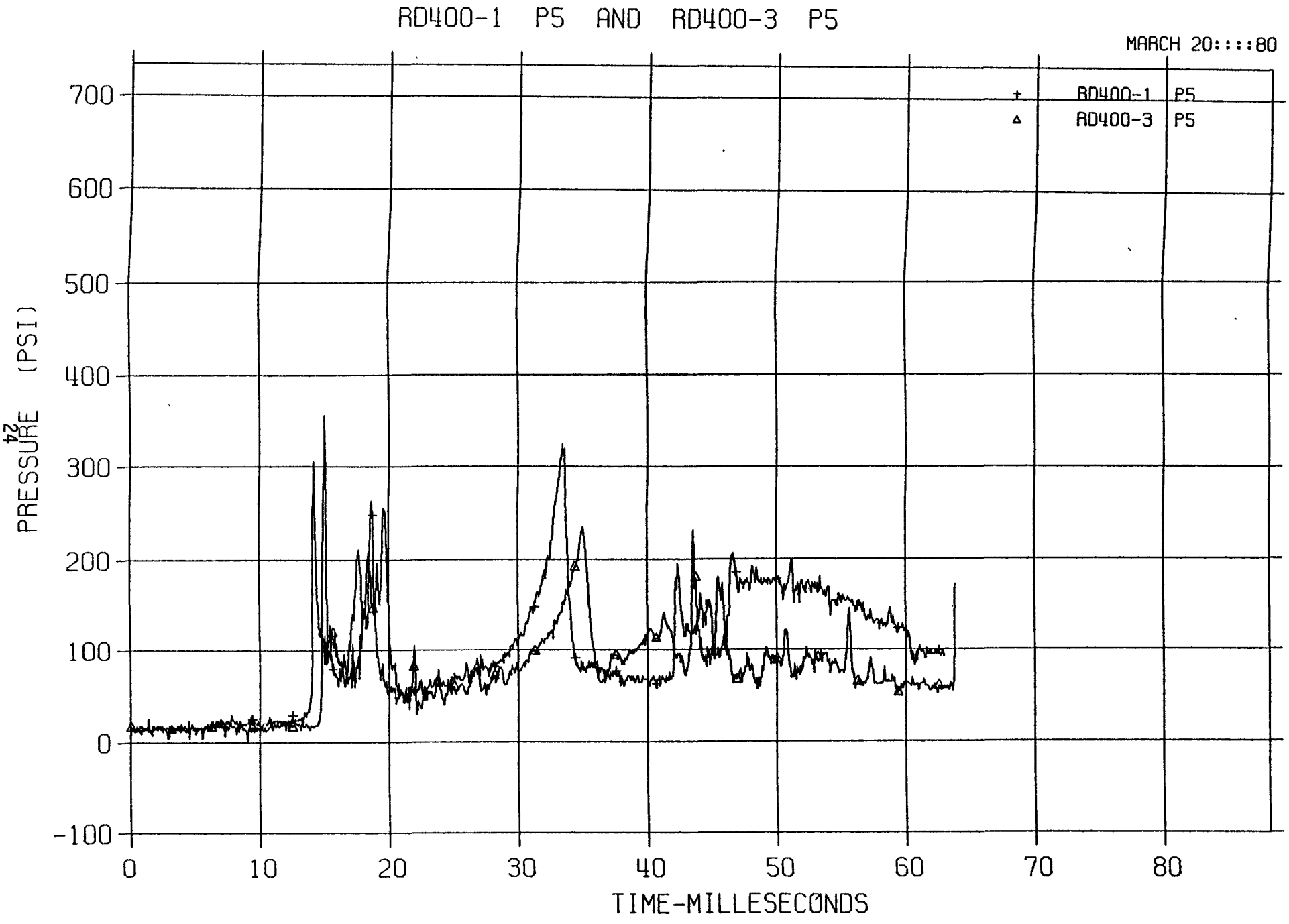

FIGURE 3.1.7, DATA COMPARISON BETWEEN SRI TESTS RD400-1 AND RD400-3.

PL 4

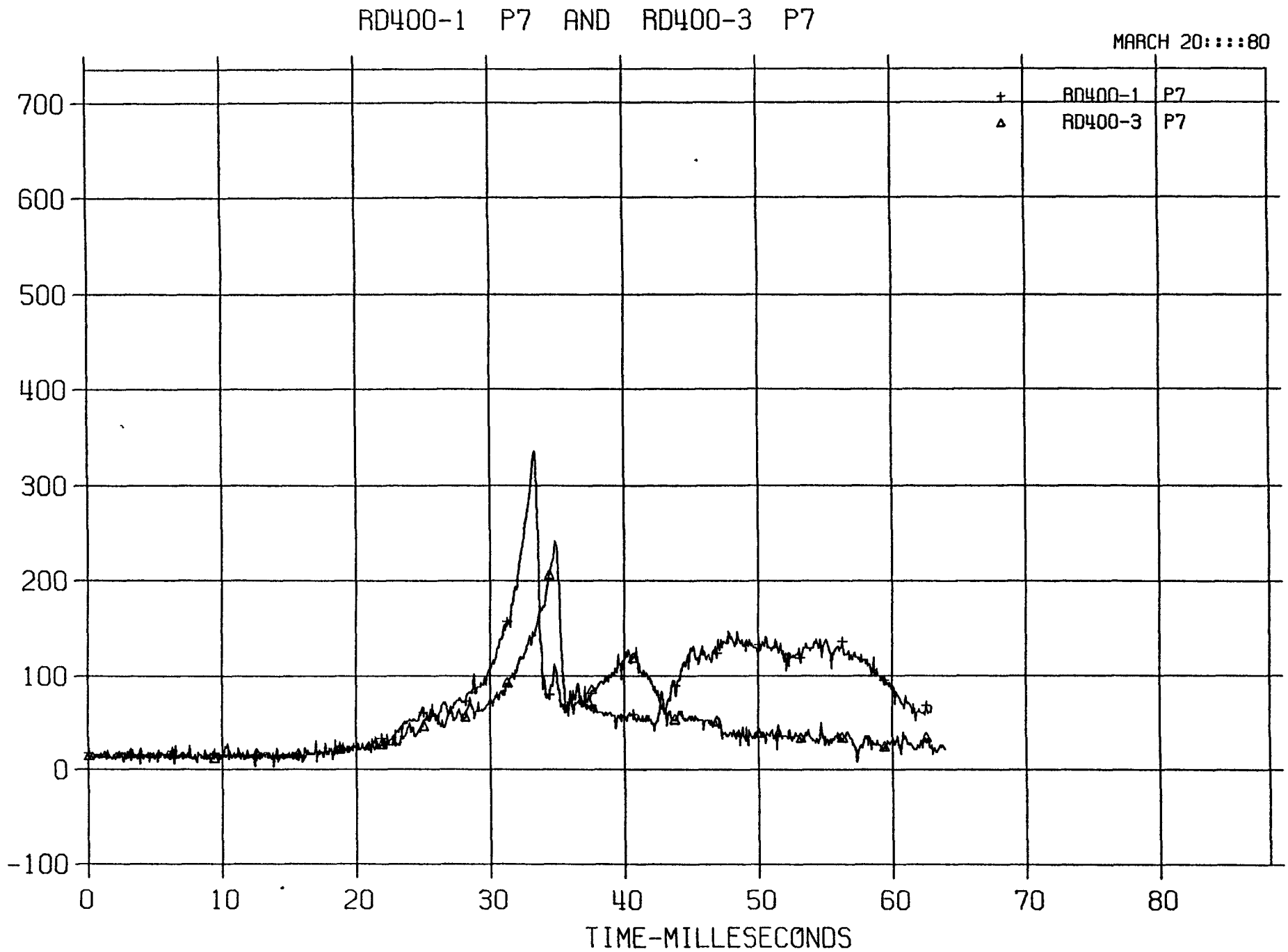

FIGURE 3.1.8, DATA COMPARISON BETWEEN SRI TESTS RD400-1 AND RD400-3.

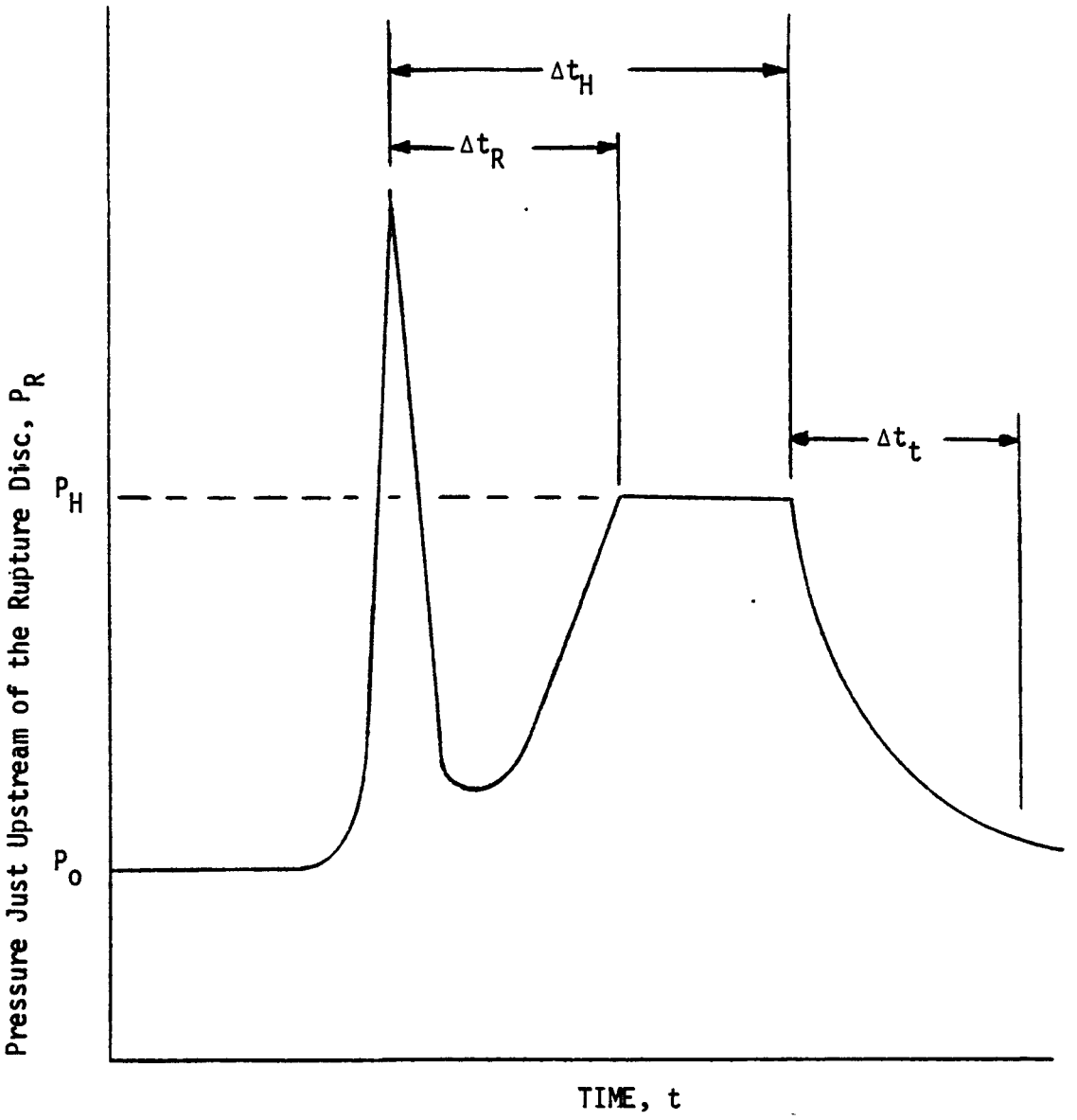

FIGURE 3.1.9, Rupture Disc Dynamic Buckling Characteristics Observed in the LLTR Series I Experiment.

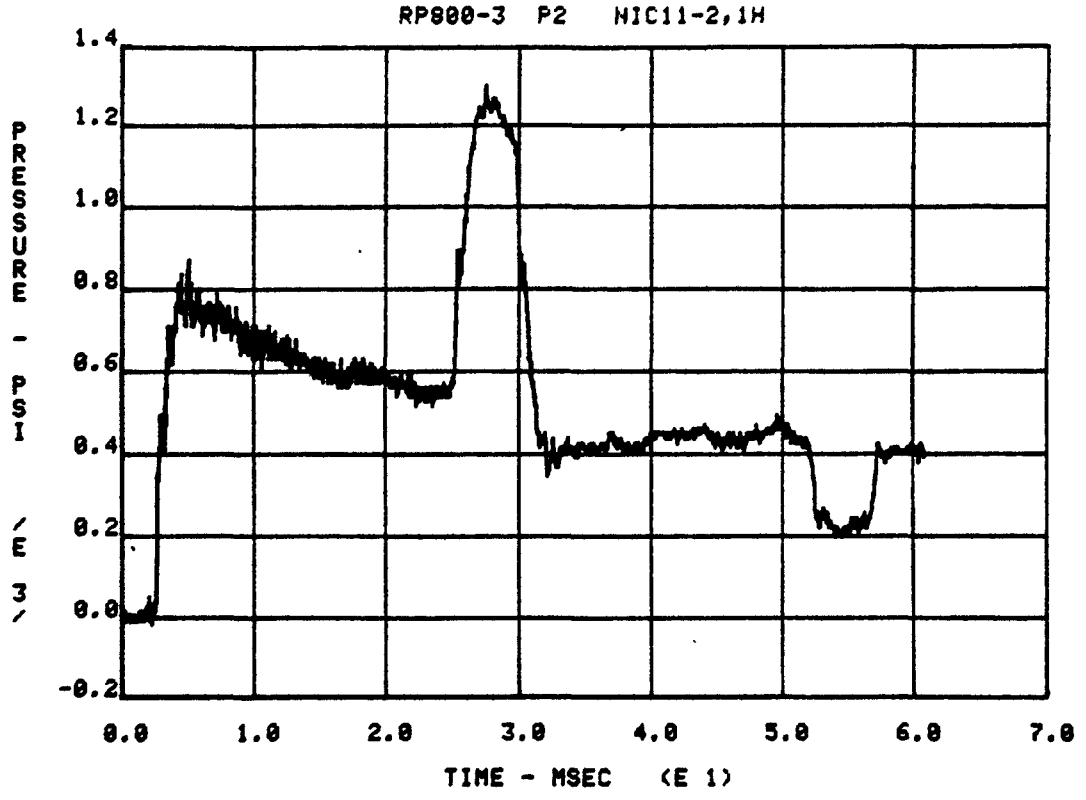

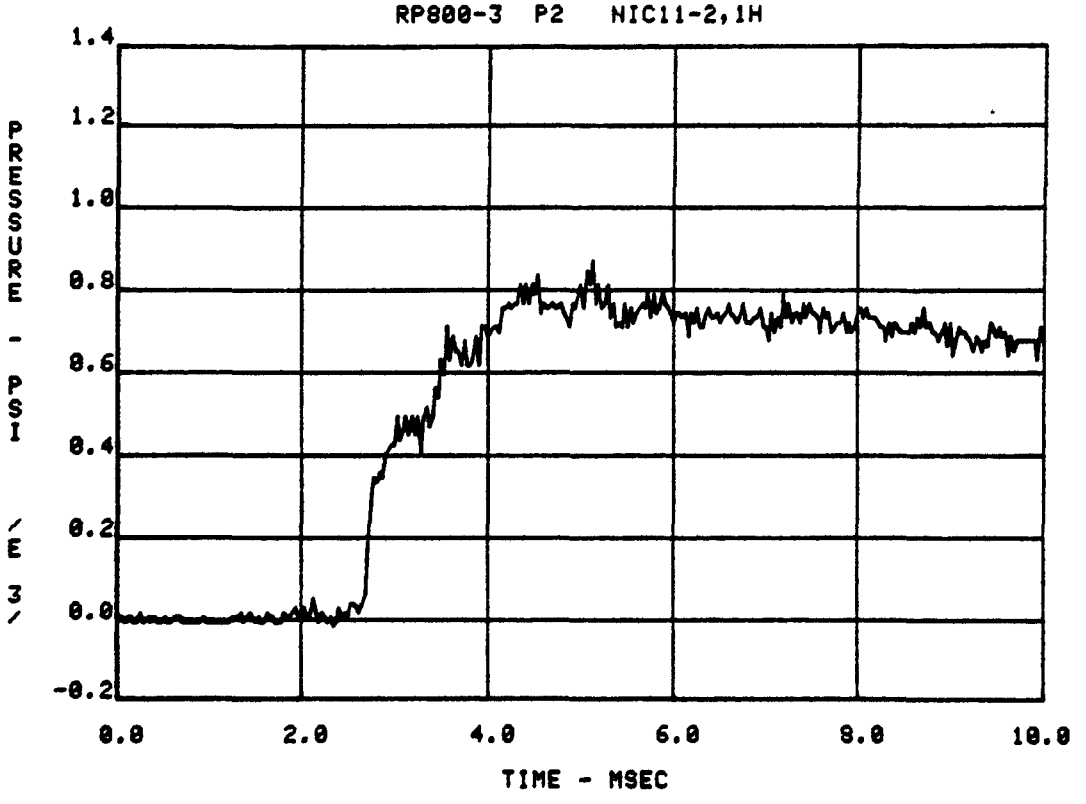

Figure 3.1.10, Pressure Data From SRI Rigid End Plug Test, RP800-3.

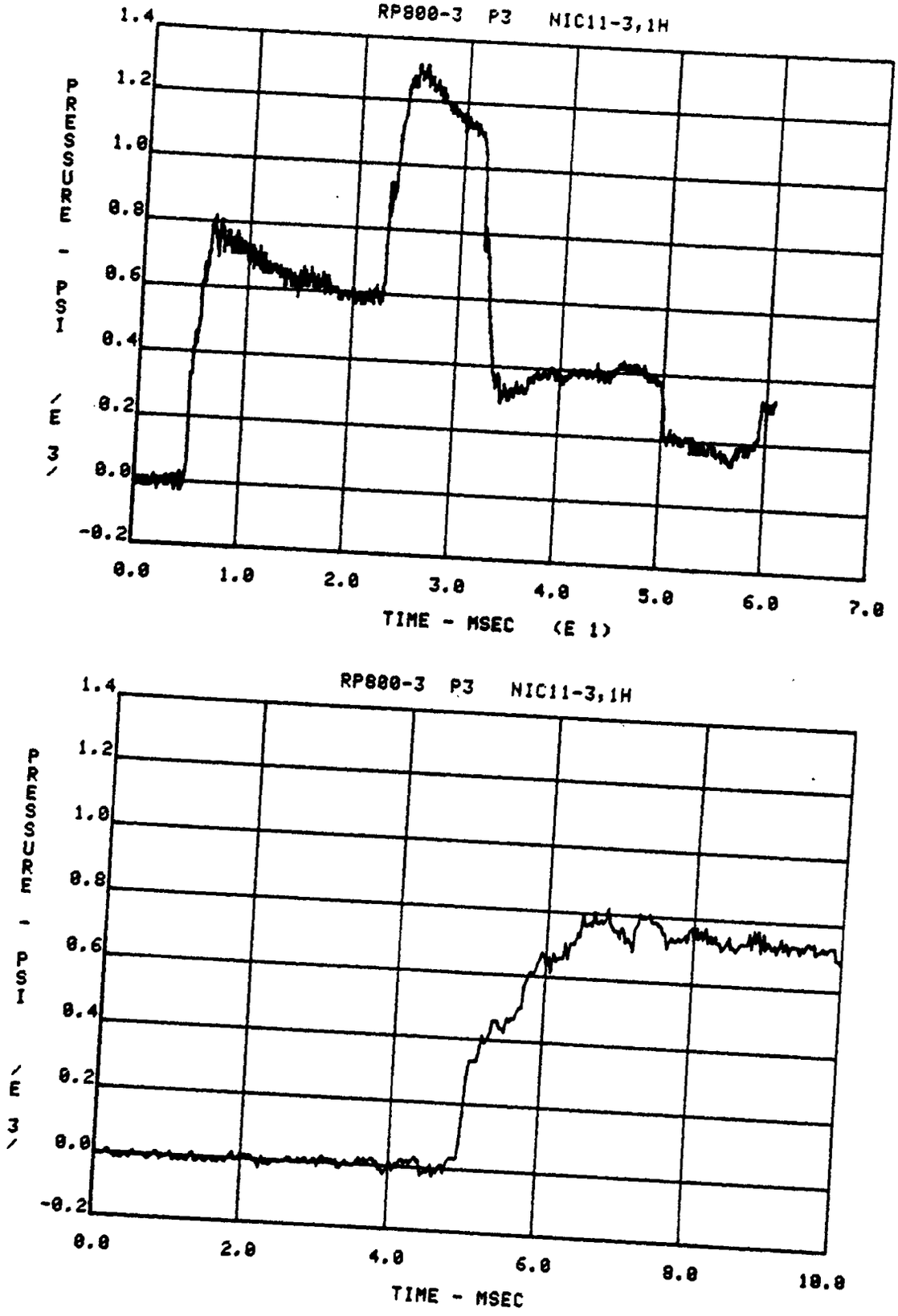

Figure 3.1.11, Pressure Data From SRI Rigid End Plug Test RP800-3.

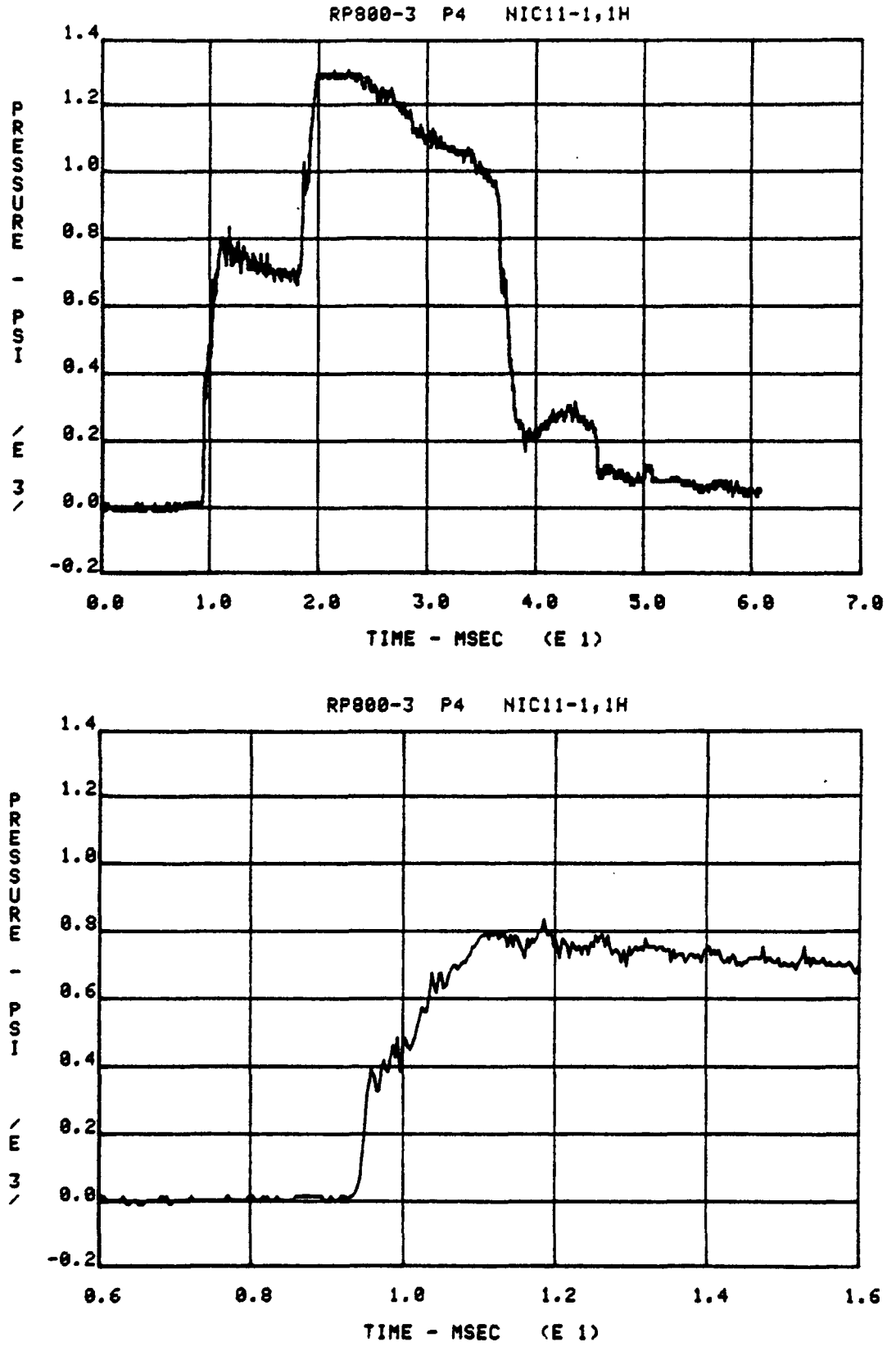

Figure 3.1.12, Pressure Data From SRI Rigid End Plug Test RP800-3.

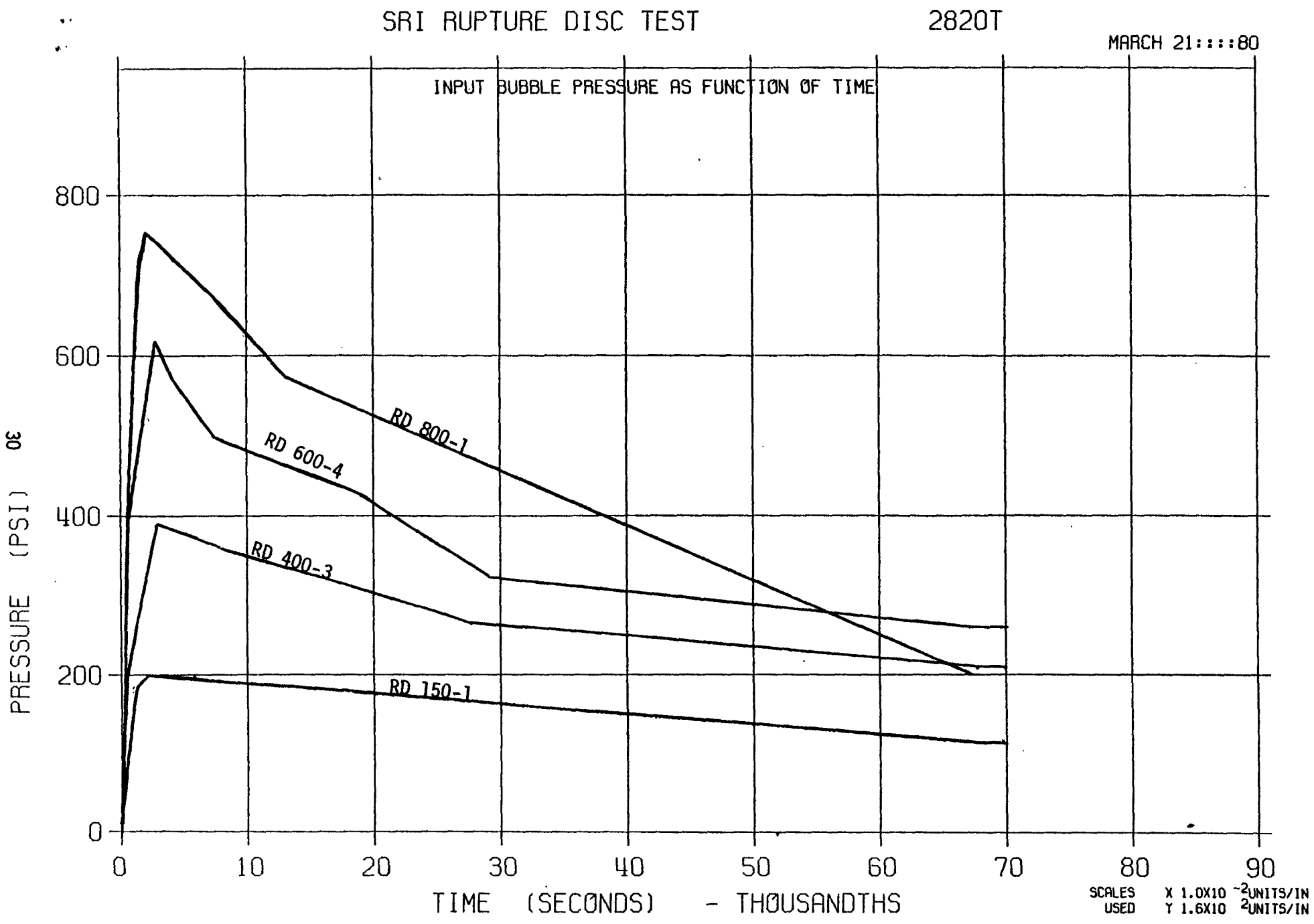

Figure 3.2.1, Source Pressure Input Data to TRANSWRAP II for SRI Tests RD150-1, RD400-3, RD600-4, and RD800-1.

PL 1

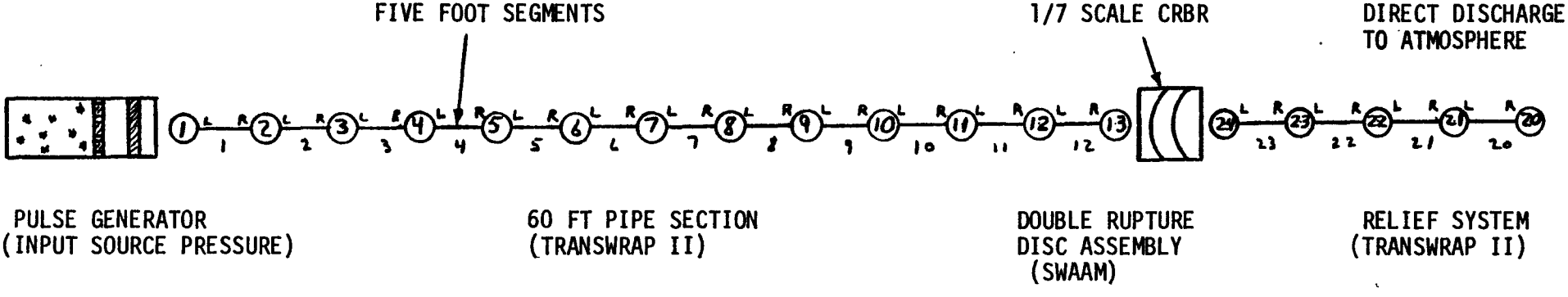

Figure 3.2.2, Schemetic TRANSWRAP II Model For Simulation of the SRI Test Apparatus.

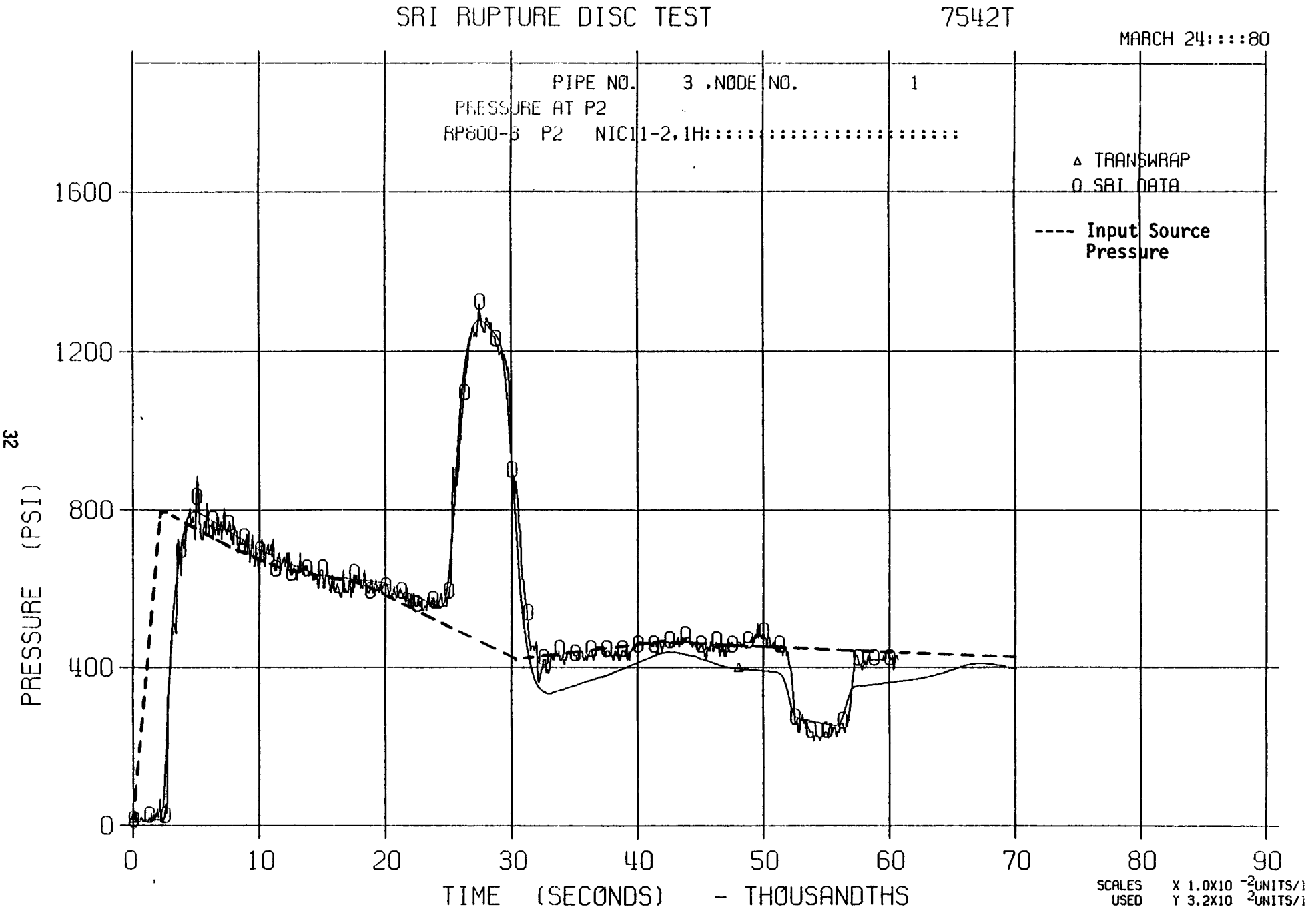

PL 2

Figure 3.2.3, Comparison Between the TRANSWRAP II Prediction and SRI Test RP800-3.

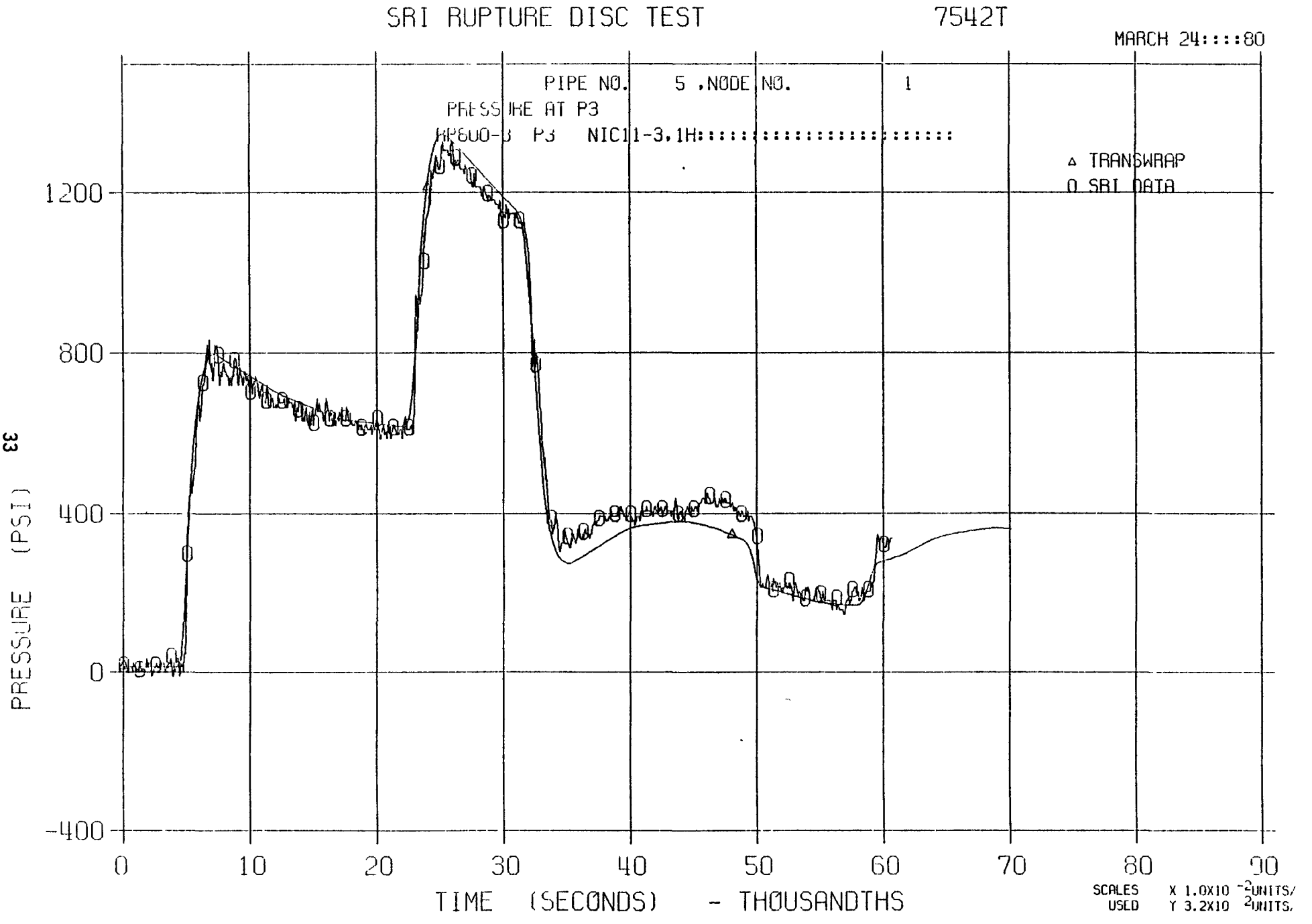

PL 3 **Figure 3.2.4, Comparison Between The TRANSWRAP II Prediction and SRI Test RP800-3.**

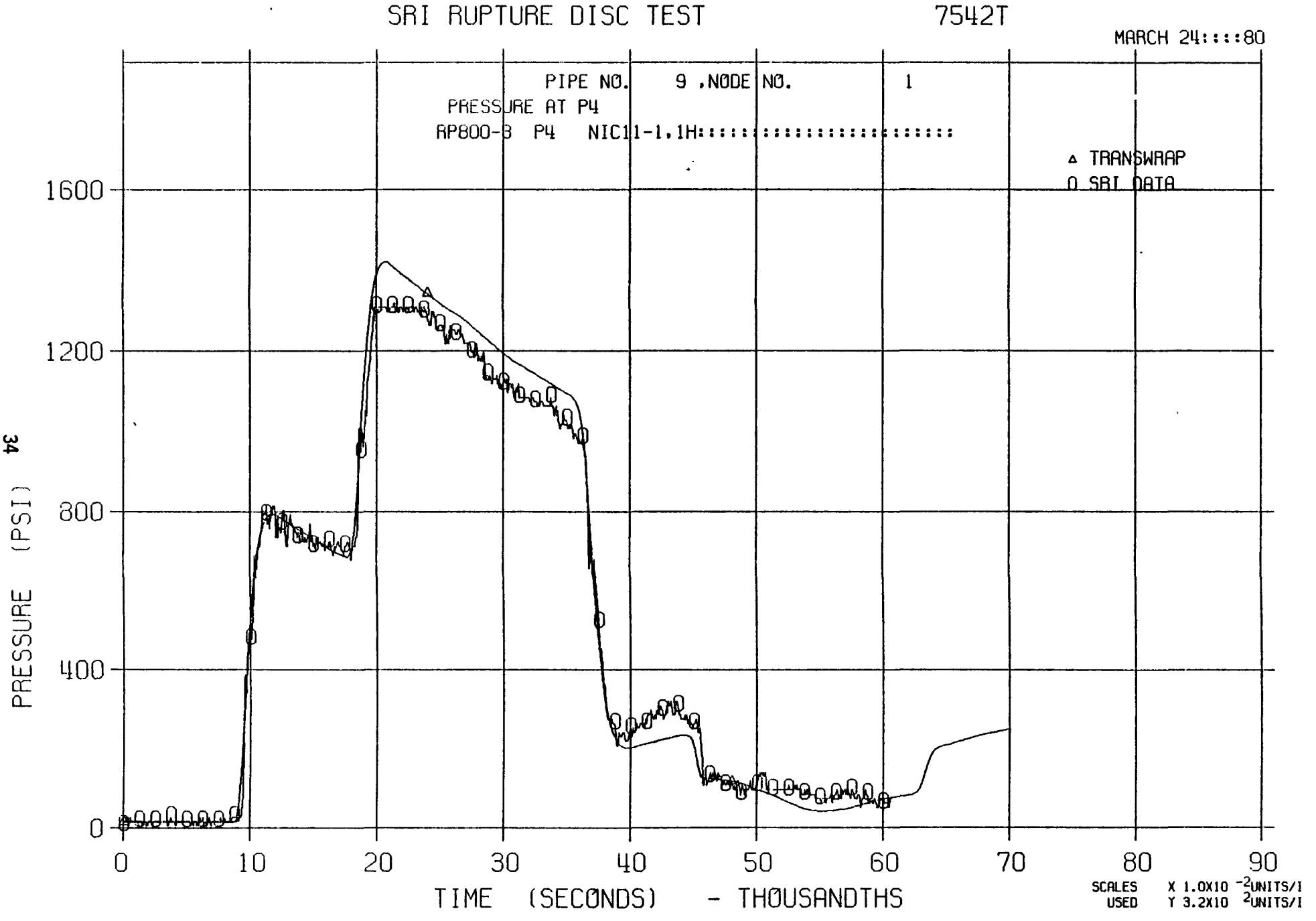

PL 4

Figure 3.2.5, Comparison Between the TRANSWRAP II Prediction and the SRI Test RP800-3.

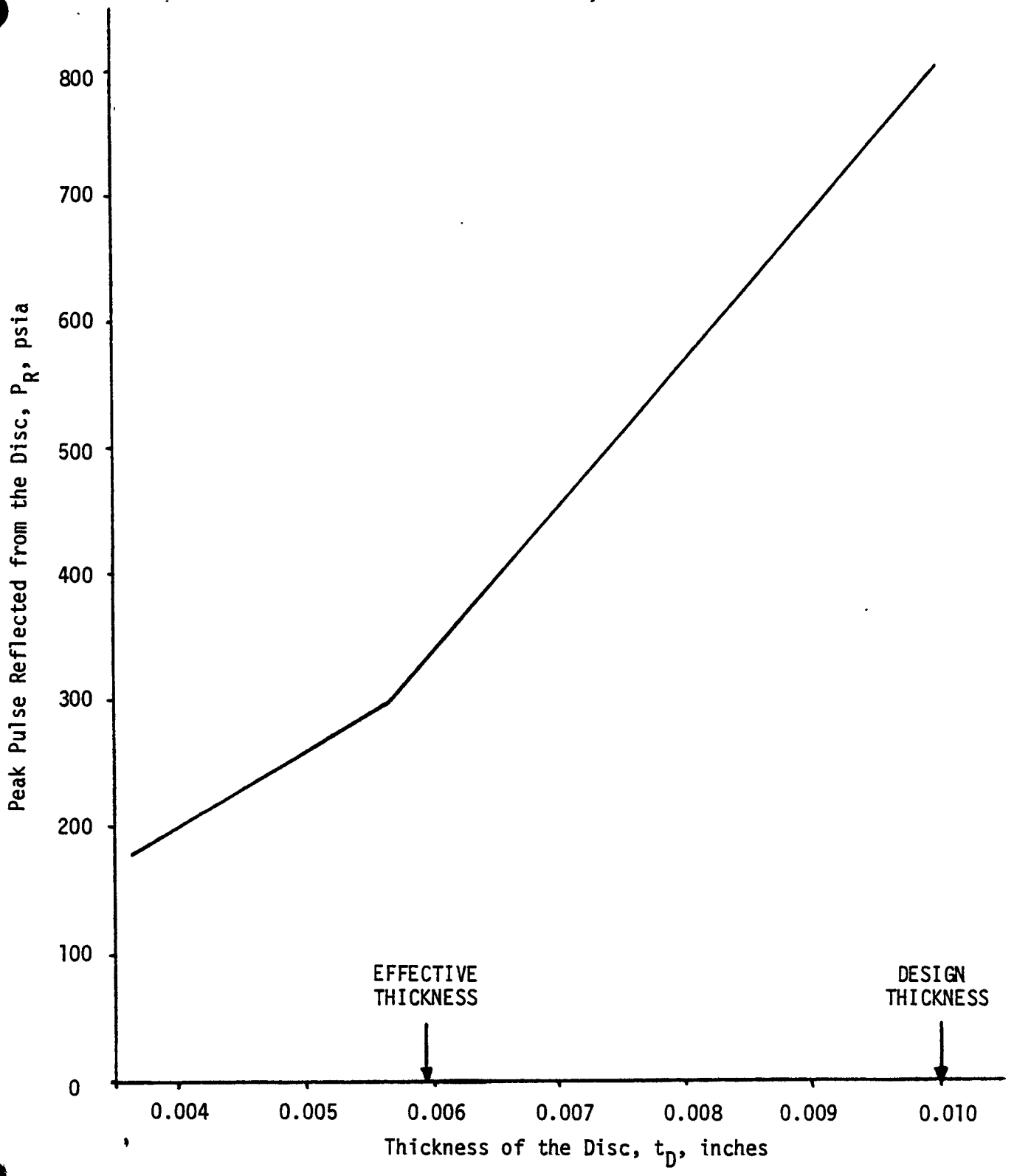

Figure 3.2.6, Effect of Membrane Strength as Reflected by Rupture Disc Thickness on Rupture Pressure.

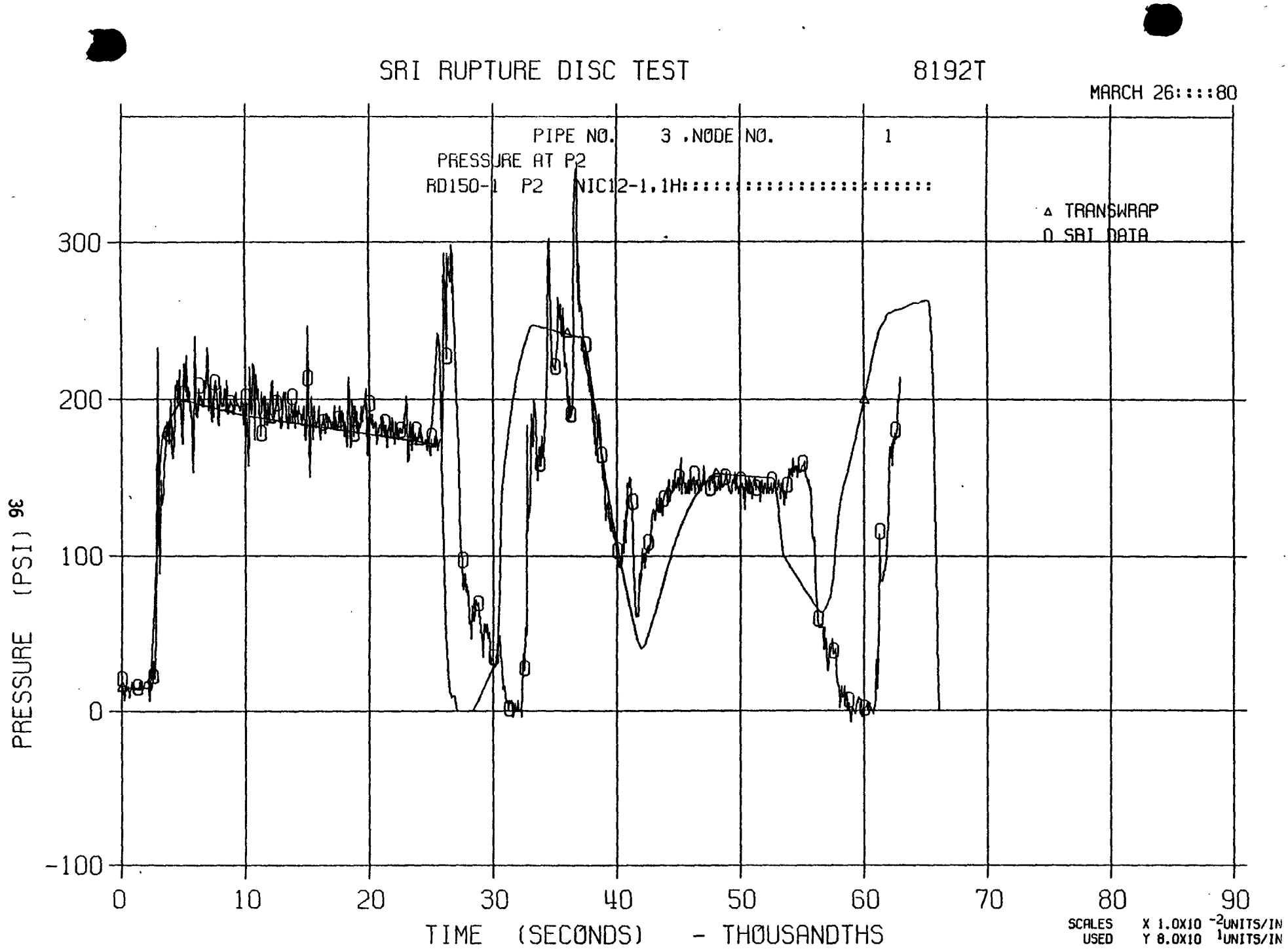

PL 2

Figure 3.2.7, Comparison Between the TRANSWRAP II Prediction and SRI Test RD150-1.

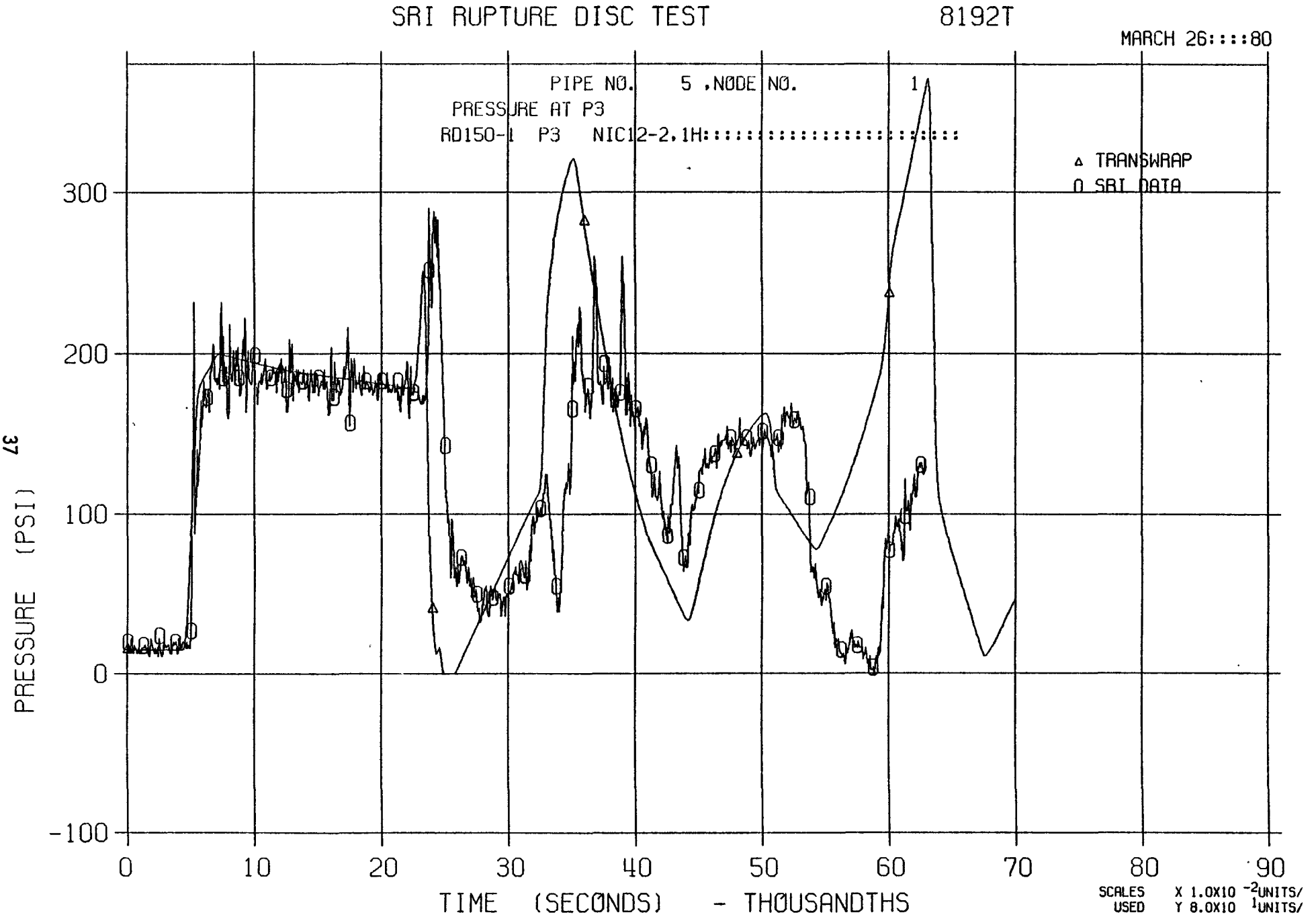

PL 3

Figure 3.2.8, Comparison Between the TRANSWRAP II Prediction and SRI Test RD150-1.

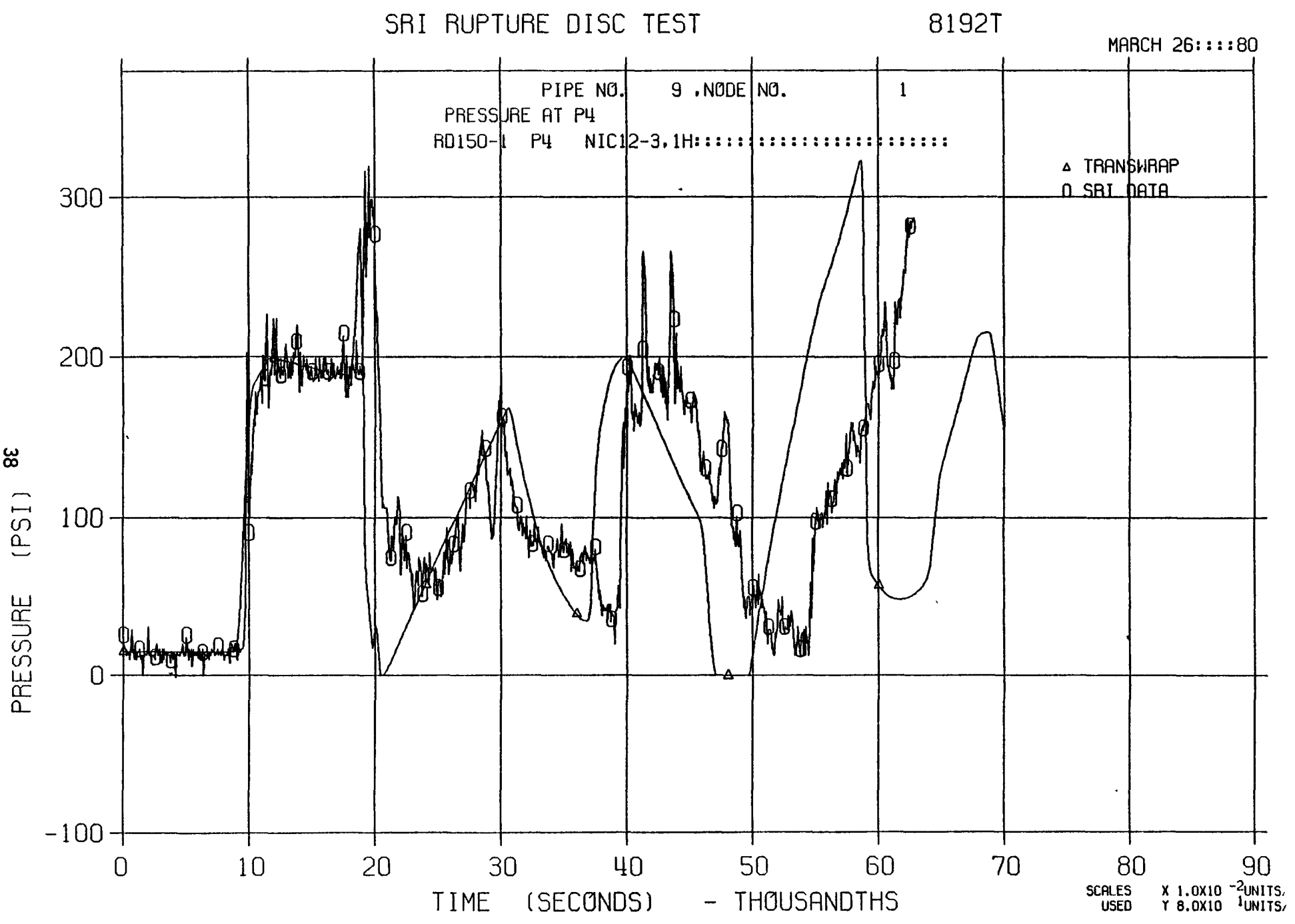

PL 4 **Figure 3.2.9, Comparison Between the TRANSWRAP II Prediction and SRI Test RD150-1.**

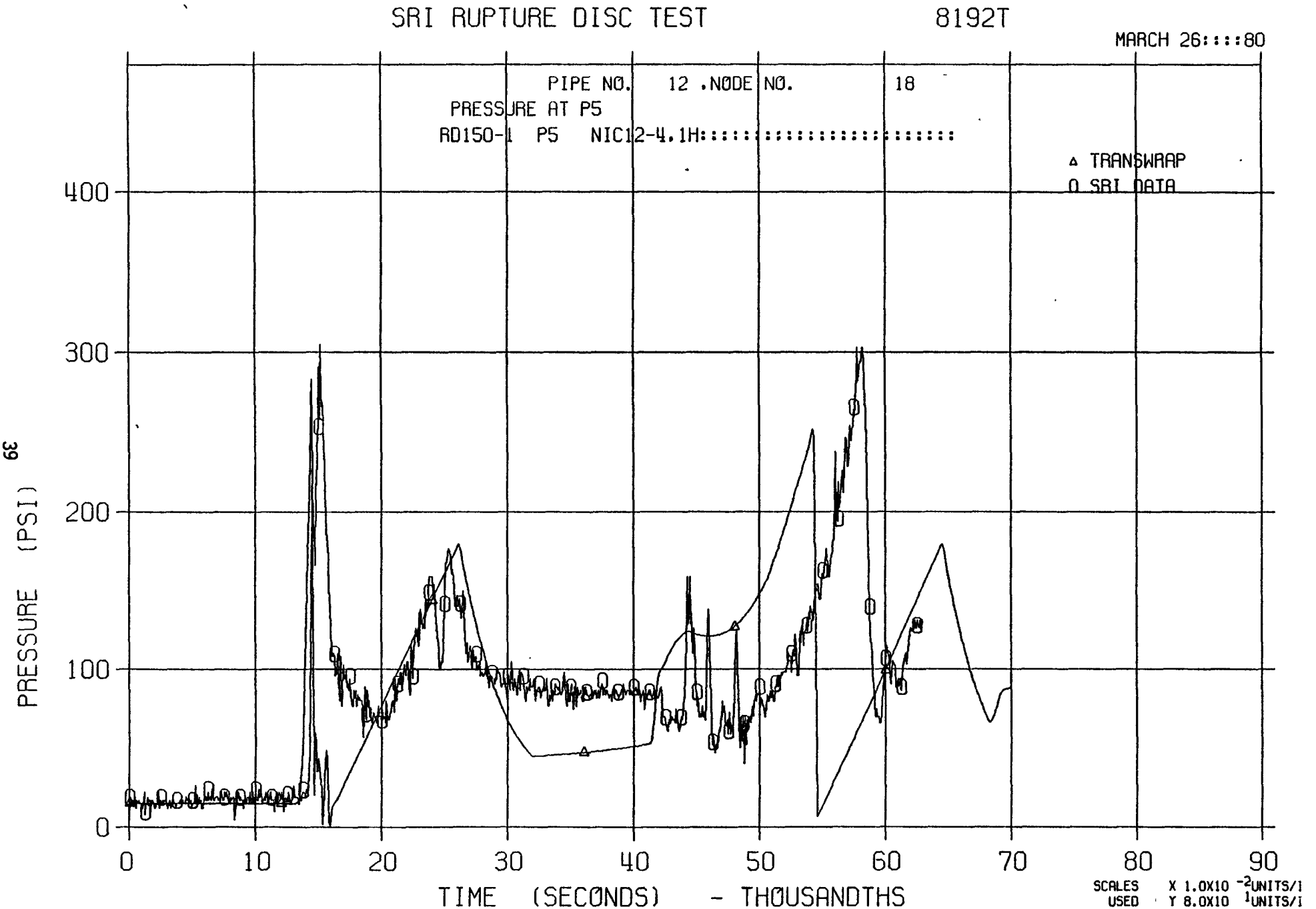

PL 5

Figure 3.2.10, Comparison Between the TRANSWRAP II Prediction and SRI Test RD150-1.

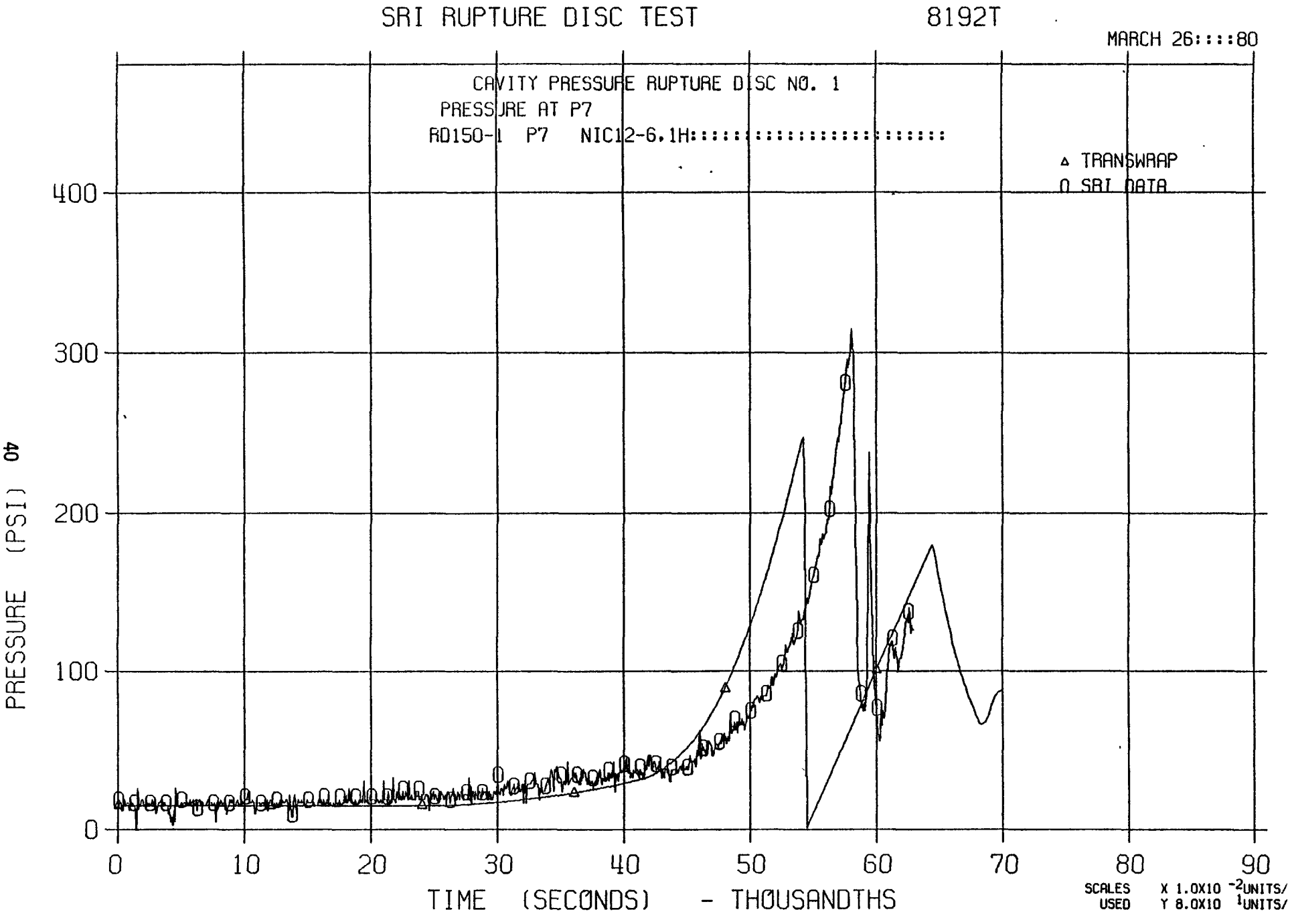

Figure 3.2.11, Comparison Between the TRANSWRAP II Prediction and SRI Test RD150-1

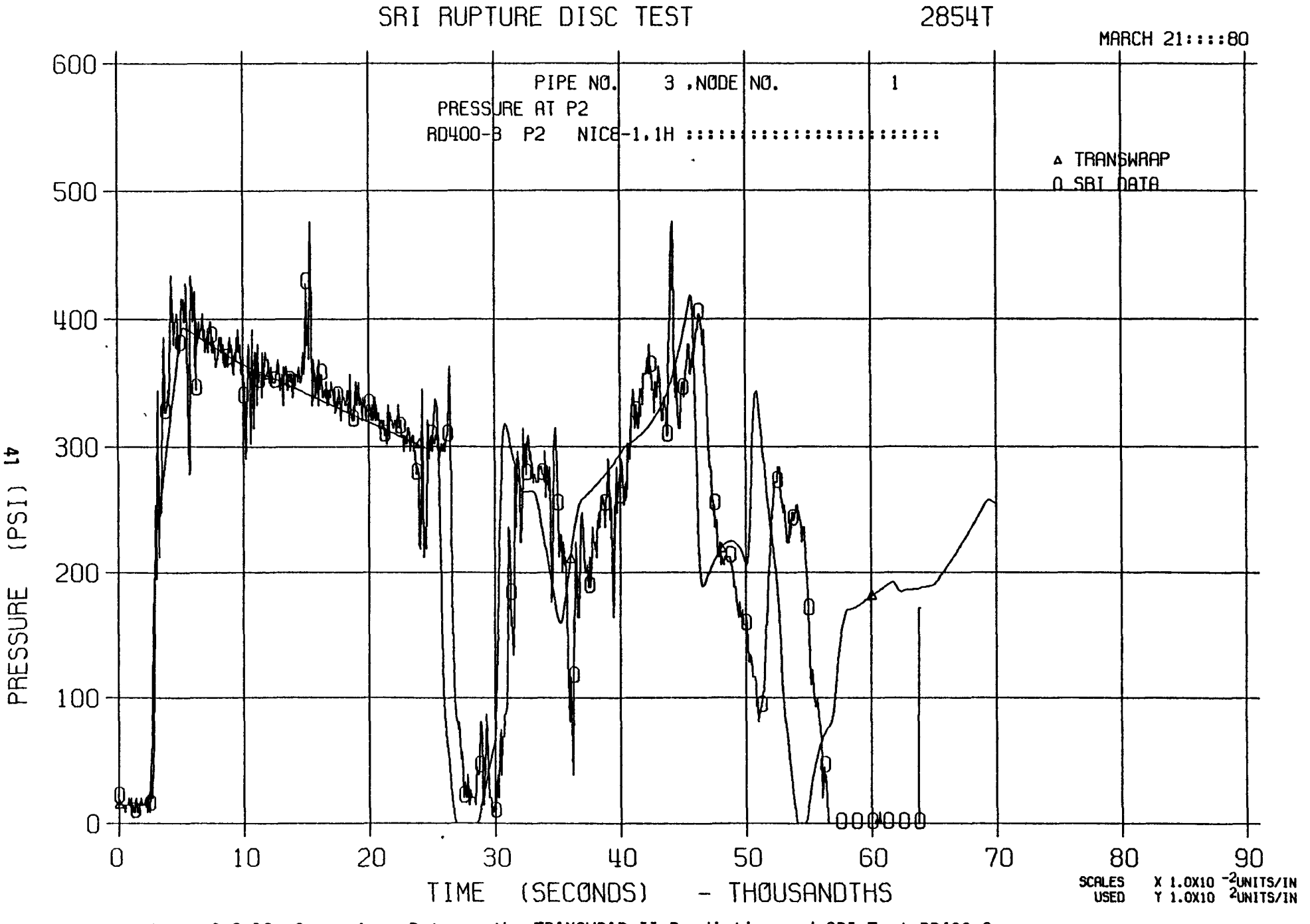

Figure 3.2.12, Comparison Between the TRANSWRAP II Prediction and SRI Test RD400-3

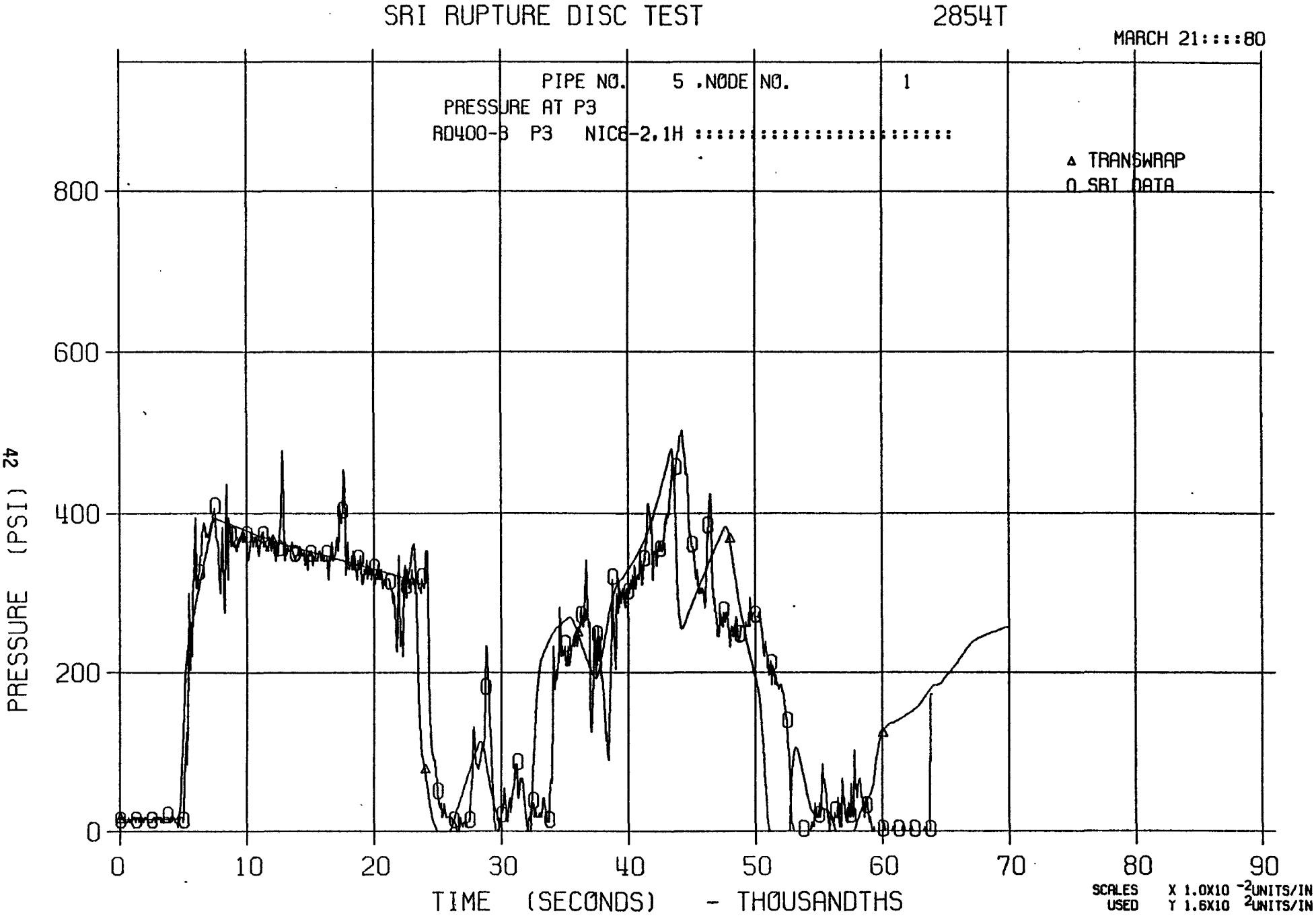

Figure 3.2.13, Comparison Between the TRANSWRAP II Prediction and SRI Test RD400-3

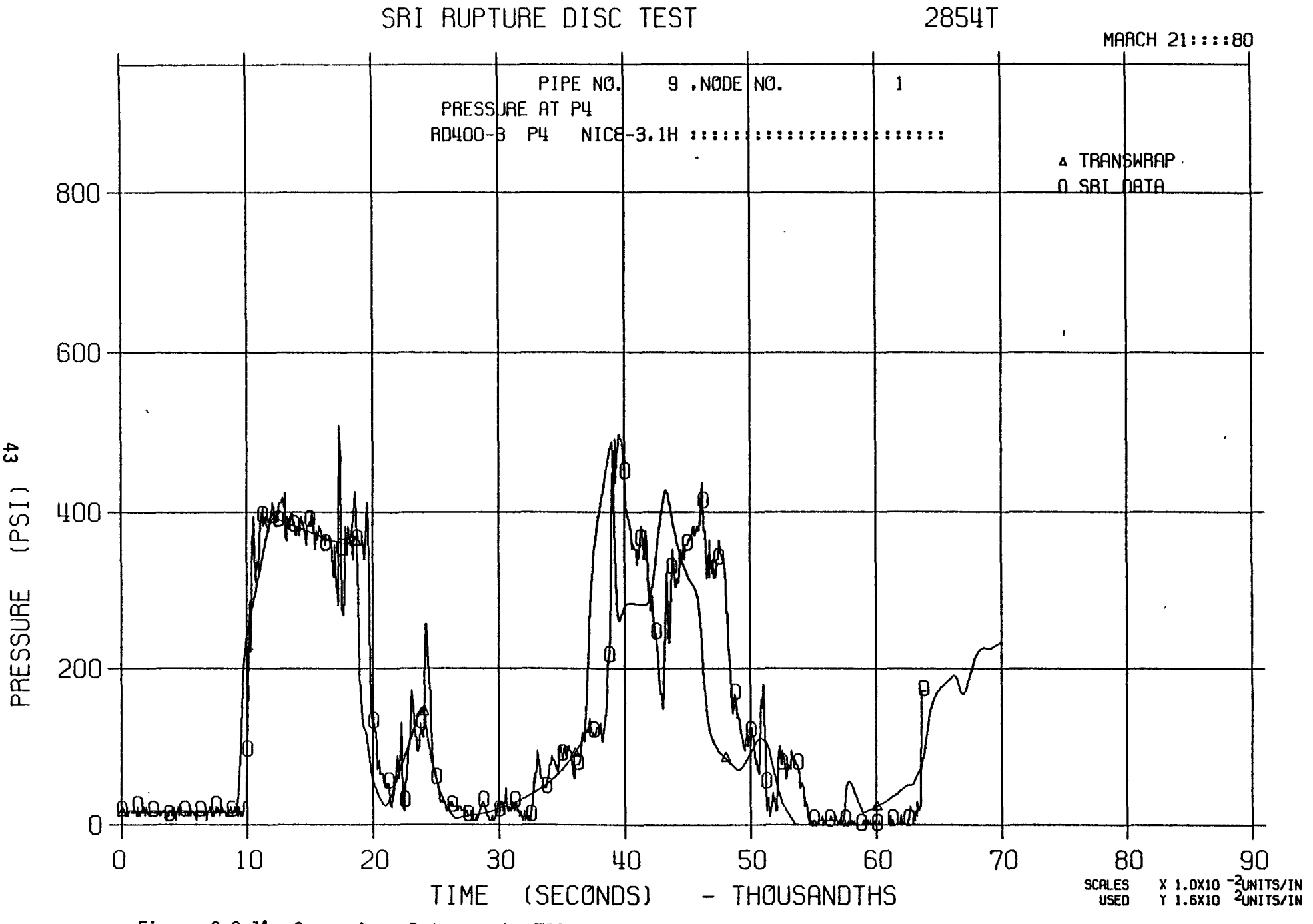

Figure 3.2.14, Comparison Between the TRANSWRAP II Prediction and SRI Test RD400-3

PL 4

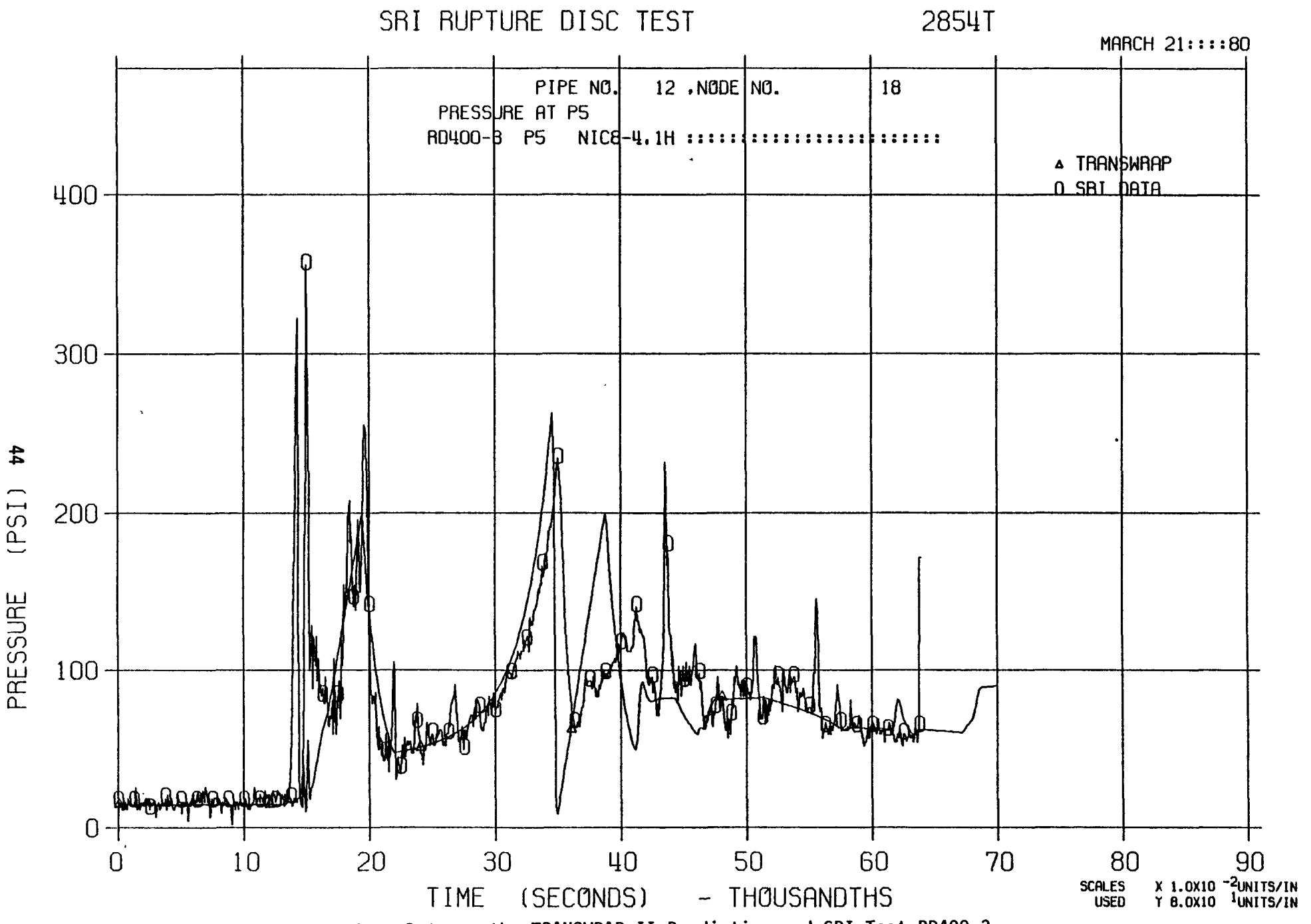

Figure 3.2.15, Comparison Between the TRANSWRAP II Prediction and SRI Test RD400-3

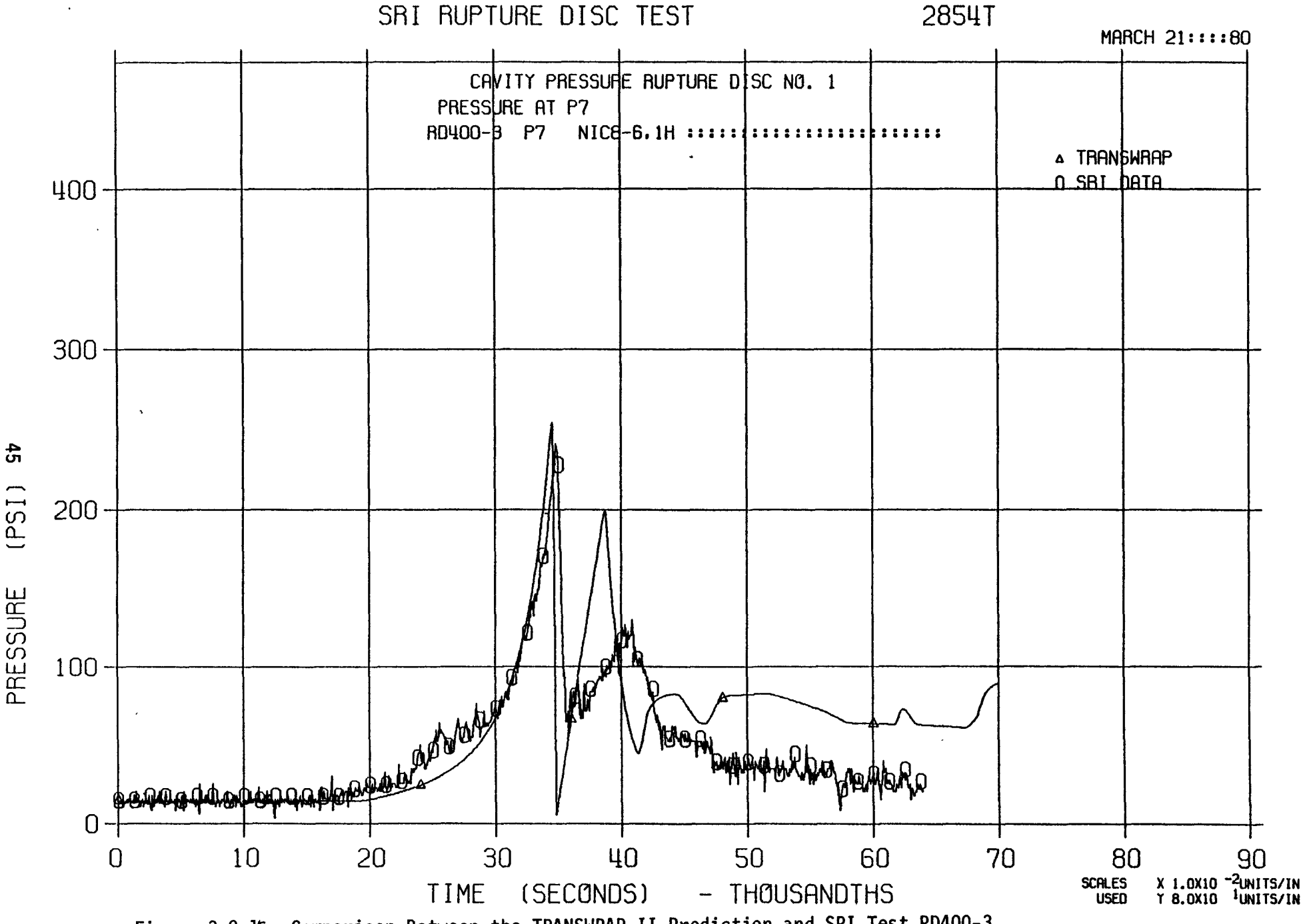

Figure 3.2.16, Comparison Between the TRANSWRAP II Prediction and SRI Test RD400-3

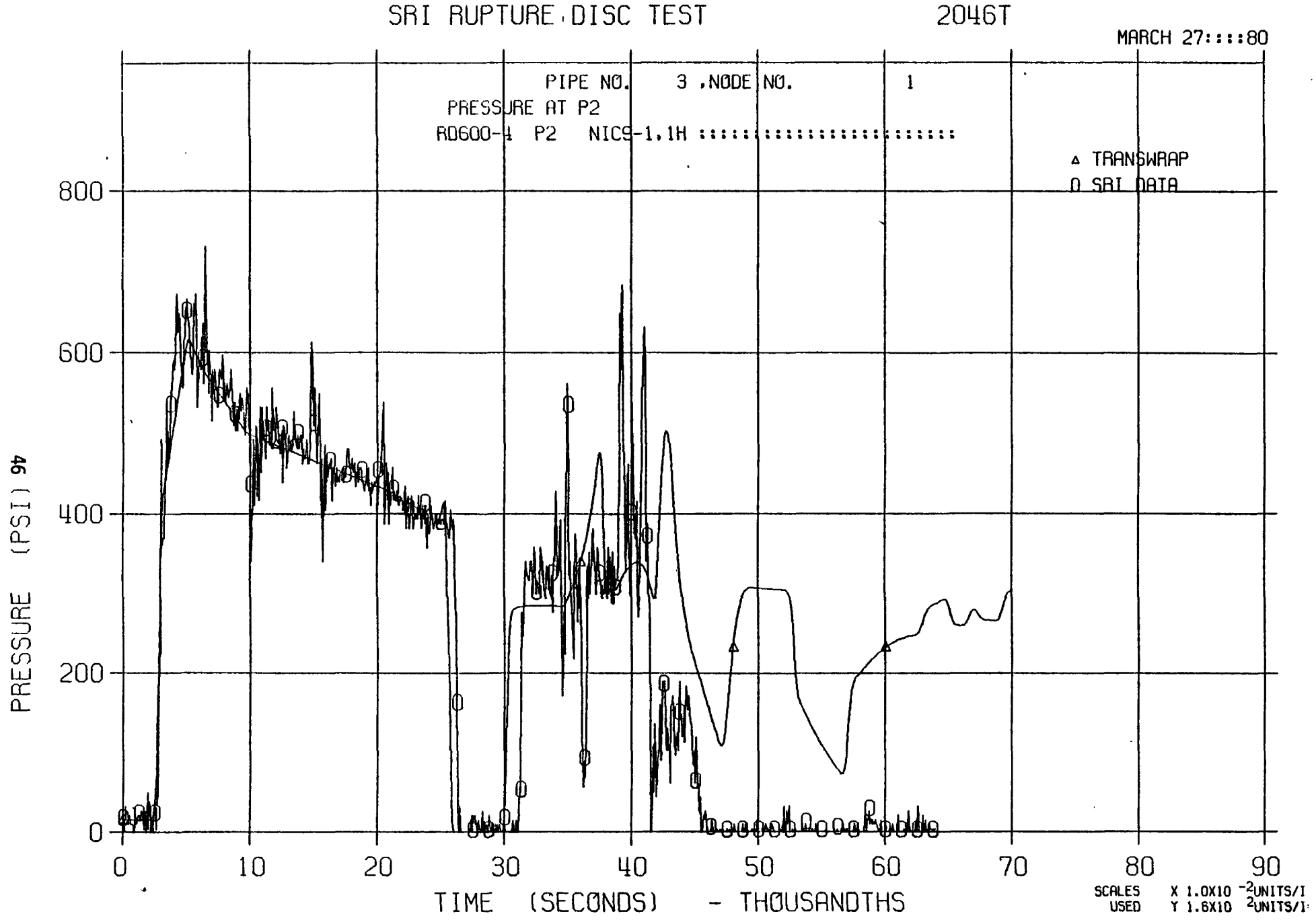

Figure 3.2.17, Comparison Between the TRANSWRAP II Prediction and SRI Test RD600-4

PL 2

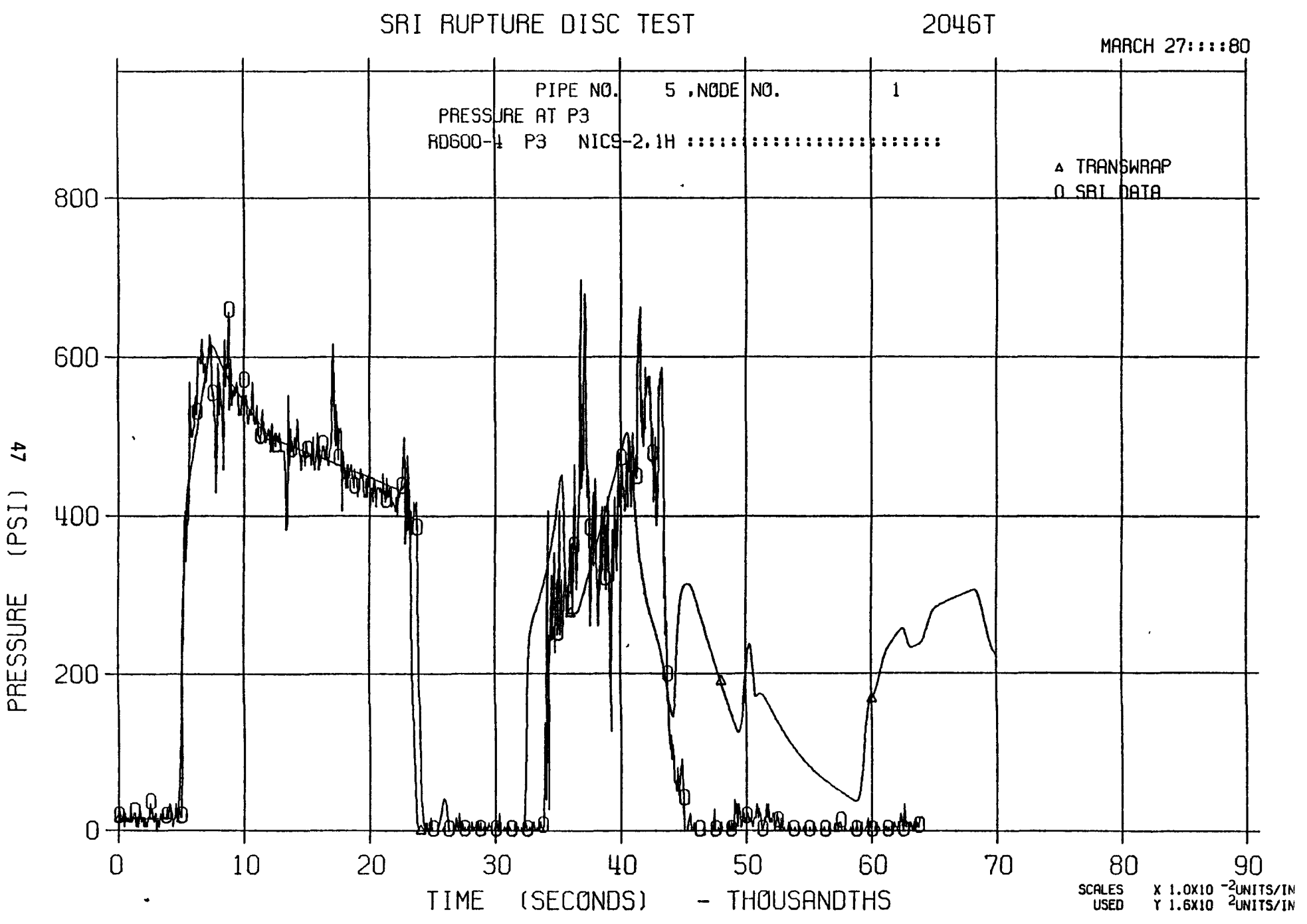

Figure 3.2.18, Comparison Between the TRANSWRAP II Prediction and SRI Test RD600-4

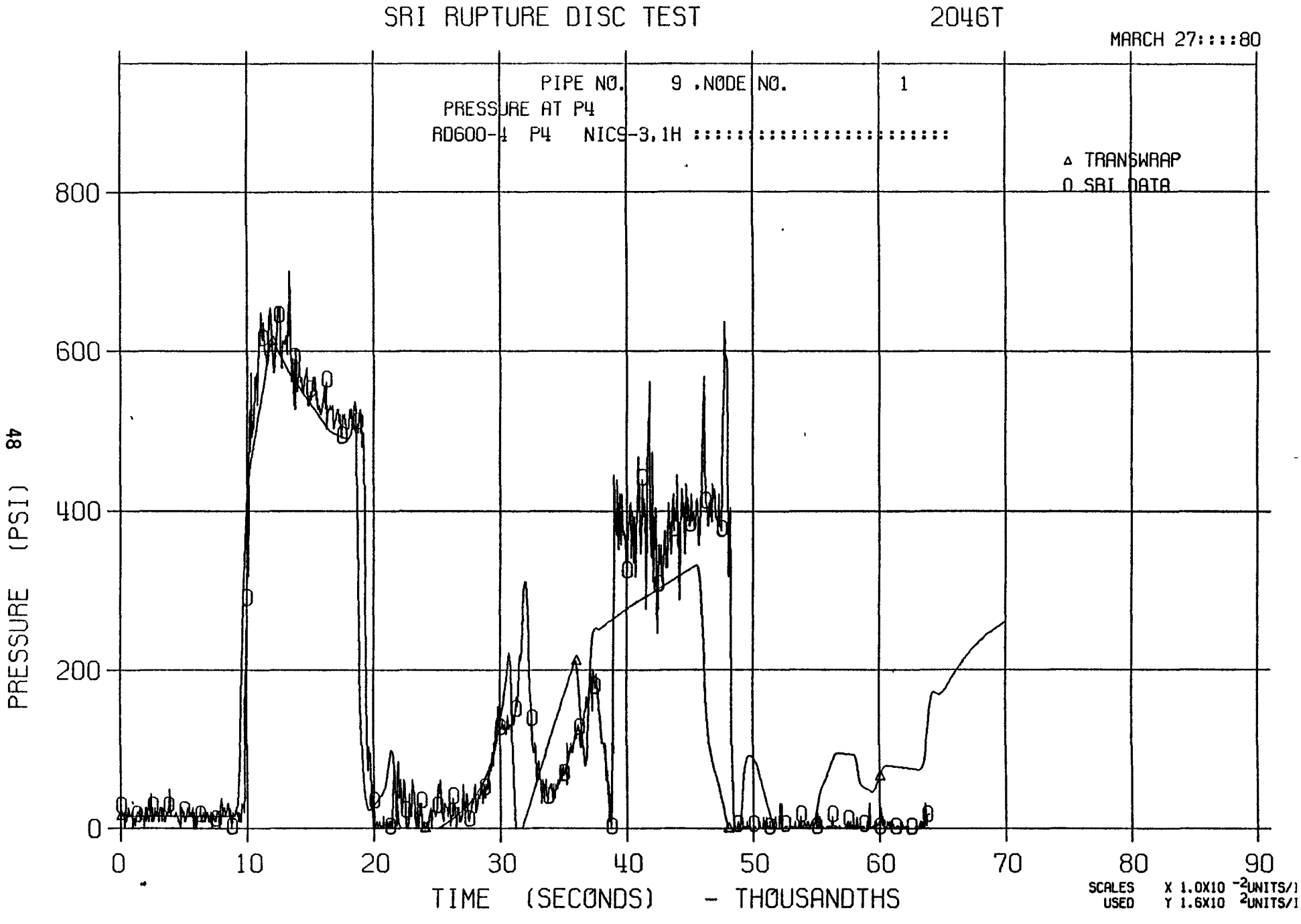

Figure 3.2.19, Comparison Between the TRANSWRAP II Prediction and SRI Test RD600-4

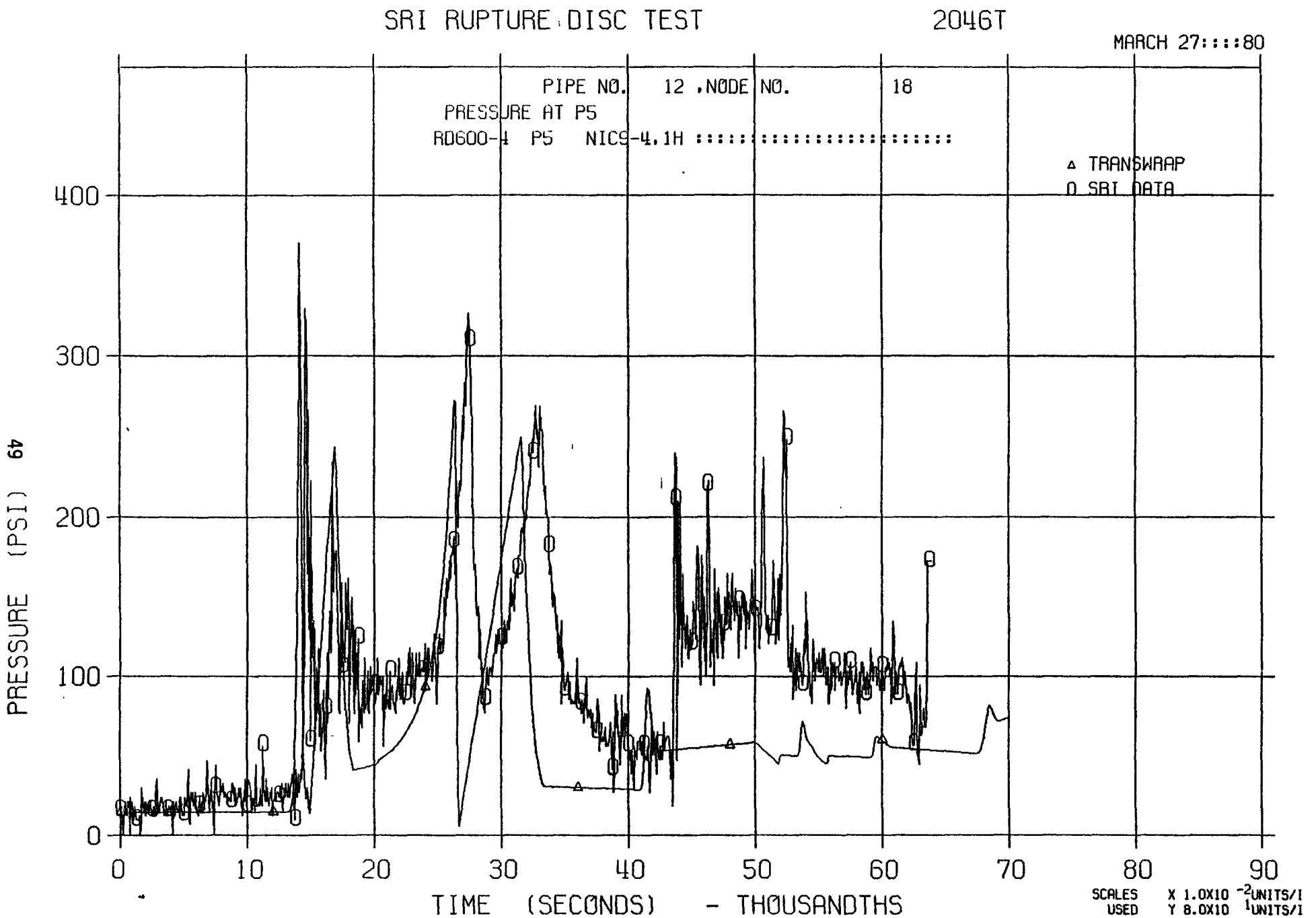

Figure 3.2.20, Comparison Between the TRANSWRAP II Prediction and SRI Test RD600-4

PL 5

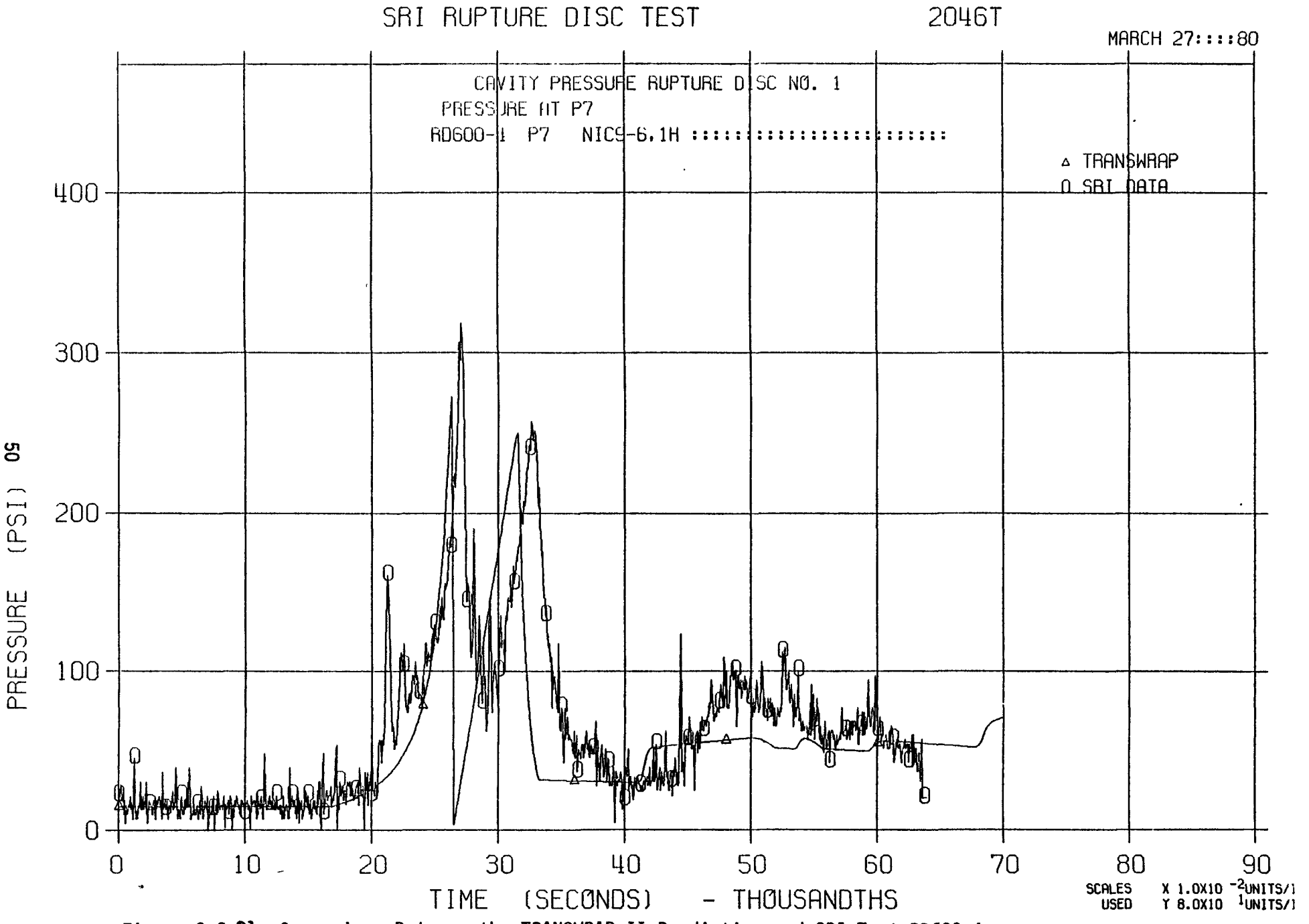

Figure 3.2.21, Comparison Between the TRANSWRAP II Prediction and SRI Test RD600-4

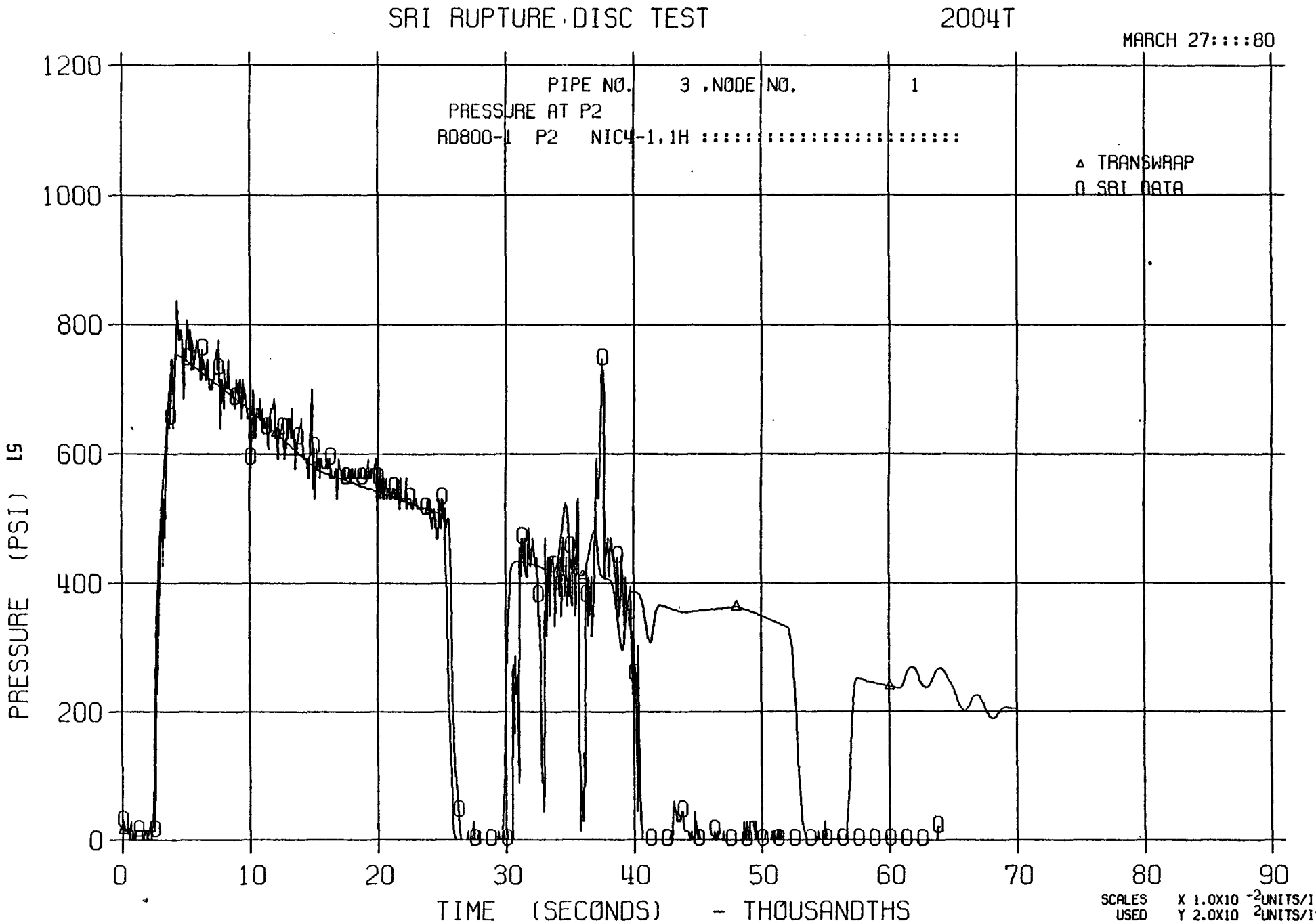

Figure 3.2.22, Comparison Between the TRANSWRAP II Prediction and SRI Test RD800-1

PL 2

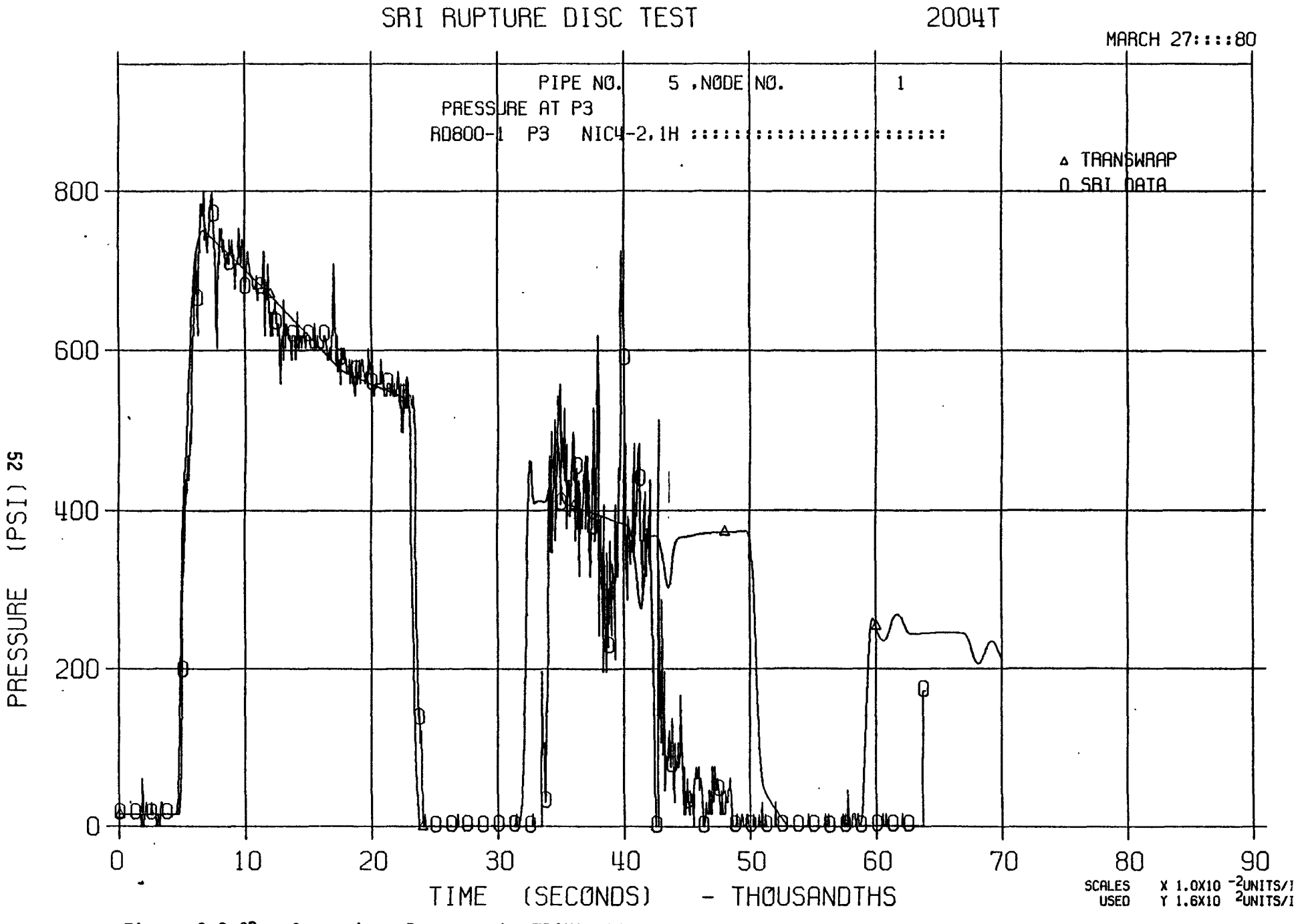

Figure 3.2.23, Comparison Between the TRANSWRAP II Prediction and SRI Test RD800-1

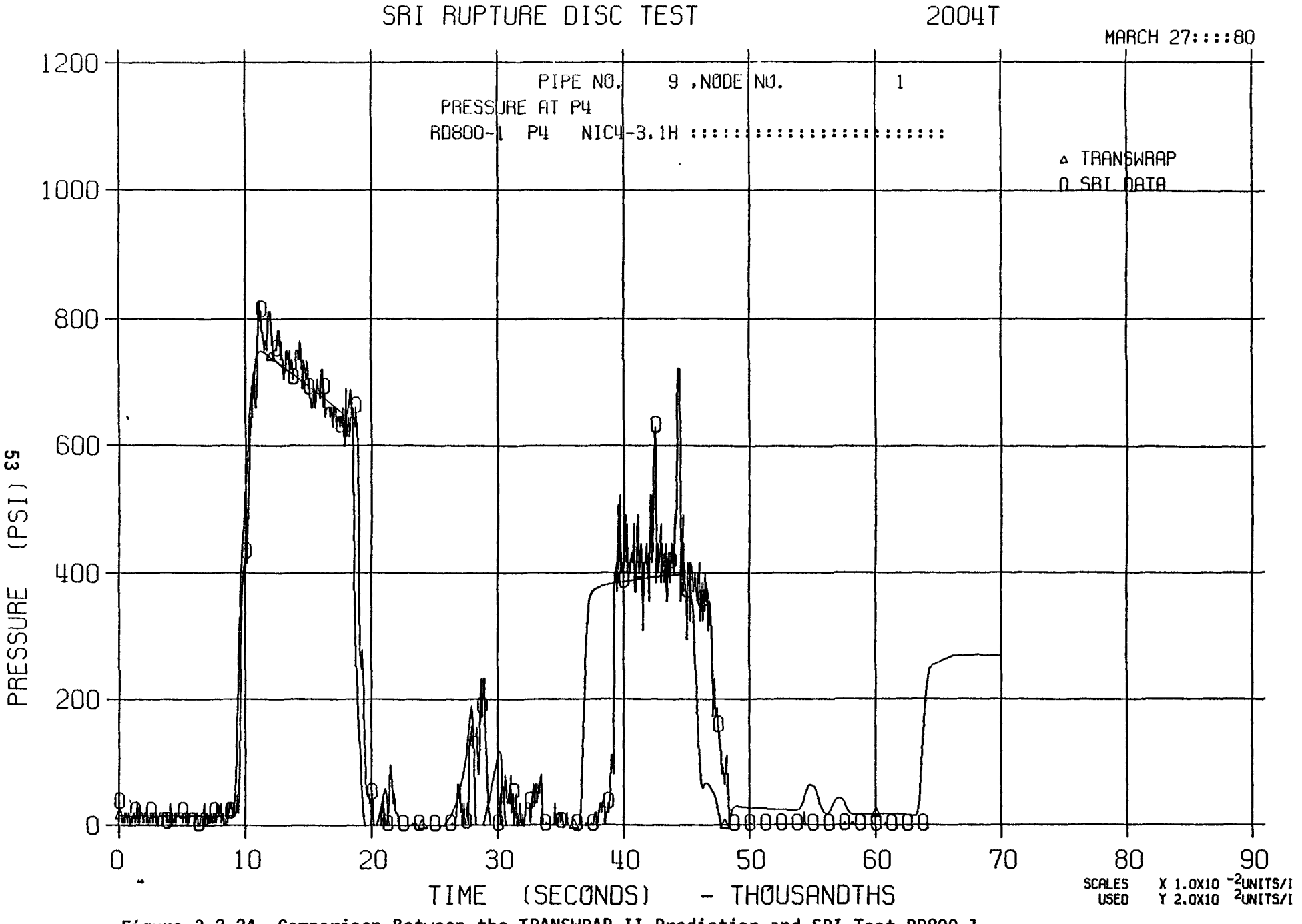

Figure 3.2.24, Comparison Between the TRANSWRAP II Prediction and SRI Test RD800-1

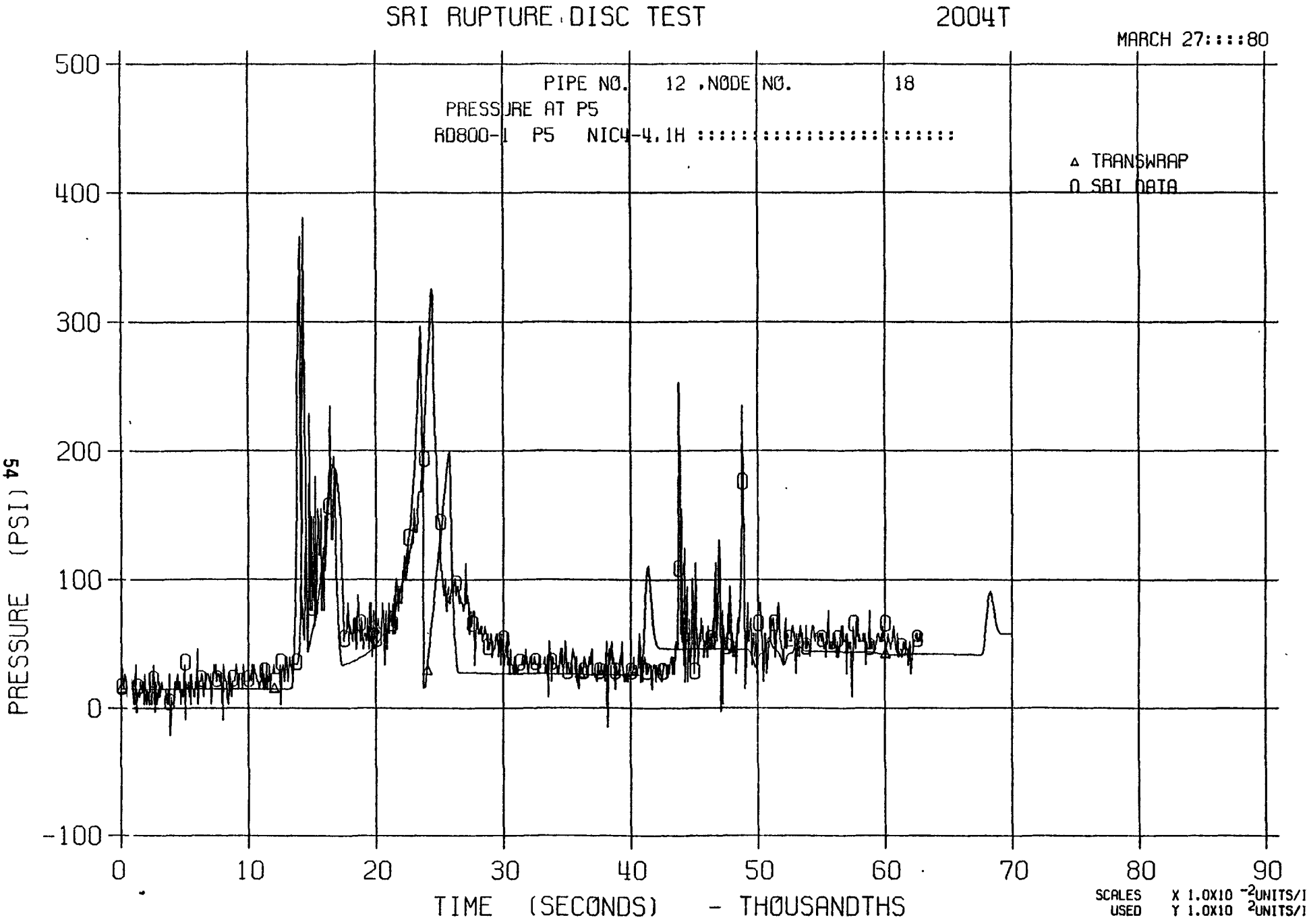

Figure 3.2.25, Comparison Between the TRANSWRAP II Prediction and SRI Test RD800-1

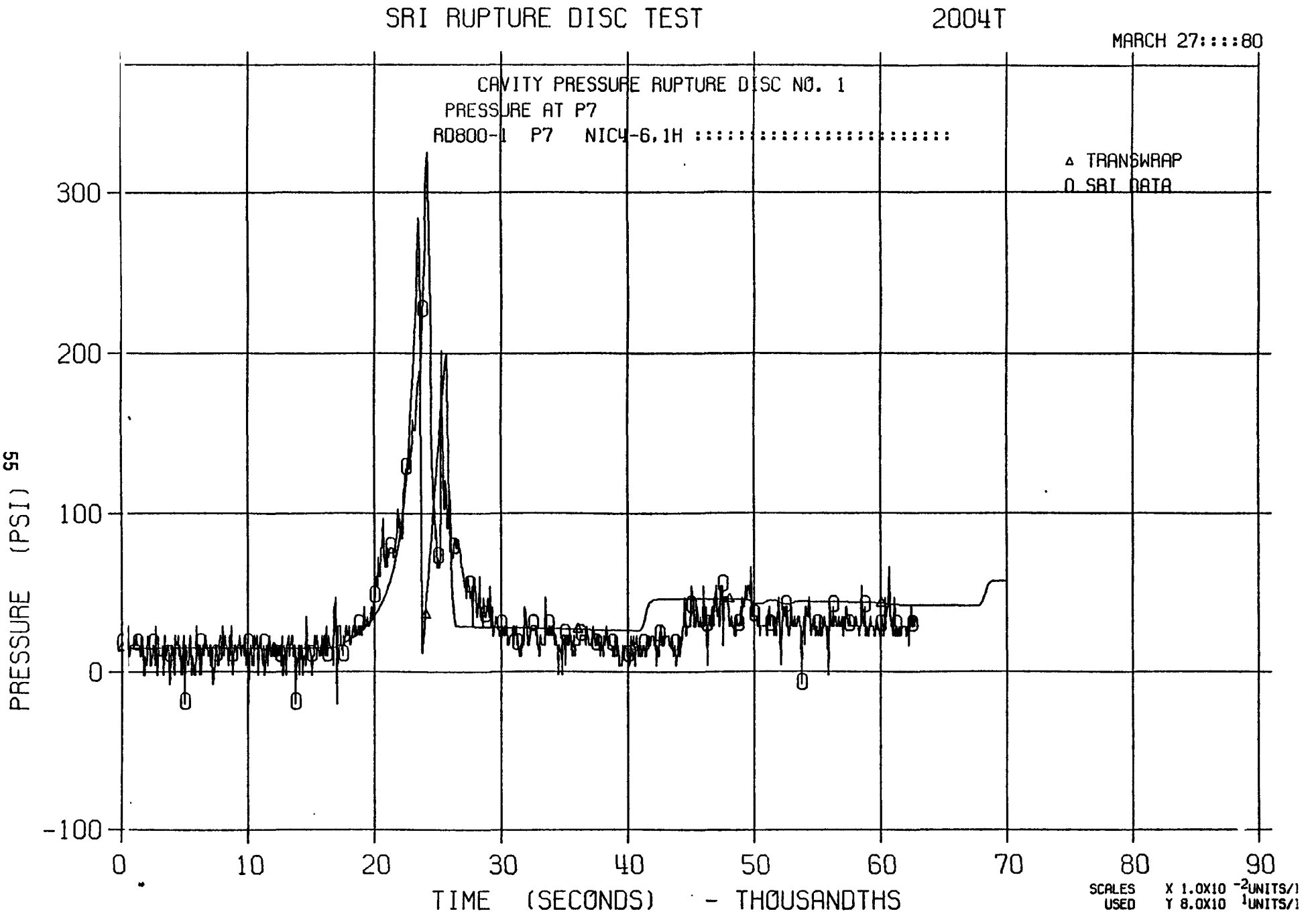

Figure 3.2.26, Comparison Between the TRANSWRAP II Prediction and SRI Test RD800-1

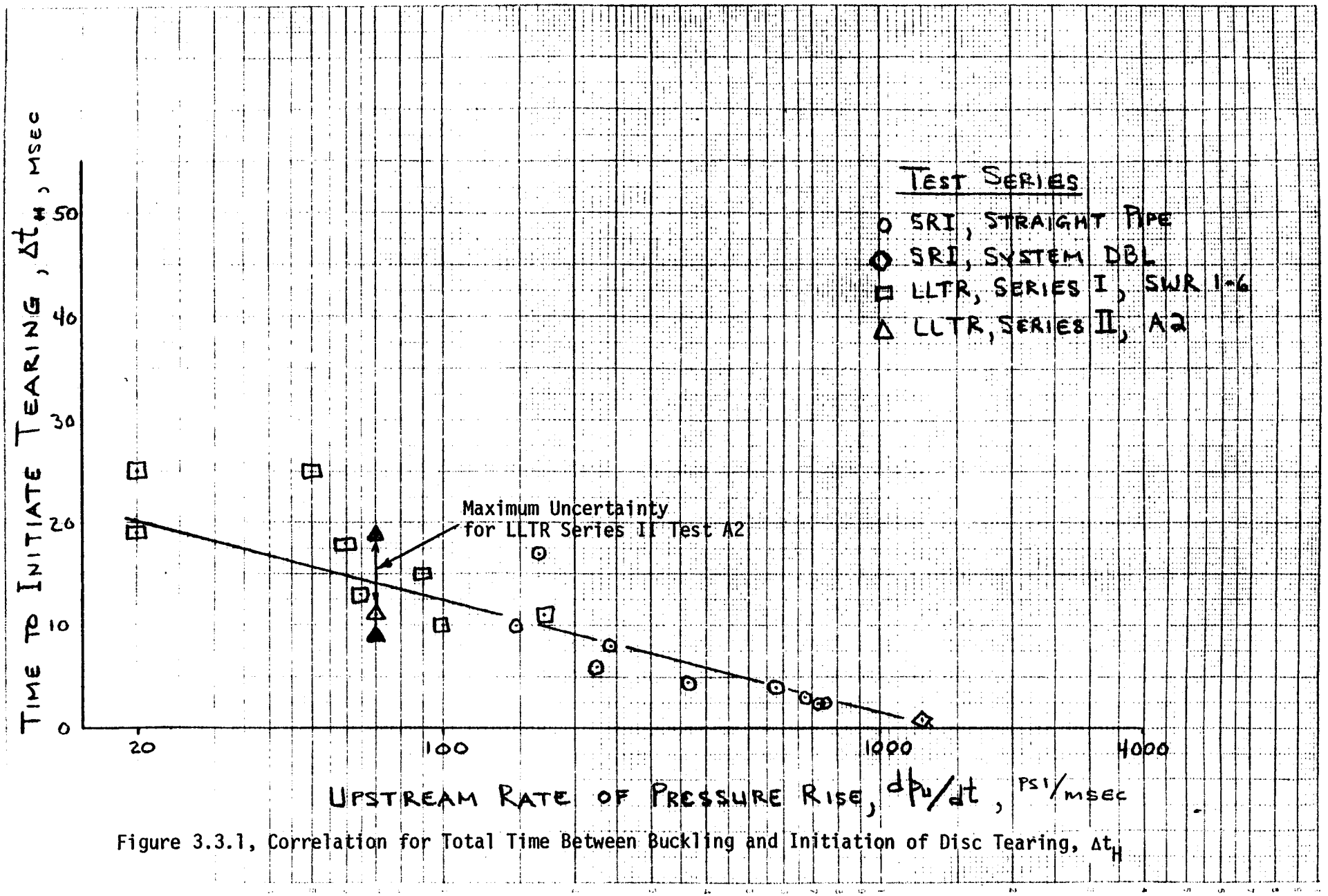

Figure 3.3.1, Correlation for Total Time Between Buckling and Initiation of Disc Tearing, Δt_H

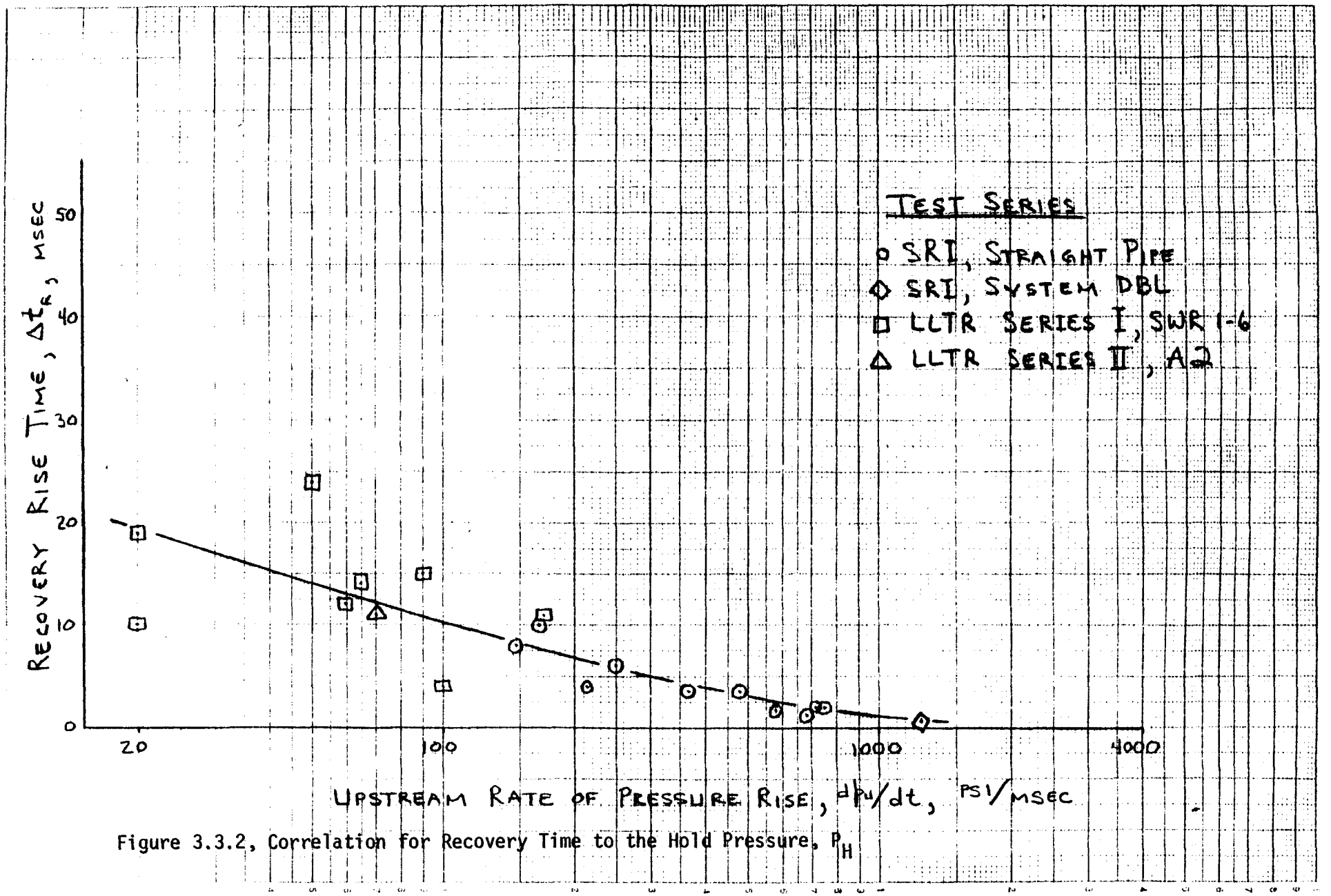

Figure 3.3.2, Correlation for Recovery Time to the Hold Pressure, P_H

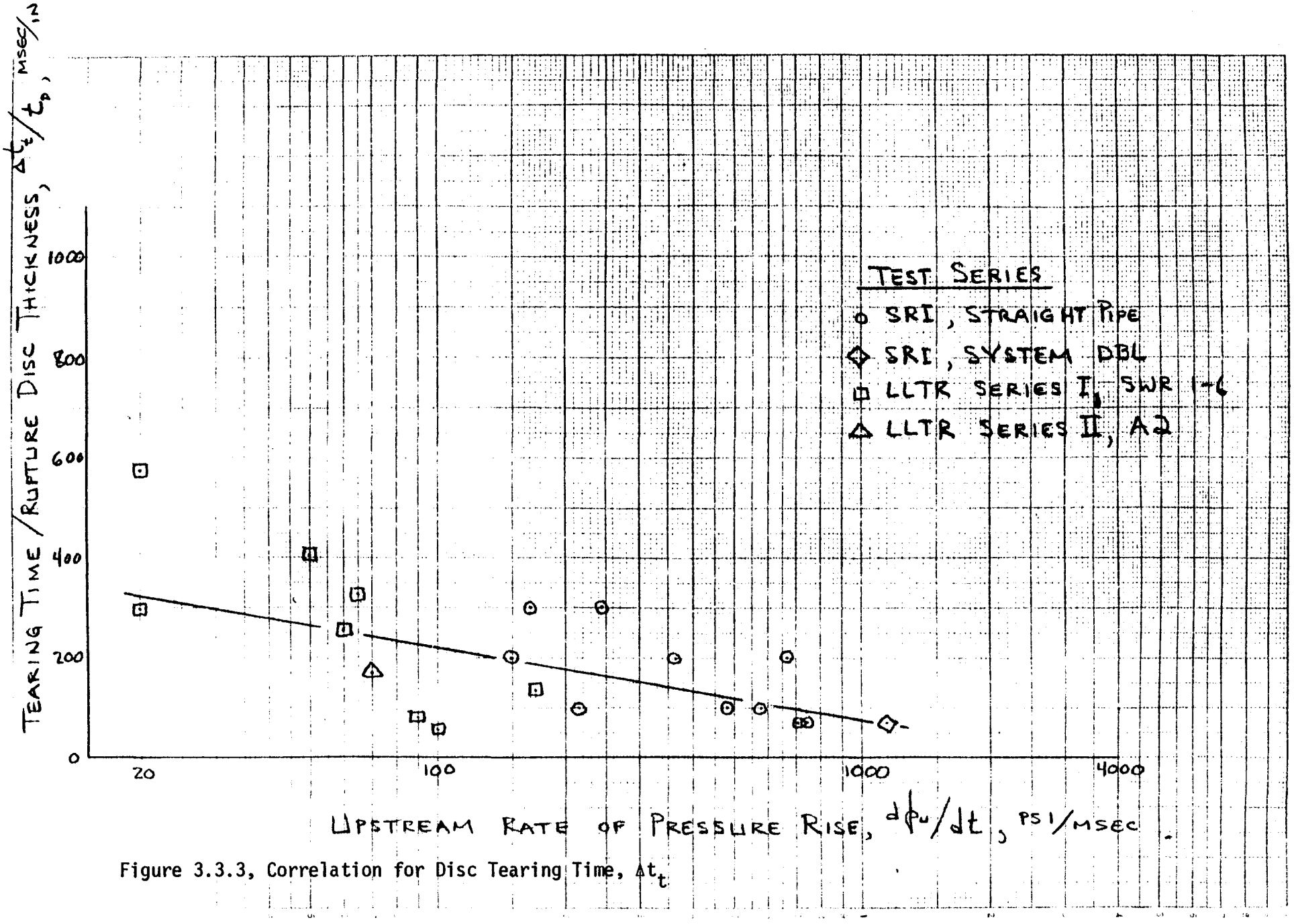

Figure 3.3.3, Correlation for Disc Tearing Time, Δt_t

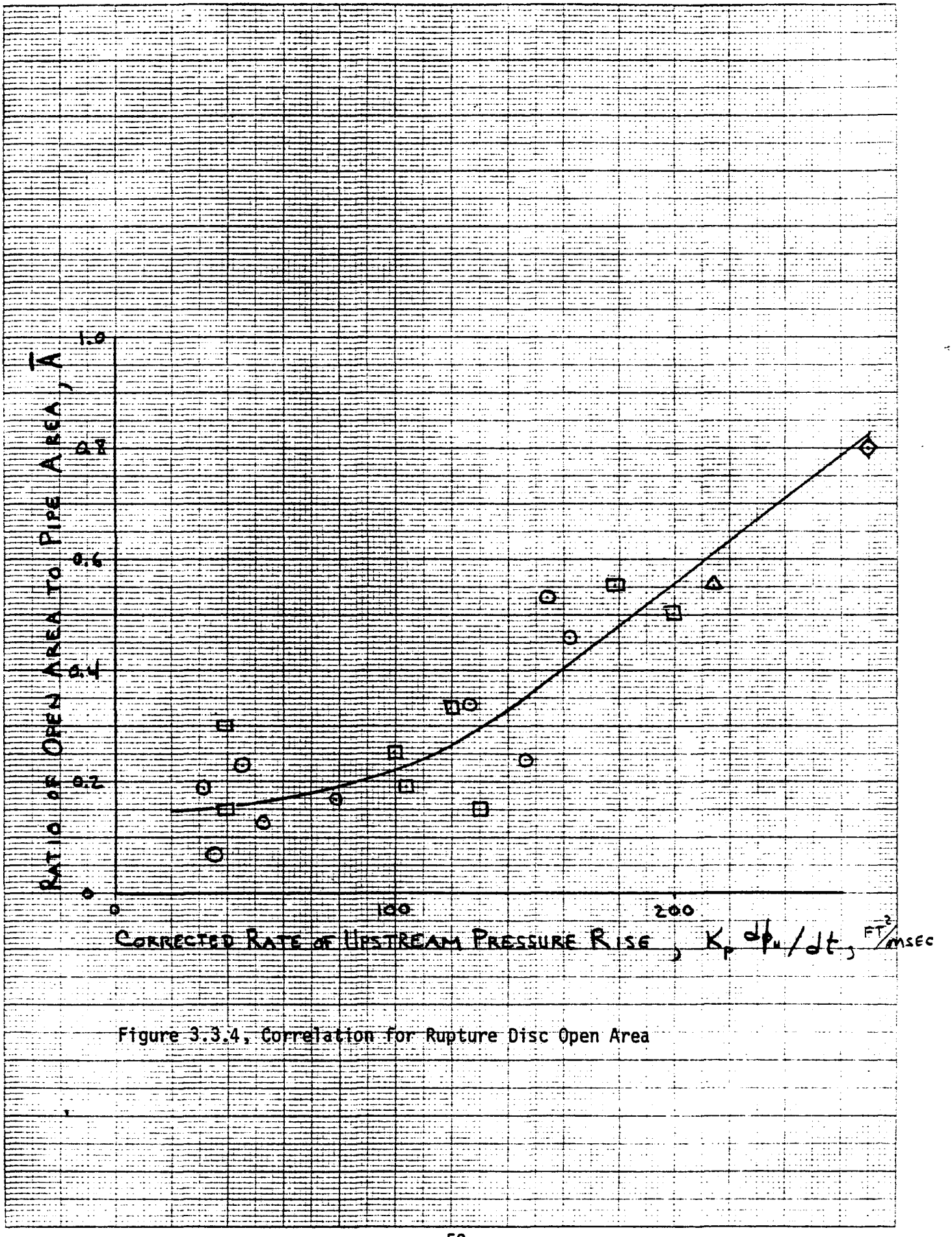

Figure 3.3.4, Correlation for Rupture Disc Open Area

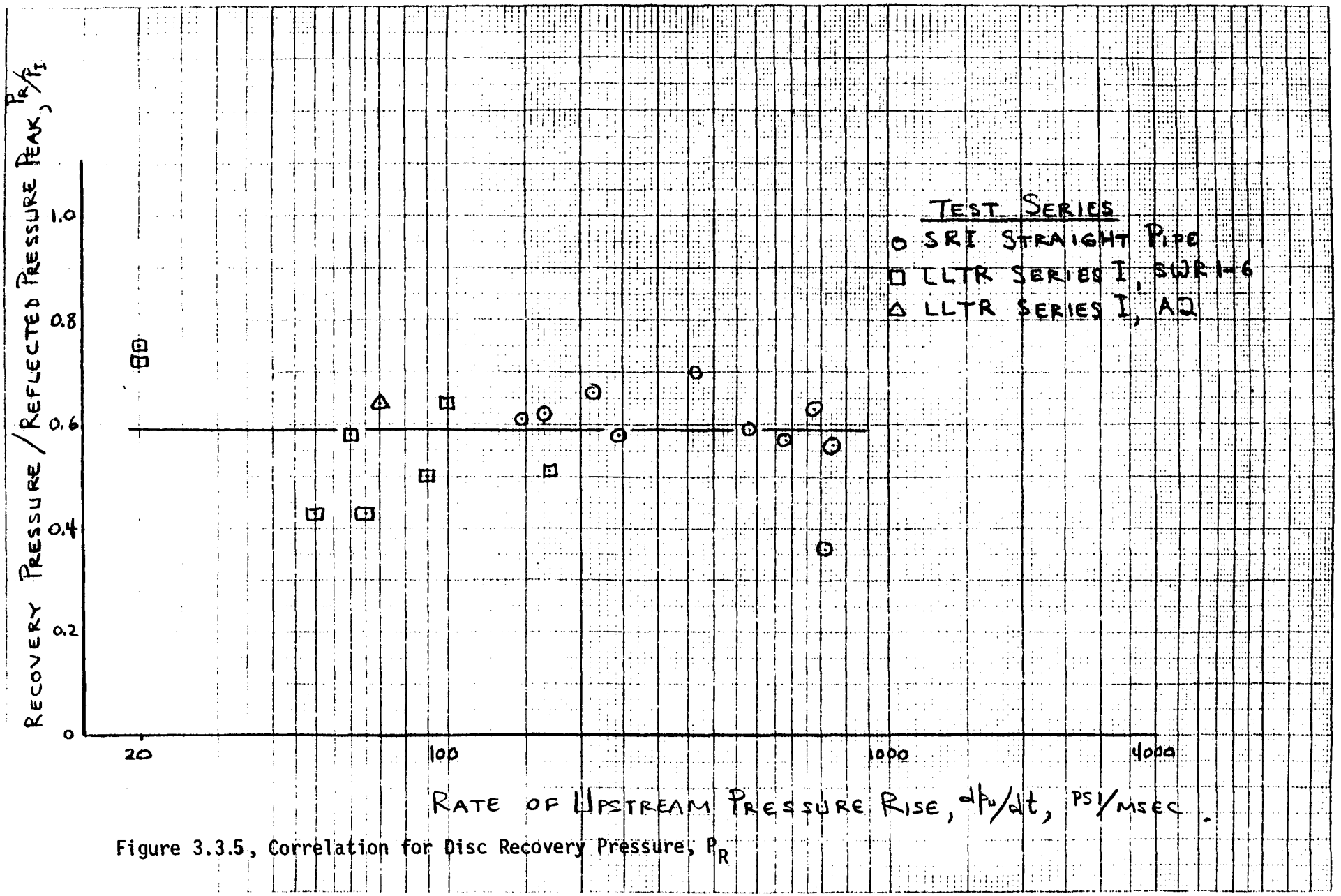

Figure 3.3.5, Correlation for Disc Recovery Pressure, P_R

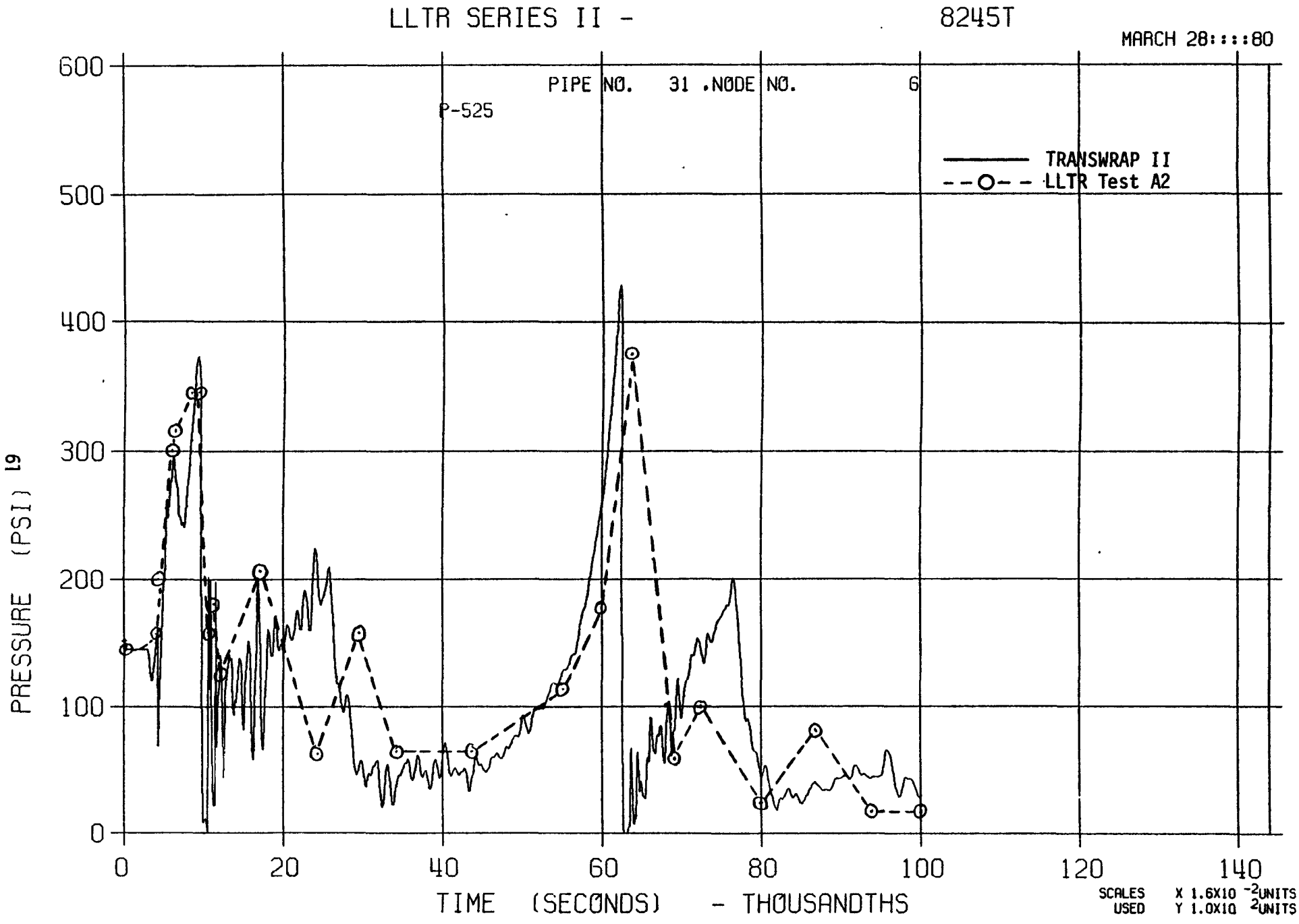

Figure 3.3.6, Comparison Between the TRANSWRAP II Prediction Using Rupture Disc Correlations and LLTR Series II Test A2.

Appendix A

Basic input data to TRANSWRAP which define the model and nominal test conditions are listed in Table A1. Source pressure and rupture disc data for the four tests selected for emphasis are listed separately in Table A2. Source pressures for three of these tests are shown in Figures A1 through A3.

TABLE A1 , BASIC TRANSWRAP INPUT DATA EXCLUSIVE OF SOURCE PRESSURE AND RUPTURE DISC DATA

```
11                                                                      CARD  1
0 999999. 999999. 999999.                                               CARD  2
00                                                                      CARD  3
    15.0    625.    62.4    41.5                                       CARD  4
                                                                        CARD  5
1                                                                       CARD  6
     .34     0.0     .33     0.0     .33     0.0                        CARD  7
                                                                        CARD  8
                                                                        CARD  9
                                                                        CARD 10
                                                                        CARD 11
     5.0     2.3     0.0                                                CARD 12
   0.001 0.00098           7.5                                          CARD 13
T190.                                                                   CONFLOW
***** SRI RUPTURE DISC TEST - SEPT 1979
***** TSS FILENAME /SRI/DBLRDM
  32  33   2   2   2   2  30  30   0   0   0                           CARD 16
       62.4        41.5     0.00006      0.0002       0.0       0.070 CARD 17
   0.000006       .00006        1.0         1.0       0.1       0.006 CARD 18
        0.0         0.0                                                CARD 19
   1   1   2  19         5.0     .2083       0.0      15.0      15.0
    4400.0     0.012
   2   2   3  19         5.0     .2083       0.0      15.0      15.0
    4400.0     0.012
   3   3   4  19         5.0     .2083       0.0      15.0      15.0
    4400.0     0.012
   4   4   5  19         5.0     .2083       0.0      15.0      15.0
    4400.0     0.012
   5   5   6  19         5.0     .2083       0.0      15.0      15.0
    4400.0     0.012
   6   6   7  19         5.0     .2083       0.0      15.0      15.0
    4400.0     0.012
   7   7   8  19         5.0     .2083       0.0      15.0      15.0
    4400.0     0.012
```

TABLE A1 , CONTINUED

8	8	9	19	5.0	.2083	0.0	15.0	15.0
4400.0			0.012					
9	9	10	19	5.0	.2083	0.0	15.0	15.0
4400.0			0.012					
10	10	11	19	5.0	.2083	0.0	15.0	15.0
4400.0			0.012					
11	11	12	19	5.0	.2083	0.0	15.0	15.0
4400.0			0.012					
12	12	13	19	5.0	.2083	0.0	15.0	15.0
4400.0			0.012					
13	0	0	3	0.555	.2083	0.0	15.0	15.0
4400.0			0.012					
14	0	0	3	0.555	.2083	0.0	15.0	15.0
4400.0			0.012					
15	0	0	3	0.555	.2083	0.0	15.0	15.0
4400.0			0.012					
16	0	0	3	0.555	.2083	0.0	15.0	15.0
4400.0			0.012					
17	0	0	3	0.555	.2083	0.0	15.0	15.0
4400.0			0.012					
18	0	0	3	0.555	.2083	0.0	15.0	15.0
4400.0			0.012					
19	0	0	3	0.555	.2083	0.0	15.0	15.0
4400.0			0.012					
20	21	20	3	0.555	10.0	0.0	15.0	15.0
4400.0			0.012					
21	22	21	3	0.555	10.0	0.0	15.0	15.0
4400.0			0.012					
22	23	22	3	0.555	10.0	0.0	15.0	15.0
4400.0			0.012					
23	24	23	3	0.555	10.0	0.0	15.0	15.0
4400.0			0.012					
24	0	0	3	0.555	10.0	0.0	15.0	15.0
4400.0			0.012					
25	0	0	3	0.555	10.0	0.0	15.0	15.0
4400.0			0.012					
26	0	0	3	0.555	10.0	0.0	15.0	15.0
4400.0			0.012					

TABLE A1 , CONTINUED

27	0	0	3	0.555	10.0	0.0	15.0	15.0
	4400.0		0.012					
28	0	0	3	0.555	10.0	0.0	15.0	15.0
	4400.0		0.012					
29	0	0	3	0.555	10.0	0.0	15.0	15.0
	4400.0		0.012					
30	0	0	3	0.555	10.0	0.0	15.0	15.0
	4400.0		0.012					
1	1		16					
2	1	2	10					
3	2	3	10					
4	3	4	10					
5	4	5	10					
6	5	6	10					
7	6	7	10					
8	7	8	10					
9	8	9	10					
10	9	10	10					
11	10	11	10					
12	11	12	10					
13	12		14					
14			10					
15			10					
16			10					
17			10					
18			10					
19			10					
20	20		15	10000.0	34.0			
21	21	20	10					
22	22	21	10					
23	23	22	10					
24	23		18	100.0	34.0			
25			13		34.0			
26			13		34.0			
27			13		34.0			
28			13		34.0			
29			13		34.0			
30			13		34.0			

TABLE A1 , CONTINUED

```
$CKKIN CKKI(3,20) = 10000.0, CKKI(3,24) = 100.0 $
          3          20                                                    CARD 61
         20         1.4  939470.          .559        15.0                CARD 62
         24         1.4  939470.          .559        15.0                CARD 62
        169         1.4  939470.          .559        15.0                CARD 62
    1     1     4    20     3    20     3     4                            CARD 63
  110    70                                                                CARD 64
        0.0        15.0         1.0         70.         1.0      .0001 CARD 65
       3.8        .2396         1.3         .01        .2396       1.3CARD 66
    5000.0         20.0        10.0        .2396      5000.0       20.0CARD 67
      10.0        .2396                                                  CARD 67
       1.0         12.0         0.0         0.0         0.0        .375CARD 68
      0.5          0.5          0.0         0.0         0.0         0.6  CARD 69
     15.0   1500.0                                                        CARD 70
        20         30         20         30         25         24        CARD 71
        20                                                               CARD 72
     3194.      .0012         0.       41.5       62.4  0.001805      .0341 CARD 74
    9000.       4400.     2160.0   264960.       623.       860.         CARD 75
         1         -1                                  1                 CARD 76
    200. 99999. 99999. 99999. 99999. 99999. 99999. 99999. 99999. 99999. CARD 77
  31 170   1 170 170  31 170   1 170 170  30  30                         CARD 78
  12 170 170 170 170 170 170 170 170 170                                 CARD 79
  23 170 170 170 170 170 170 170 170 170                                 CARD 80
  13 170 170 170 170 170 170 170 170 170                                 CARD 81
  24 170 170 170 170 170 170 170 170 170                                 CARD 82
FT                                                                       CARD 84
                                                                         CARD 85
 0 0 0 0 0 0 0 0 0 0 0 0 1 1 1 1 1 1 1 1 1 1 1 1 1 1 1 1 1 0 0          CARD 86
 0 0 0 0 0 0 0 0 0 0 0 0 0 0 1 1 1 1 1 1 0 1 1 1 1 1 1 1 1 1 0 0 0      CARD 87
         0.0      0.00017          0.5   0                              CARD 89
SRI RUPTURE DISC TEST
TT                                                                       CARD 91
  2  4  3  0  1  0  1  0  0  0  0  0                                      CARD 92
 PRESSURE AT P2
 PRESSURE AT P3
 PRESSURE AT P4
 PRESSURE AT P5
 PRESSURE AT P7
 VELOCITY AT P1
```

TABLE A1 , CONTINUED

```
VELOCITY AT P2
VELOCITY AT P3
DISPLACEMENT AT RD1
 3  1  5  1  9  1 12 18                                          CARD 93
 3  1  5  1 12 18                                                CARD 94
    1                                                           CARD 95
          1.          0.5         0.1         0.0               CARD 96
```

TABLE A2 , SOURCE PRESSURE AND RUPTURE DISC INPUT DATA FOR TESTS
RD150-1 , RD400-3 , RD600-4 , RD800-1

RD150-1 SOURCE PRESSURE (INSERTED AFTER CARD 72)

```
 600.0      0.0075         10
   0.0      0.0002     0.0003      0.0005      0.0014      0.0020
0.0075      0.0130     0.0675      0.0800
  15.0        35.0      265.0       415.0       715.0       755.0
 670.0       575.0      200.0       200.0
```

RD150-1 RUPTURE DISC INPUT DATA (INSERTED AFTER CARD 82)

```
  2
15.         15.         .0057       1.4
2.5         .0059       3.15     E07 .29        467.4       2.15        CARD 83
0.4         .0040       .12          .0001     10 .01                  CARD 83
2.5         .0059       3.15     E07 .29        467.4       2.15        CARD 83
0.4         .0040       .12          .0001     10 .01                  CARD 83
```

RD400-3 SOURCE PRESSURE (INSERTED AFTER CARD 72)

```
 600.0      0.0075          8
   0.0      0.0003     0.0005      0.0028      0.0075      0.0275
0.0675      0.0800
  15.0        35.0      215.0       395.0       365.0       275.0
 210.0       210.0
```

RD400-3 RUPTURE DISC INPUT DATA (INSERTED AFTER CARD 82)

```
  2
15.         15.         .0057       1.4
2.5         .0059       3.15     E07 .29        467.4       2.15        CARD 83
0.4         .0030       .23          .0001     10 .004                 CARD 83
2.5         .0059       3.15     E07 .29        467.4       2.15        CARD 83
0.4         .0030       .23          .0001     10 .004                 CARD 83
```

TABLE A2 , CONTINUED

RD600-4 SOURCE PRESSURE (INSERTED AFTER CARD 72)

```
 600.0      0.0075         10
   0.0      0.0003     0.0007      0.0028      0.0041      0.0074
0.0190      0.0290     0.0675      0.0800
  15.0        45.0      415.0       620.0       575.0       500.0
 425.0       325.0      260.0       260.0
```

RD600-4 RUPTURE DISC INPUT DATA (INSERTED AFTER CARD 82)

```
   2
15.         15.          .0057       1.4
2.5         .0059        3.15     E07 .29        467.4       2.15        CARD 83
0.4         .0020        .35         .0001       10 .003                 CARD 83
2.5         .0059        3.15     E07 .29        467.4       2.15        CARD 83
0.4         .0020        .35         .0001       10 .003                 CARD 83
```

RD800-1 SOURCE PRESSURE (INSERTED AFTER CARD 72)

```
 600.0      0.0075         10
   0.0      0.0002     0.0003      0.0005      0.0014      0.0020
0.0075      0.0130     0.0675      0.0800
  15.0        35.0      265.0       415.0       715.0       755.0
 670.0       575.0      200.0       200.0
```

RD800-1 RUPTURE DISC INPUT DATA (INSERTED AFTER CARD 82)

```
   2
15.         15.          .0057       1.4
2.5         .0059        3.15     E07 .29        467.4       2.15        CARD 83
0.4         .0010        .47         .0001       10 .002                 CARD 83
2.5         .0059        3.15     E07 .29        467.4       2.15        CARD 83
0.4         .0010        .47         .0001       10 .002                 CARD 83
```

FIGURE A1, SOURCE PRESS. AND RD150-1 P2

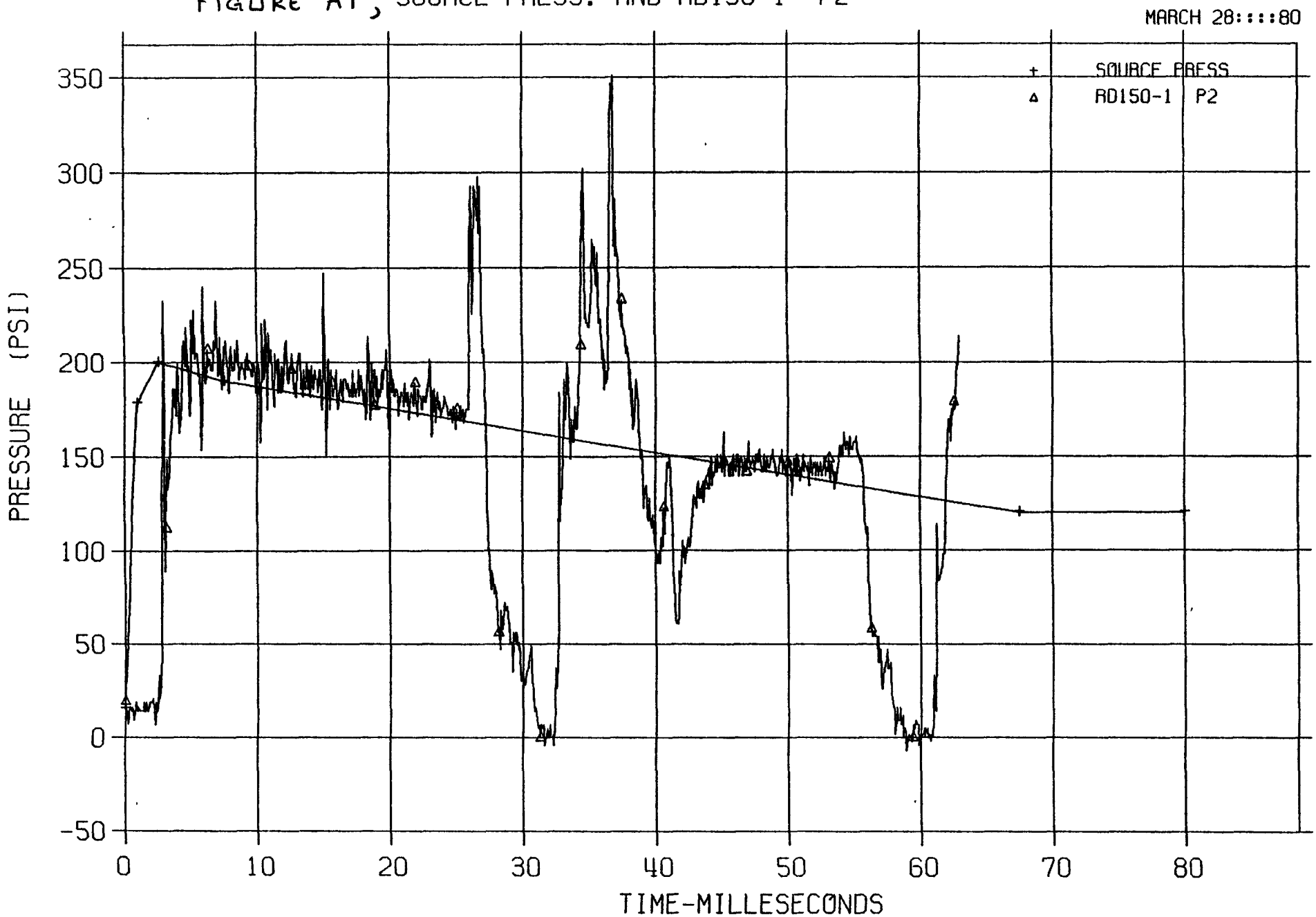

PL 1

FIGURE A2, SOURCE PRESS. AND RD400-3 P2

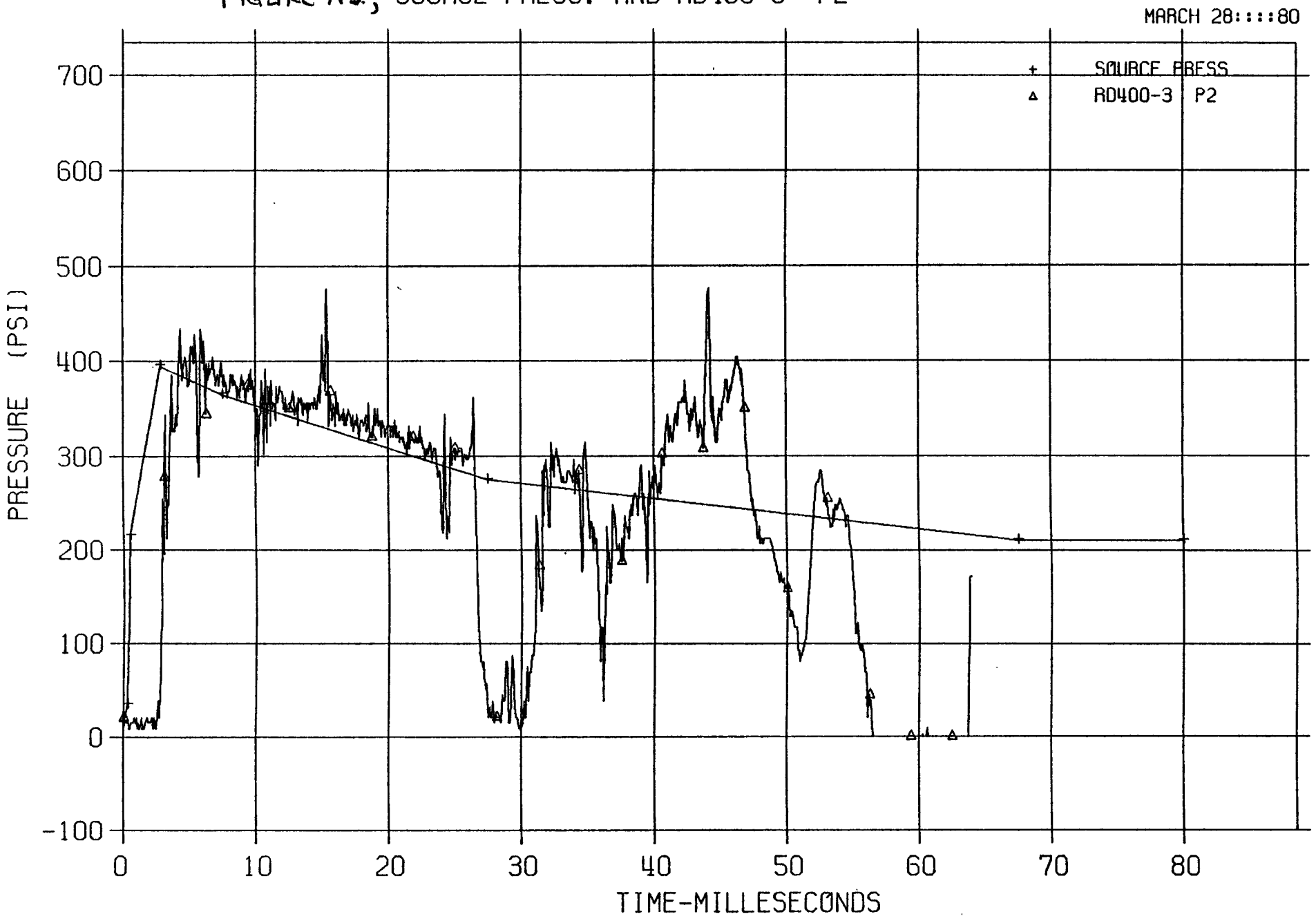

FIGURE A3, SOURCE PRESS. AND RD800-1 P2

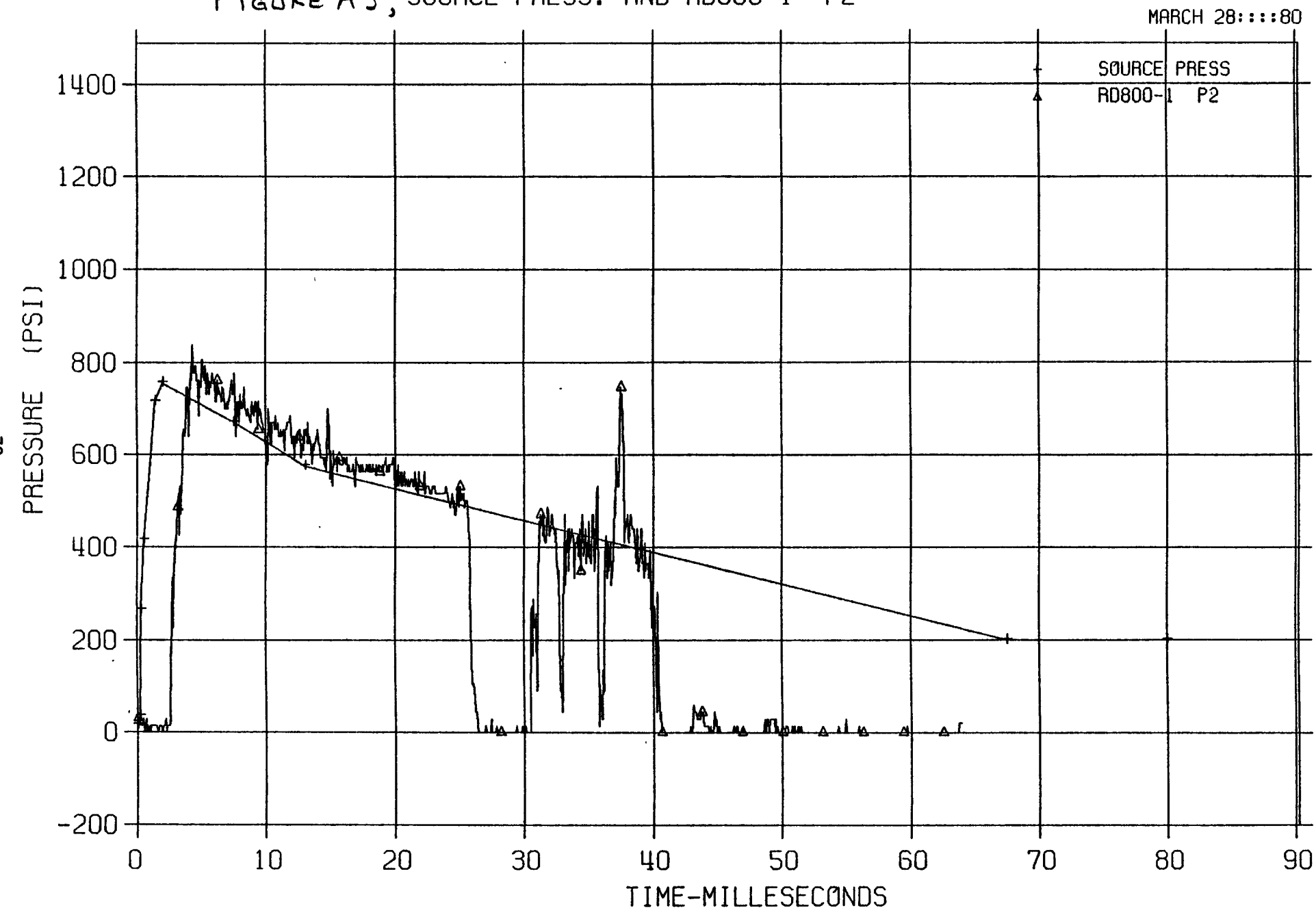

72

L 1

Appendix B

Supplemental comparisons which demonstrate the degree of repeatability achieved in the experiment and analysis are shown in Figures B1 through B. For the most part the agreement is very good with the following exceptions. At a source pressure level of 90 psi a slight compression and rarefaction are reflected to the source indicating that some buckling of the upstream disc may have occurred. Post test examination of the disc indicated no apparent damage so the buckling must have been elastic and was probably due to local imperfections in that particular disc. Note that this did not occur at the higher source pressure of 125 psi. No reason could be found for the premature buckling of the second disc in test RD200-5 predicted by TRANSWRAP except possibly that cavitation effects were predicted in the analysis and were not experienced in the test. These apparent anomolies are currently undergoing further study.

FIGURE B1, SRI RUPTURE DISC TEST, RD 50-2 8087T

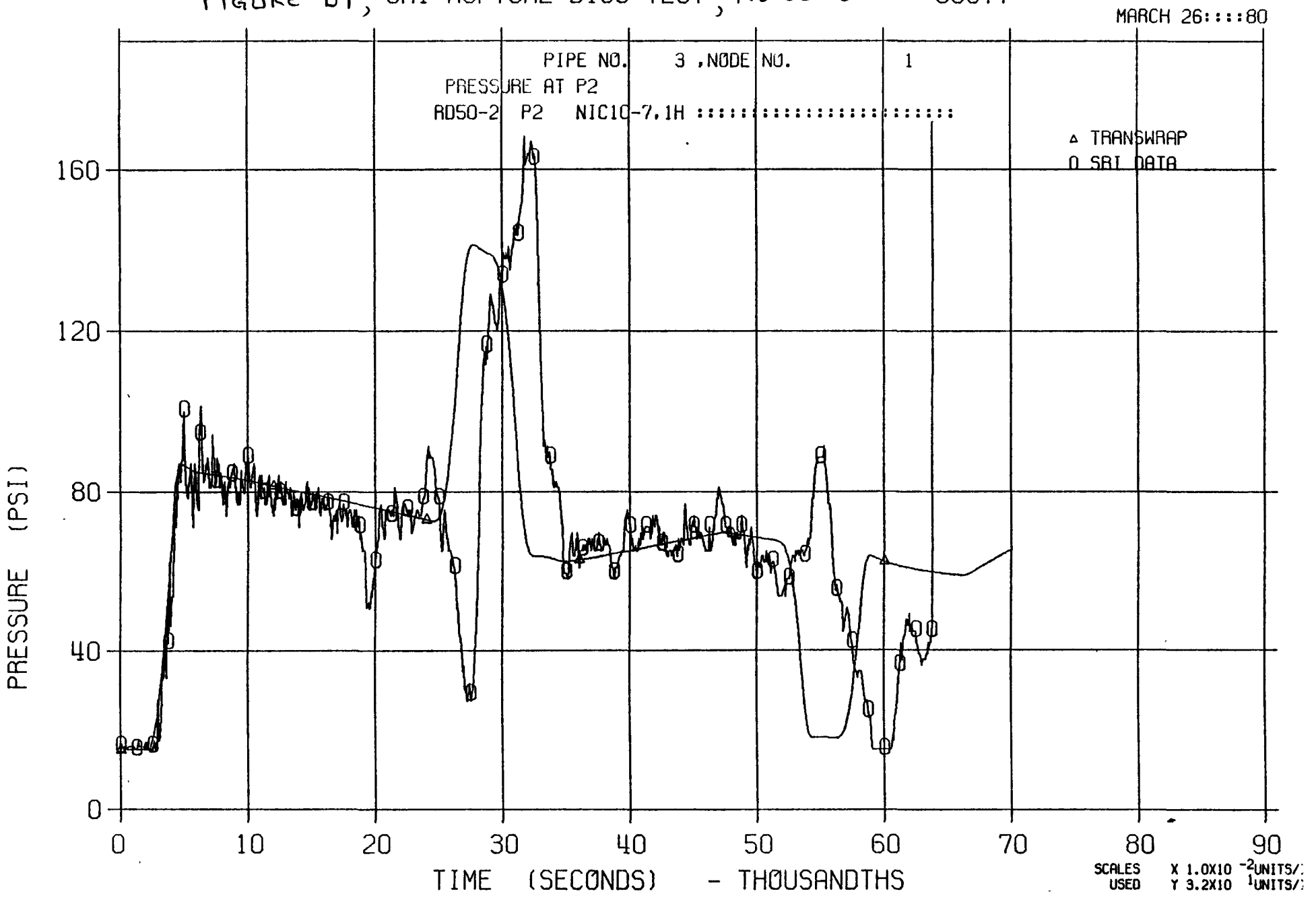

PL 2

FIGURE B2, SRI RUPTURE DISC TEST, RD 50-2 8087T

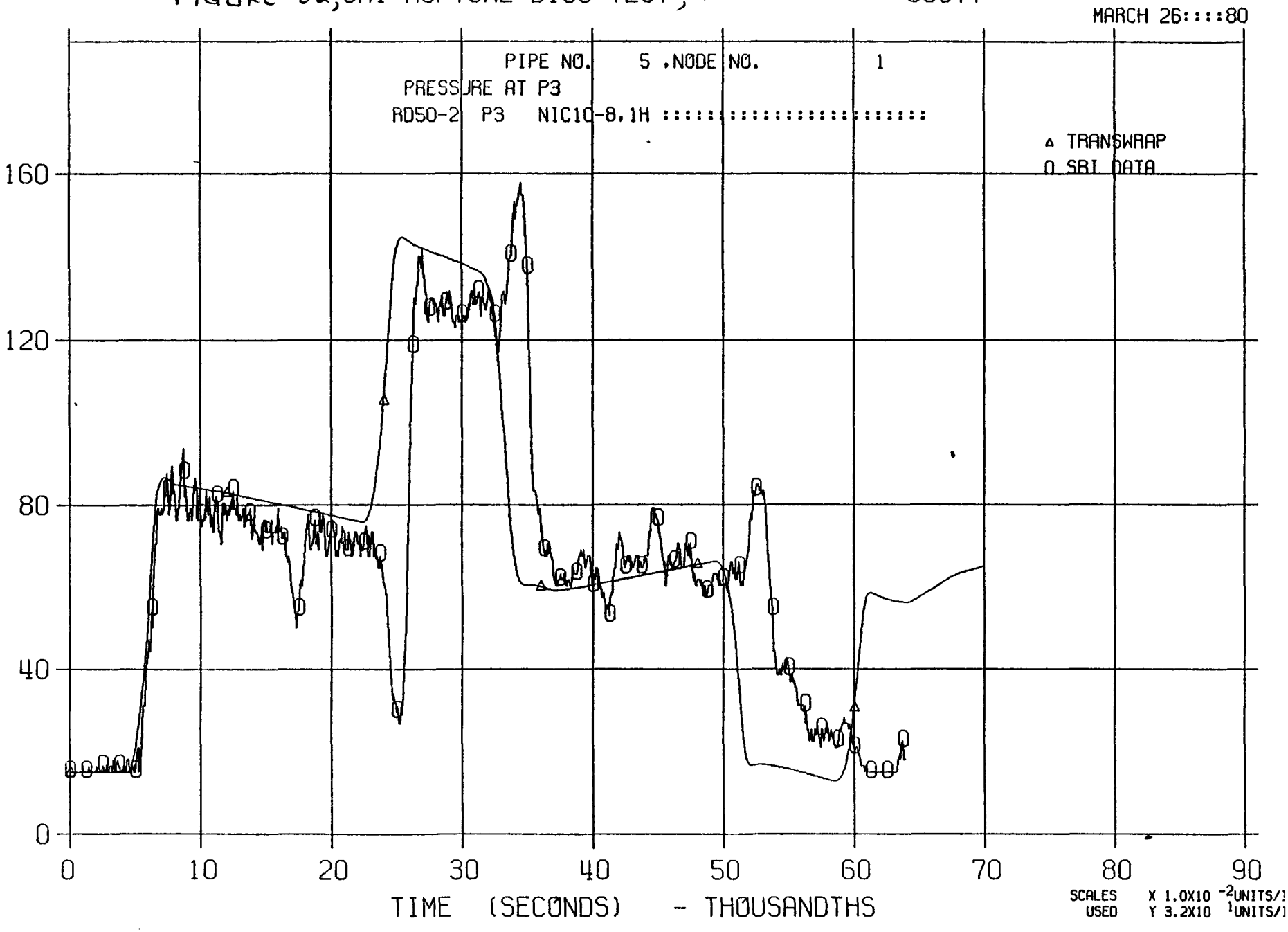

PL 3

FIGURE B3, SRI RUPTURE DISC TEST, RD 50-2 8087T

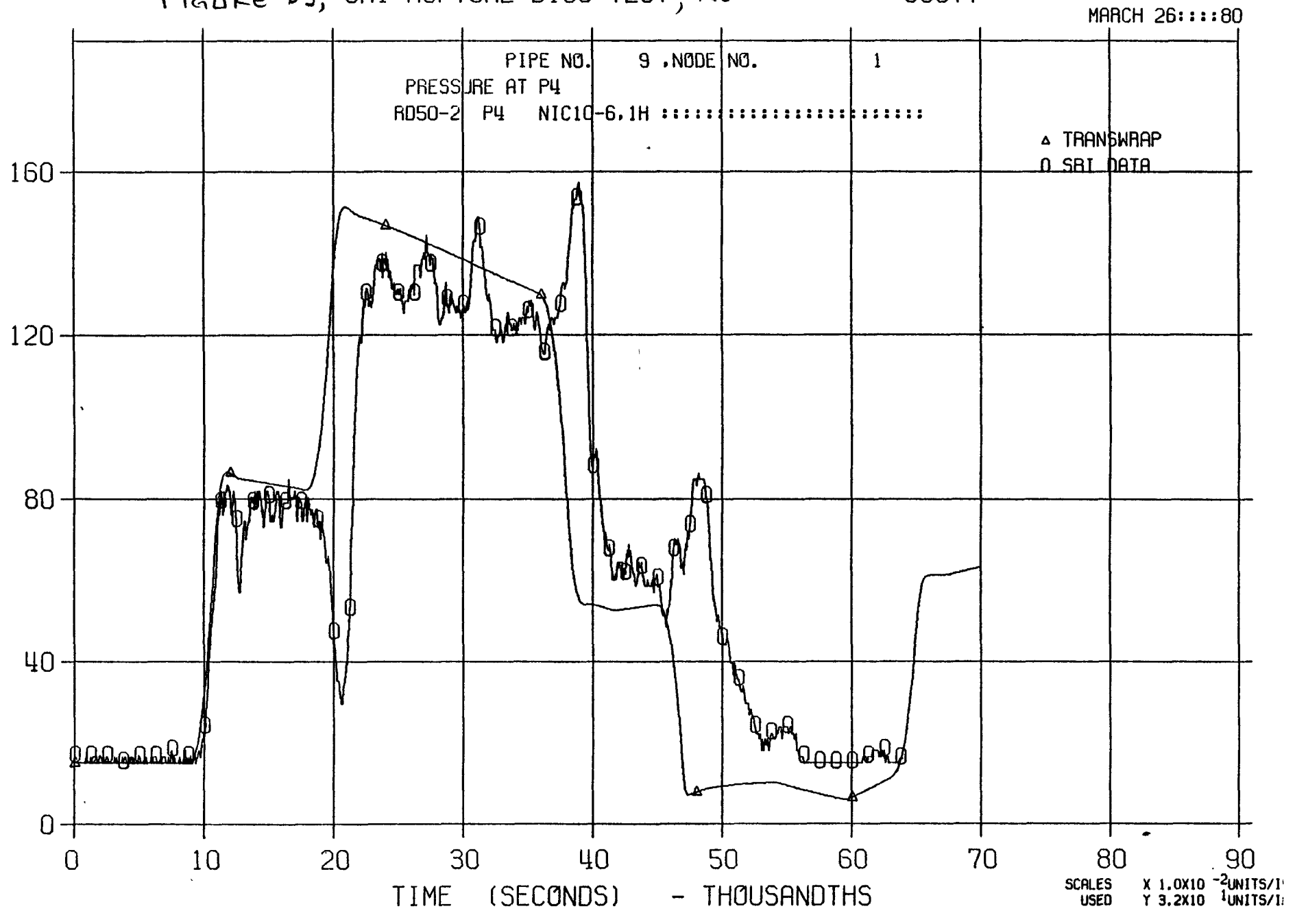

PL 4

FIGURE B4, SRI RUPTURE DISC TEST, RD 50-2 8087T

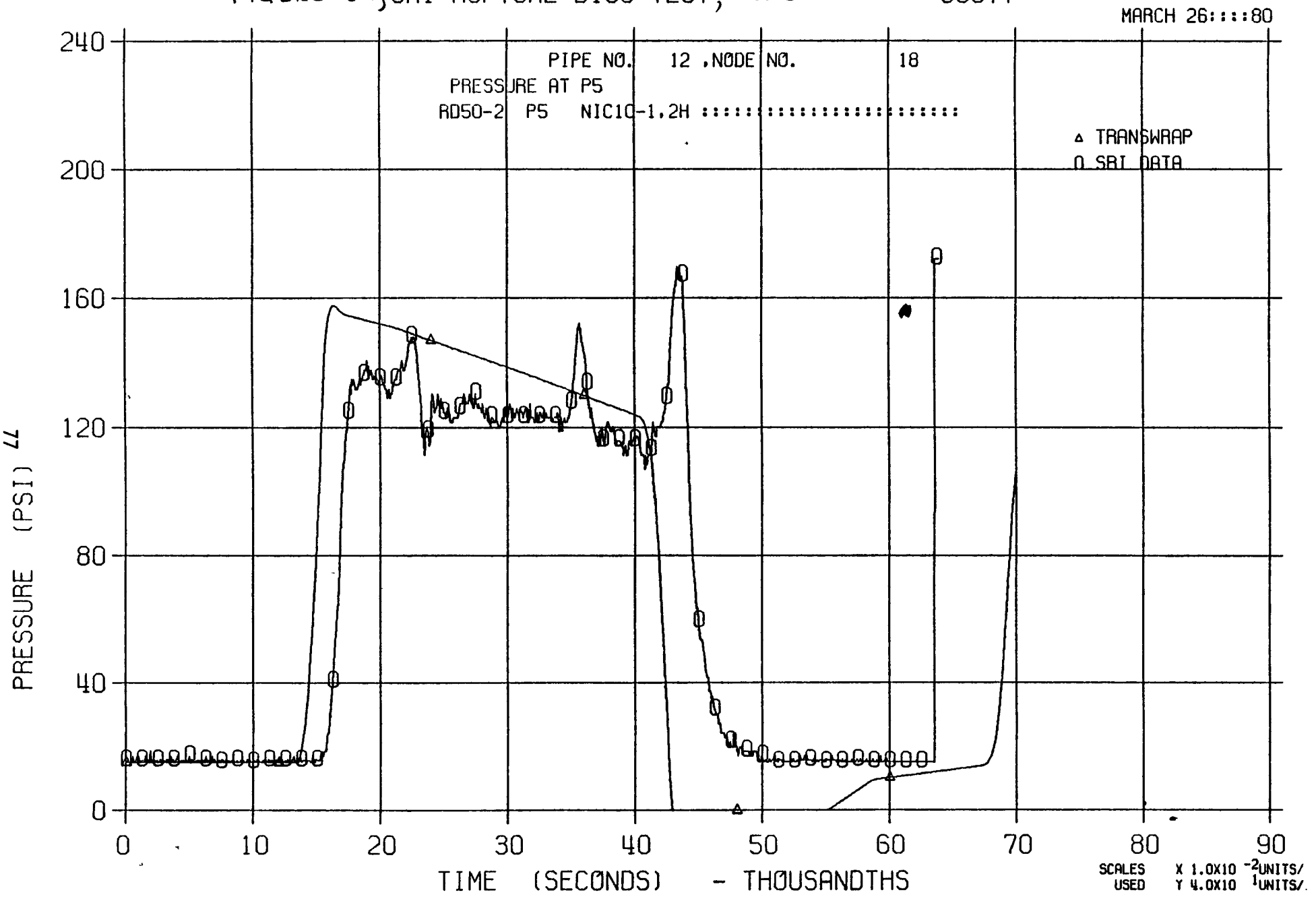

PL 5

FIGURE B5, SRI RUPTURE DISC TEST, RD 50-2 2062T

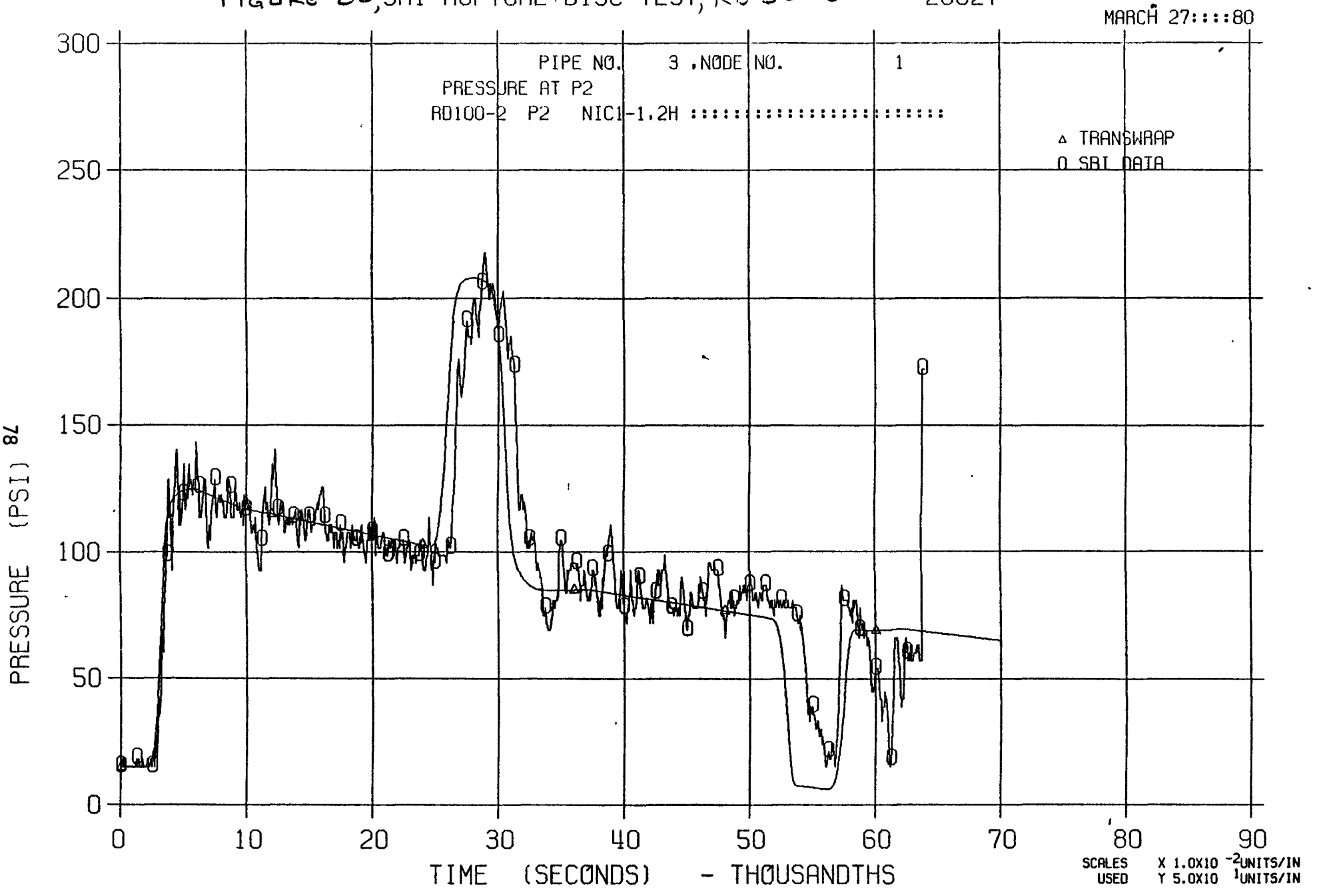

FIGURE B6, SRI RUPTURE DISC TEST, RD 100-2 2062T

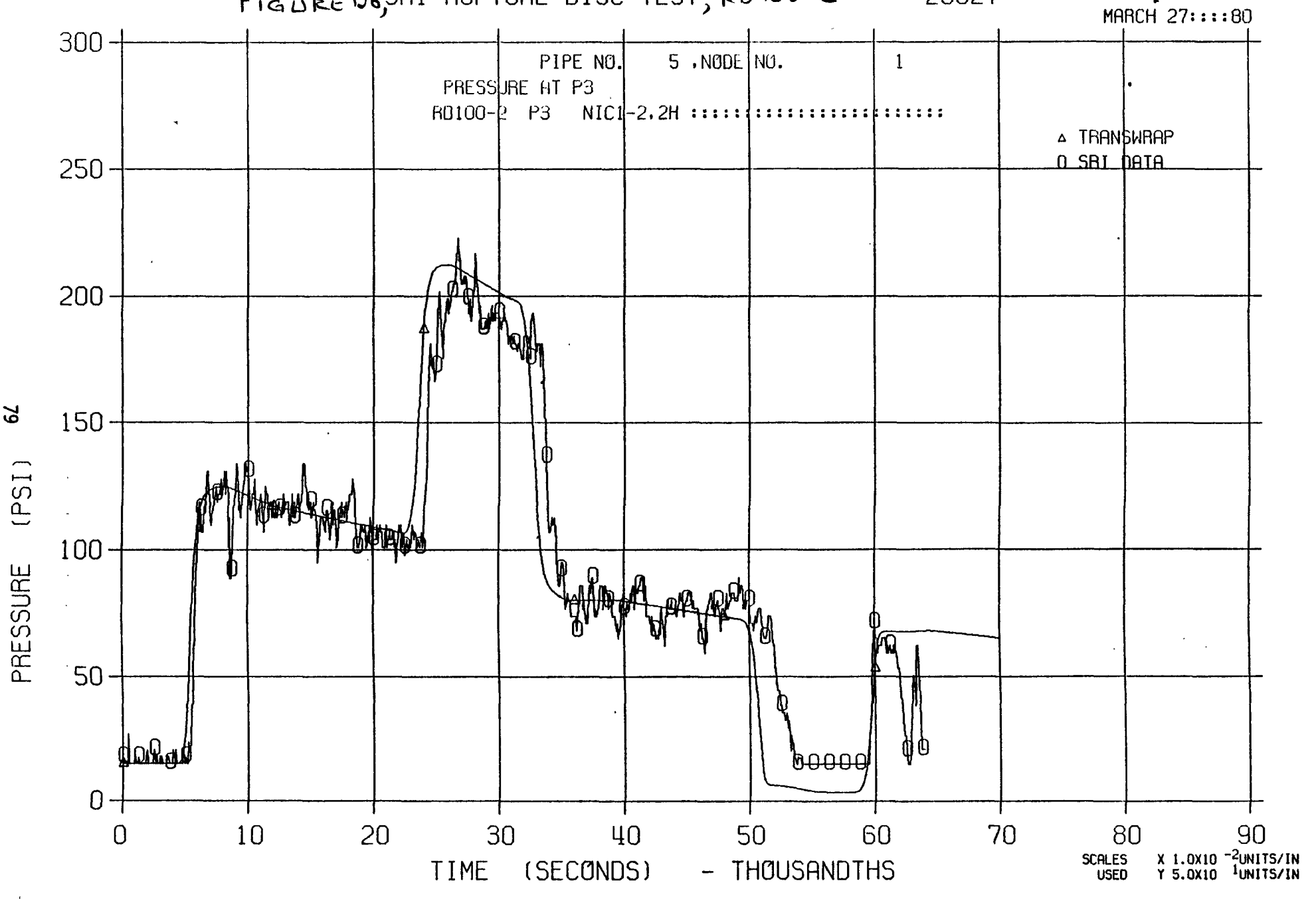

FIGURE B7, SRI RUPTURE DISC TEST, RD 100-2 2062T

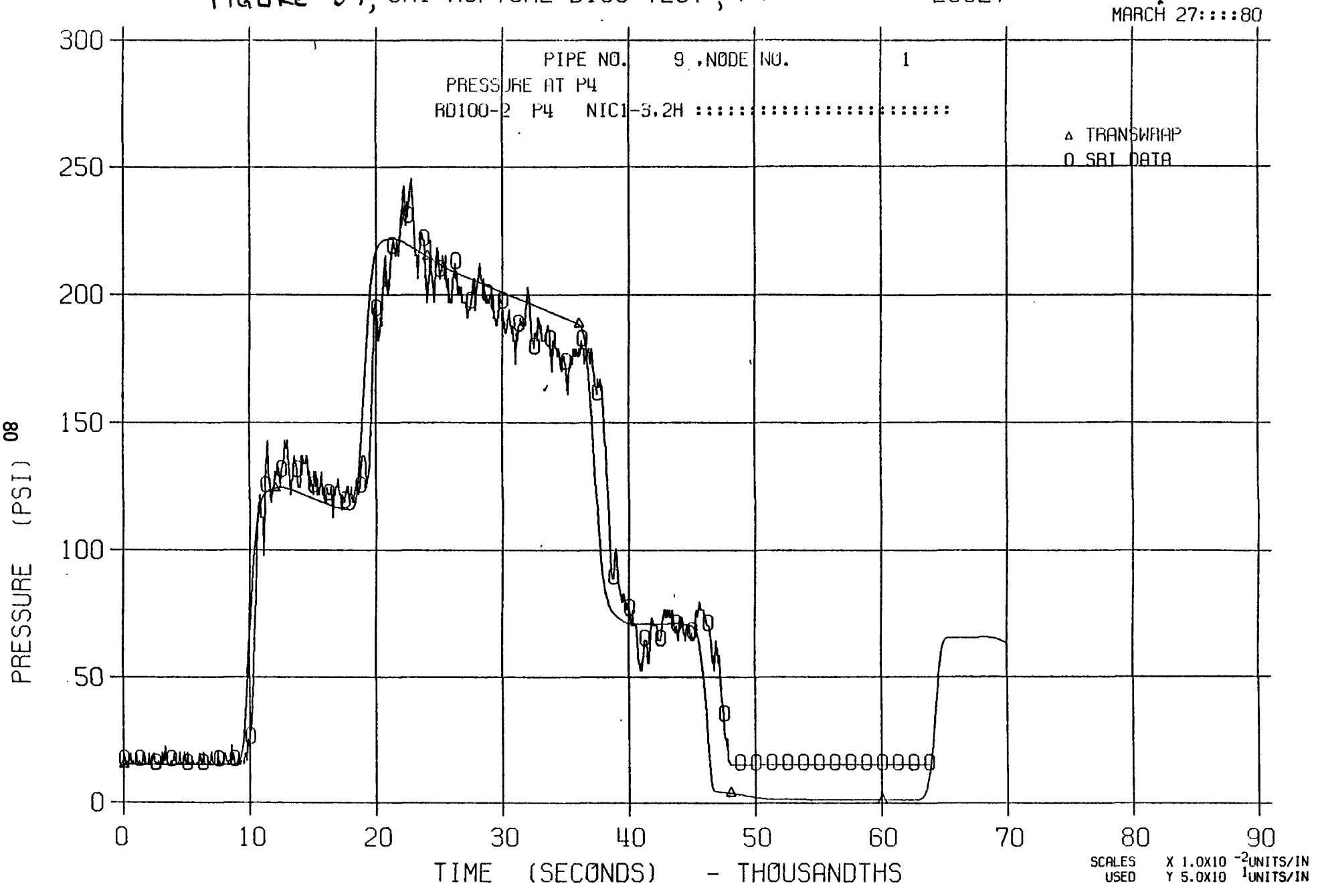

L 4

FIGURE B8, SRI RUPTURE DISC TEST, RD 100-2 2062T

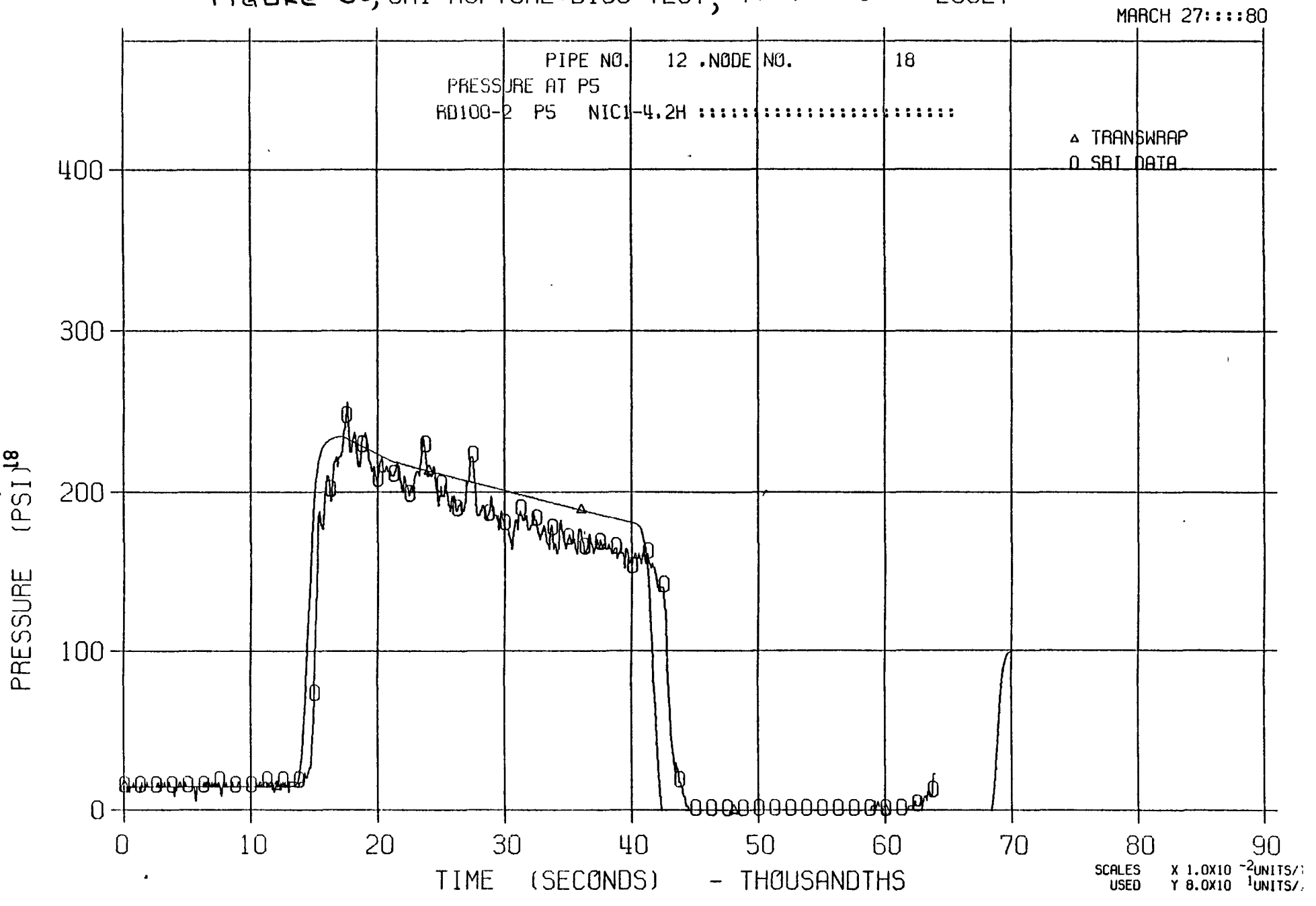

PL 5

FIGURE B9, SRI RUPTURE DISC TEST, RD 200-5 2148T

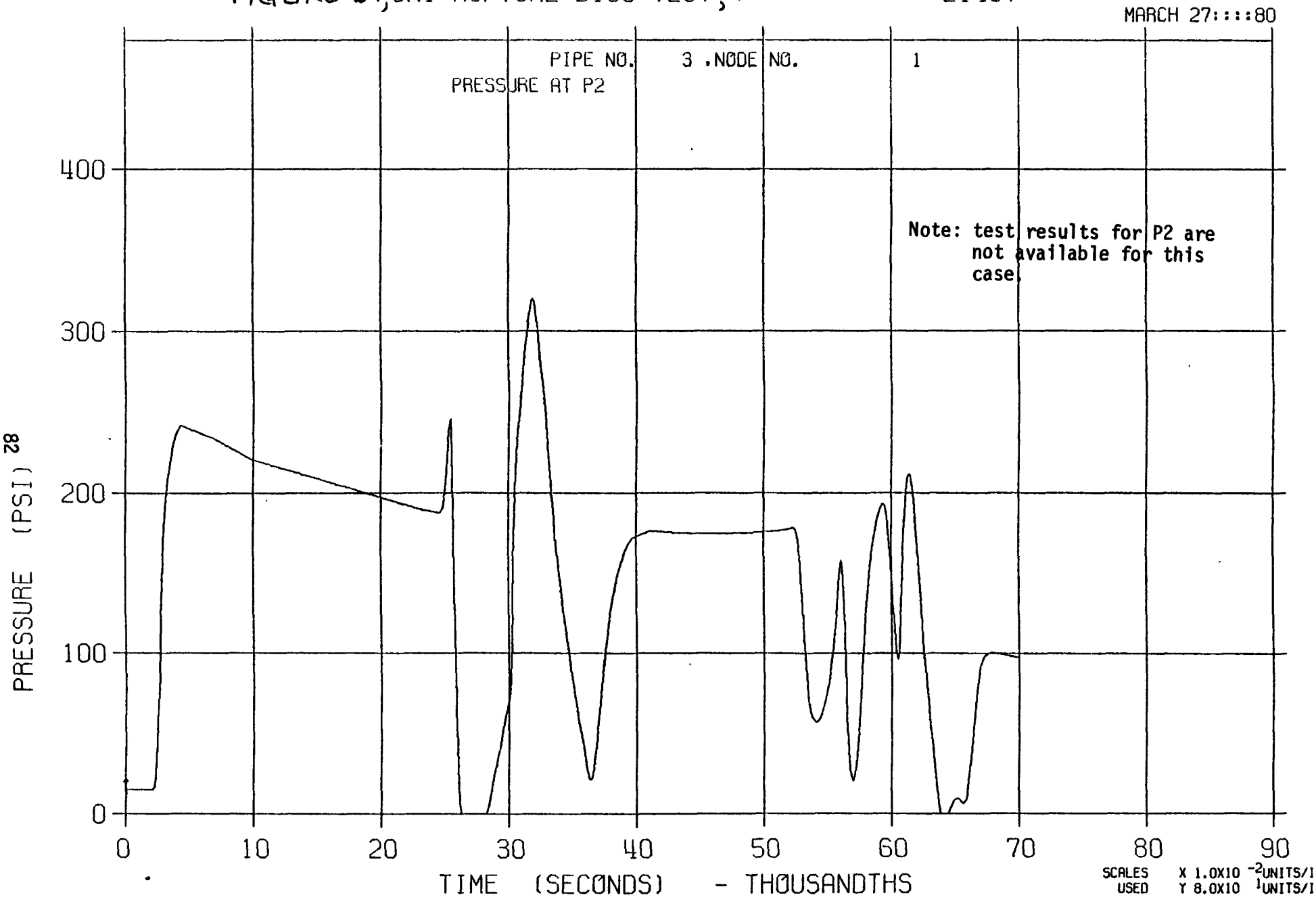

PL 2

FIGURE B10, SRI RUPTURE DISC TEST, RD 200-5 2148T

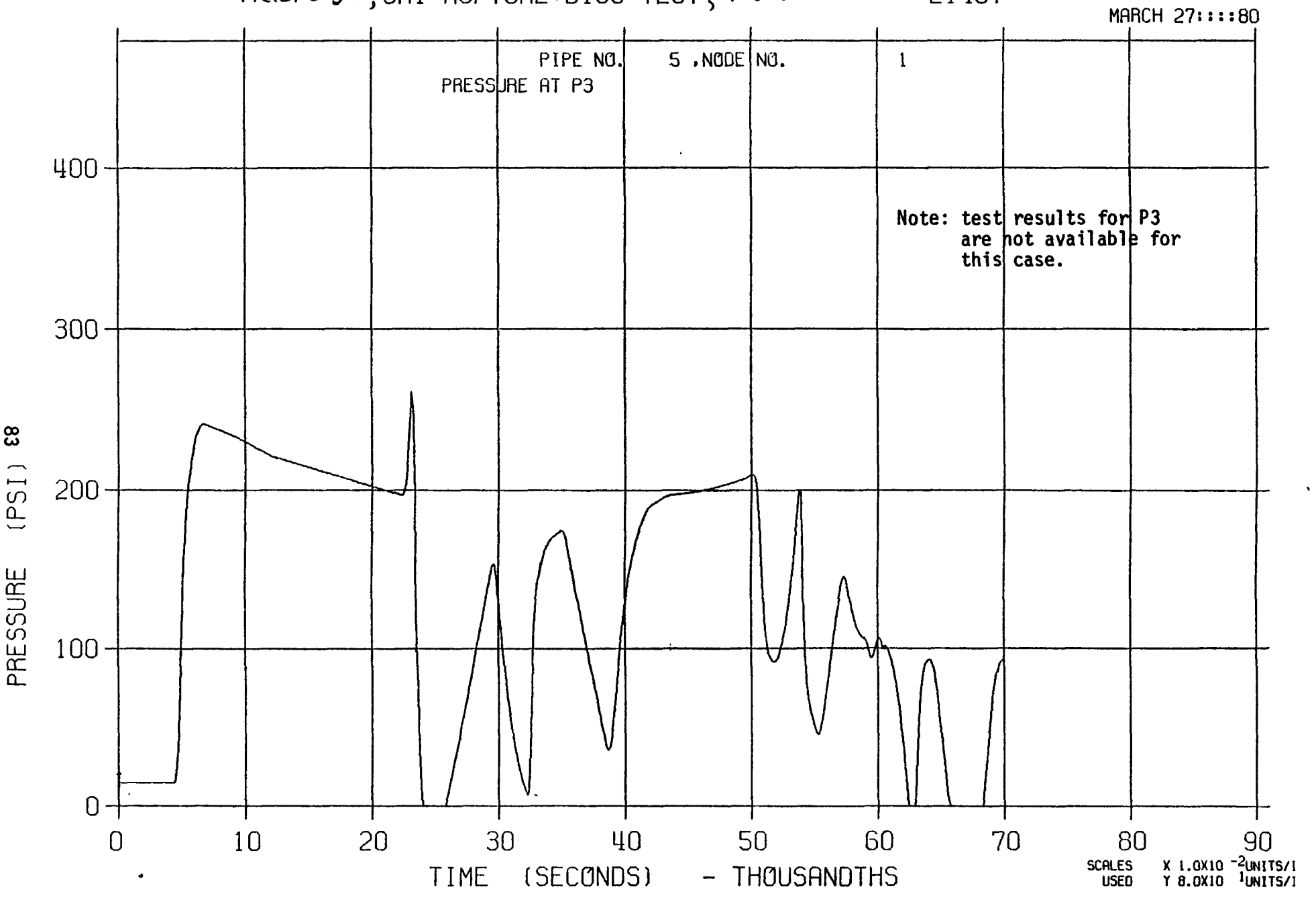

PL 3

FIGURE B11, SRI RUPTURE DISC TEST, RD 200-5 2148T

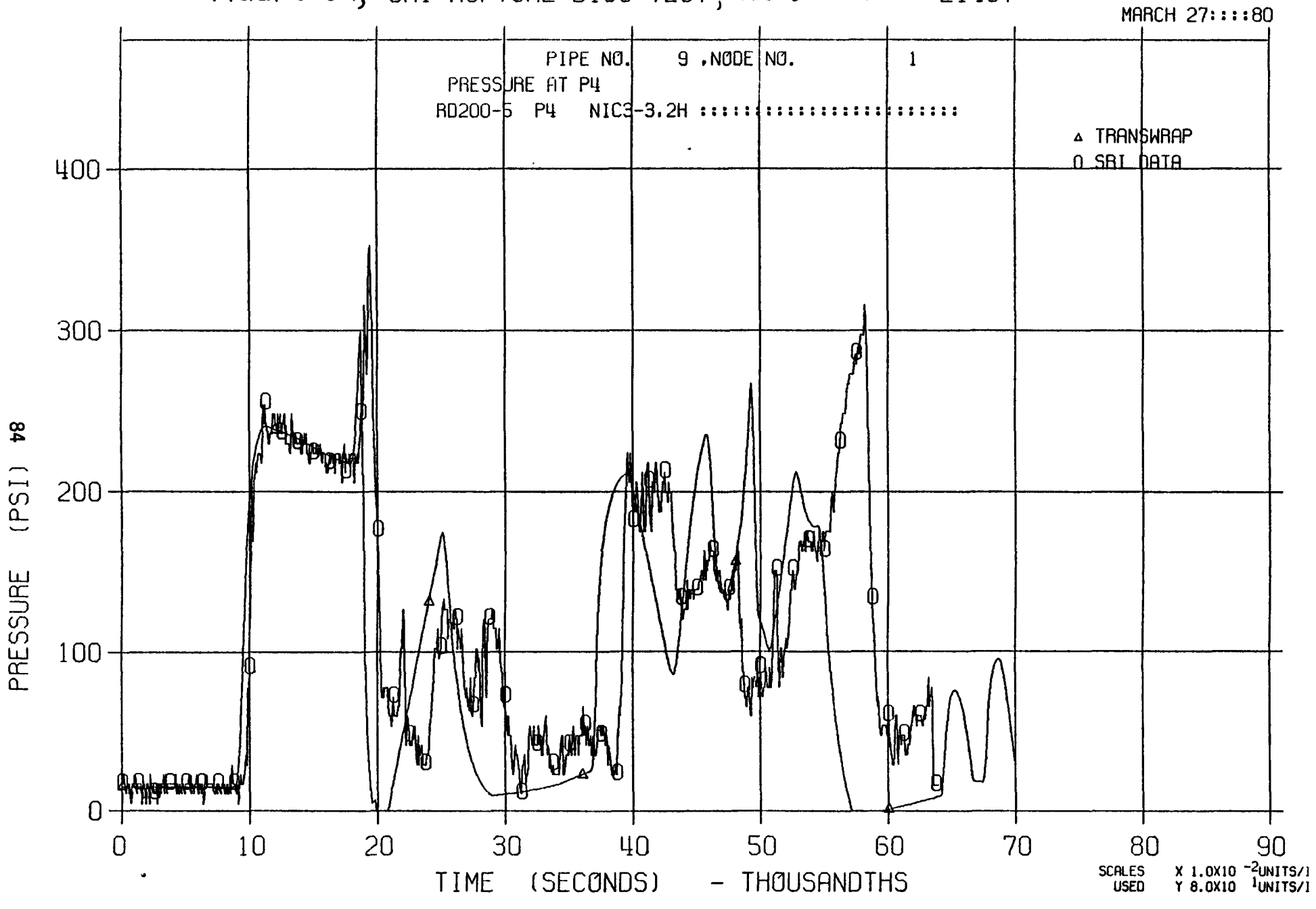

PL 4

FIGURE B12, SRI RUPTURE DISC TEST, RD 200-5 2148T

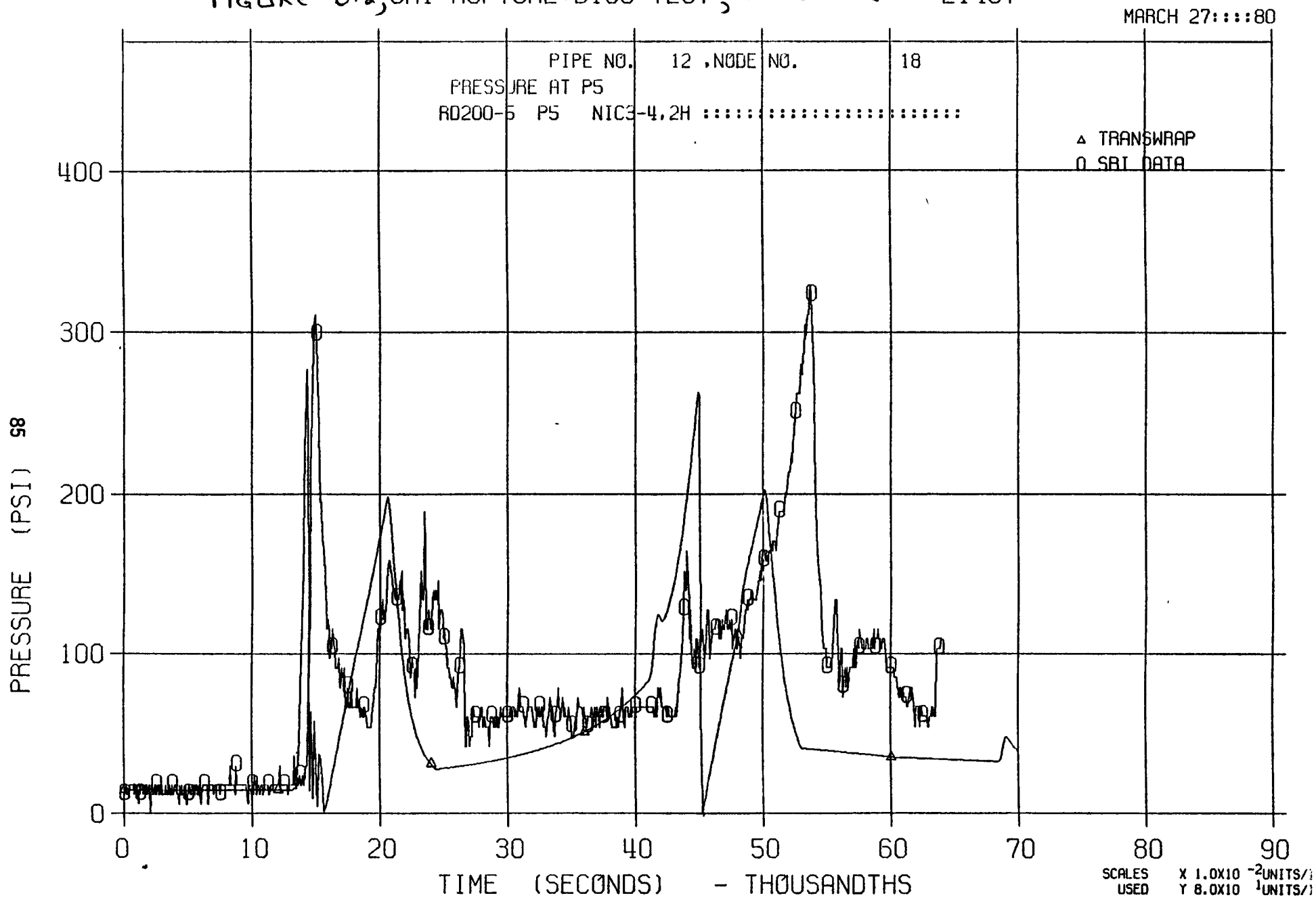

PL 5

FIGURE B13, SRI RUPTURE DISC TEST, RD 200-5 2148T

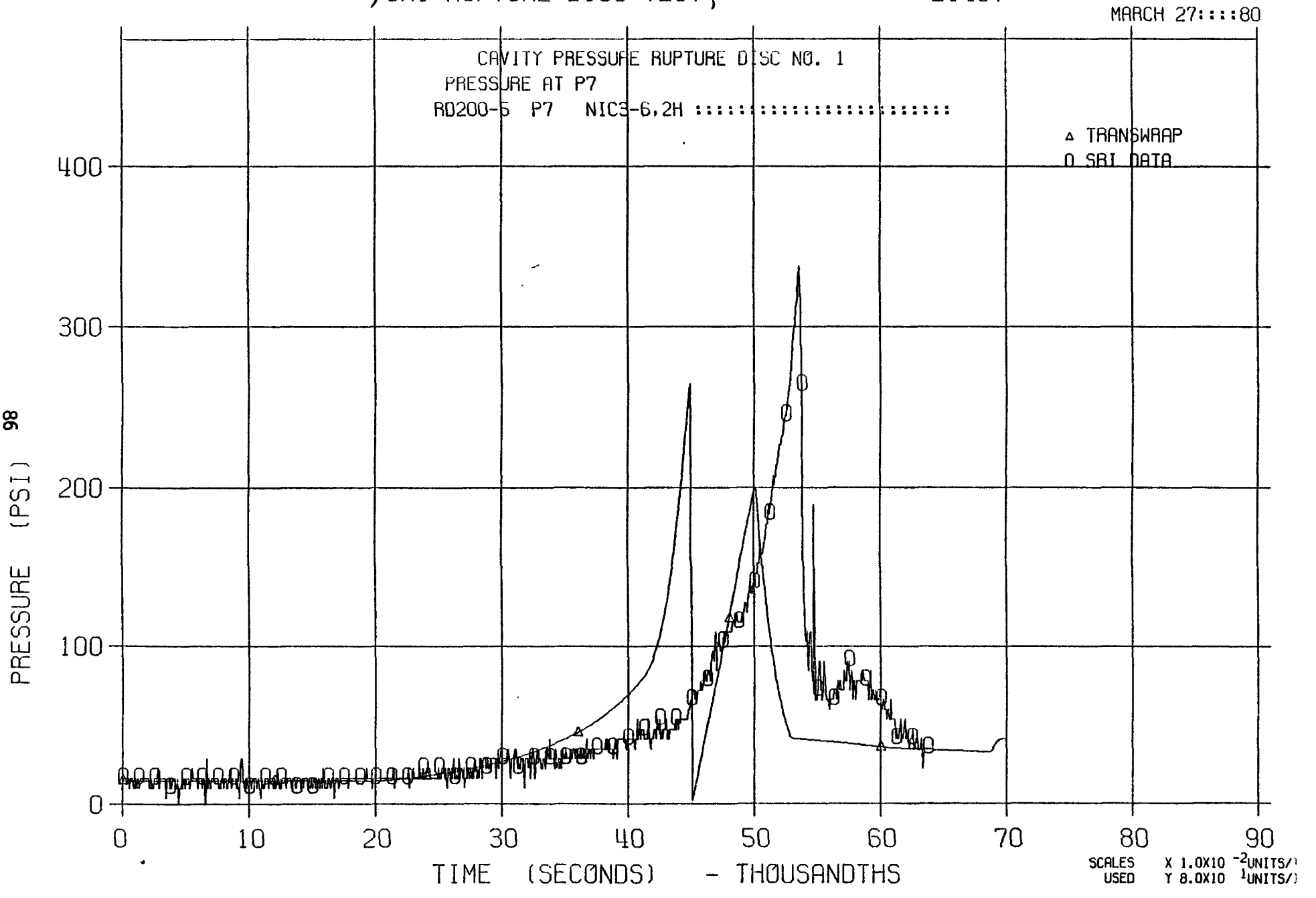

PL 6

FIGURE 214, SRI RUPTURE DISC TEST, RD400-1 8154T

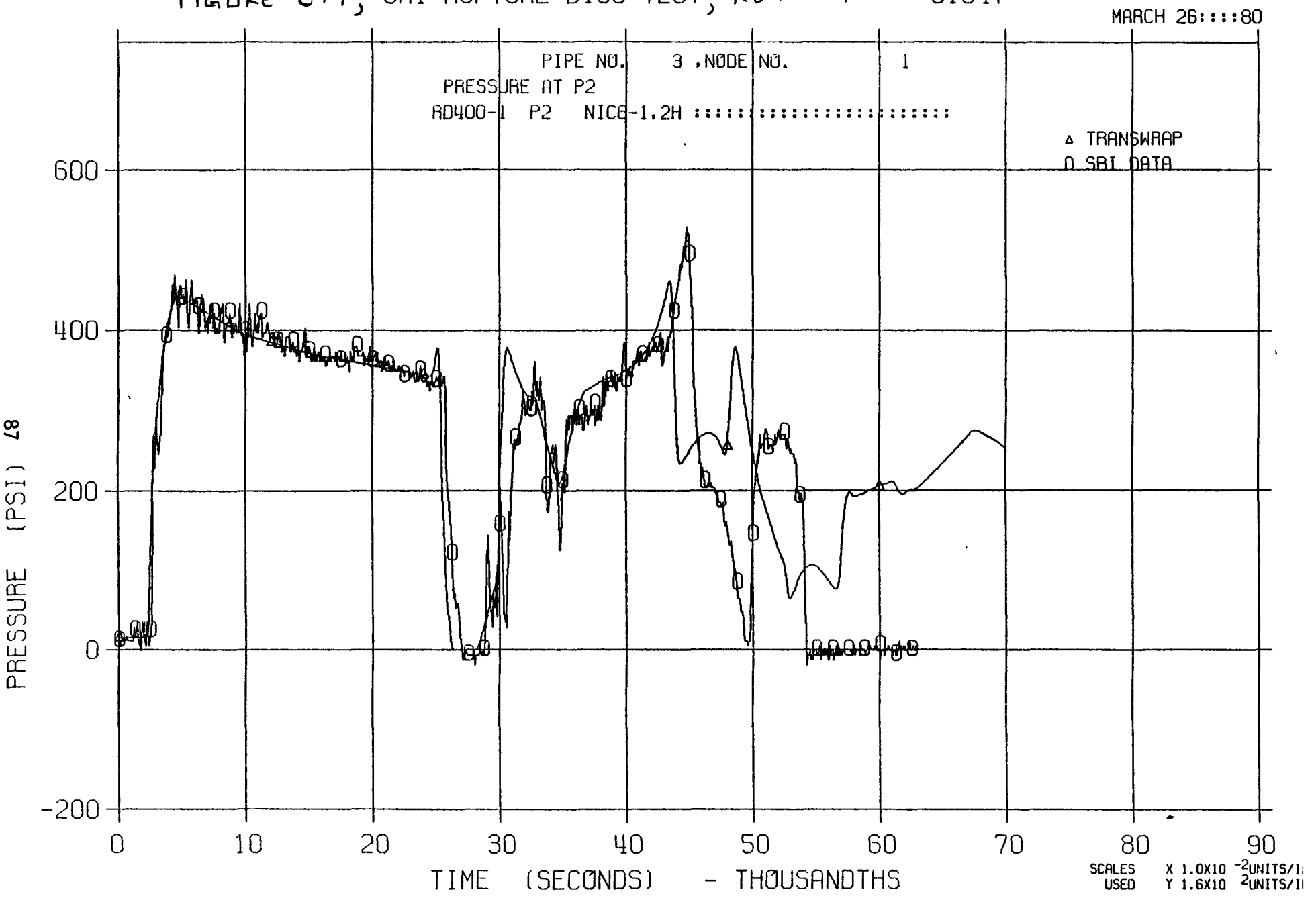

PL 2

FIGURE B15, SRI RUPTURE DISC TEST, RD 400-1 8154T

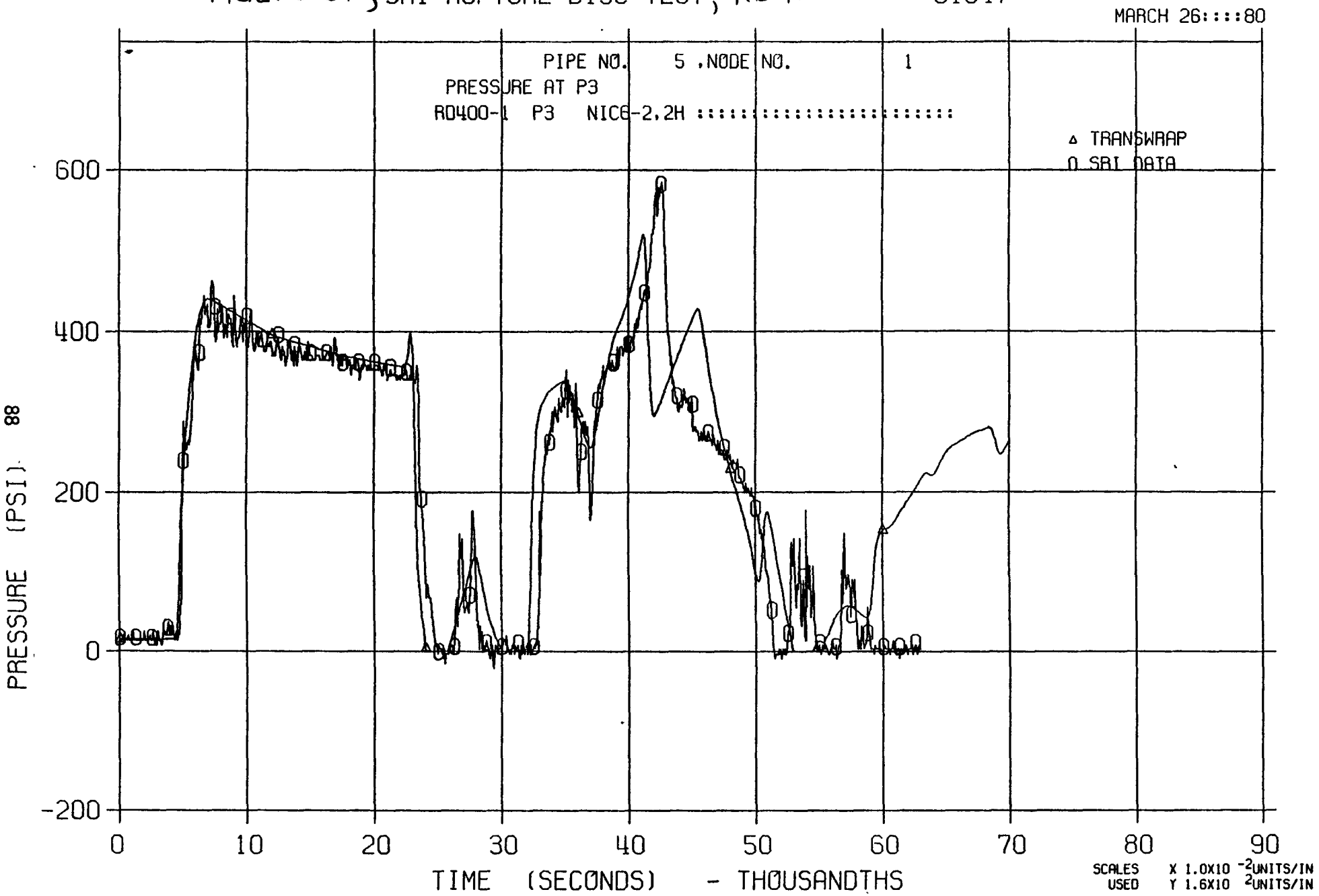

L 3

FIGURE B16, SRI RUPTURE DISC TEST, RD 400-1 8154T

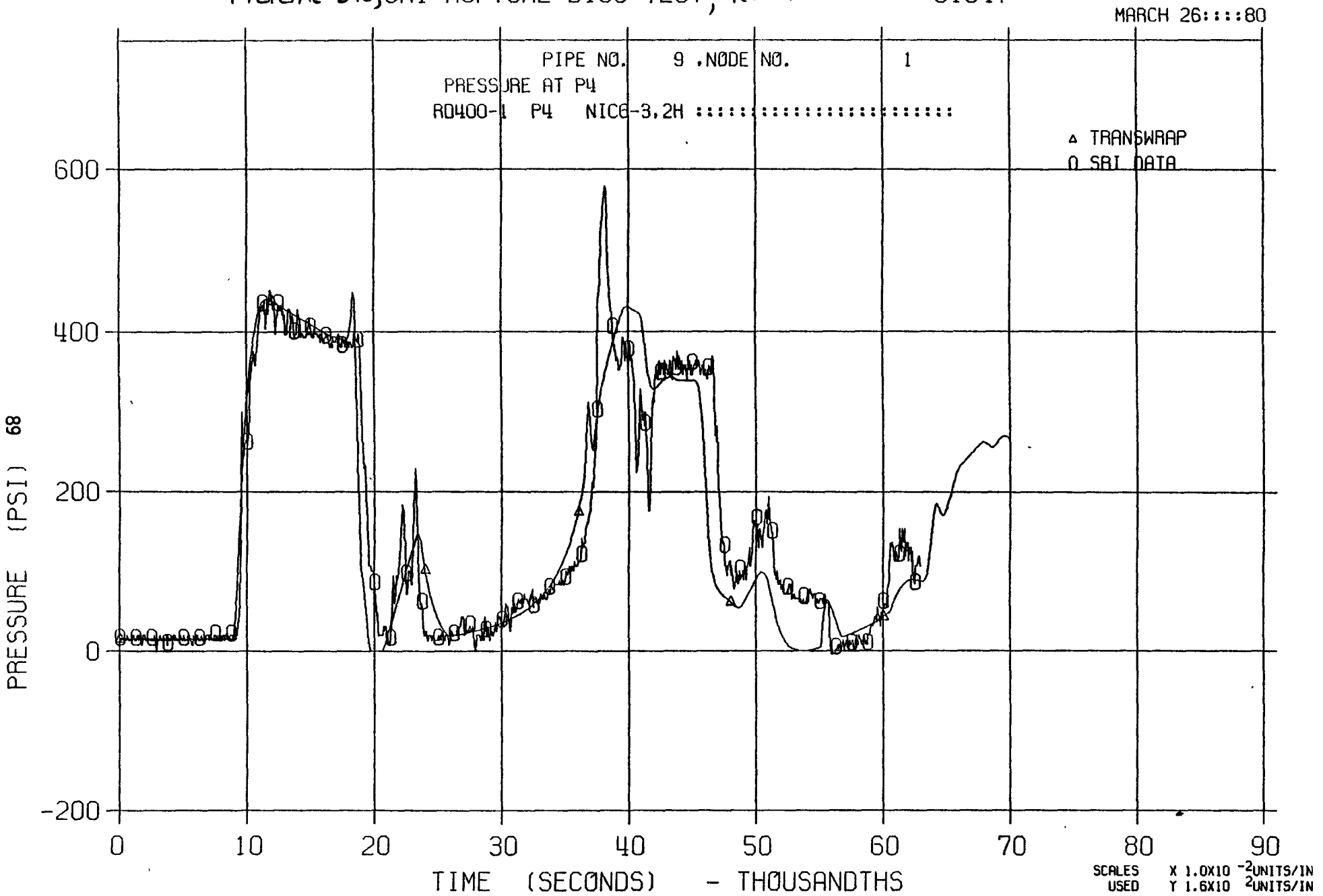

PL 4

FIGURE B17, SRI RUPTURE DISC TEST, RD 400-1 8154T

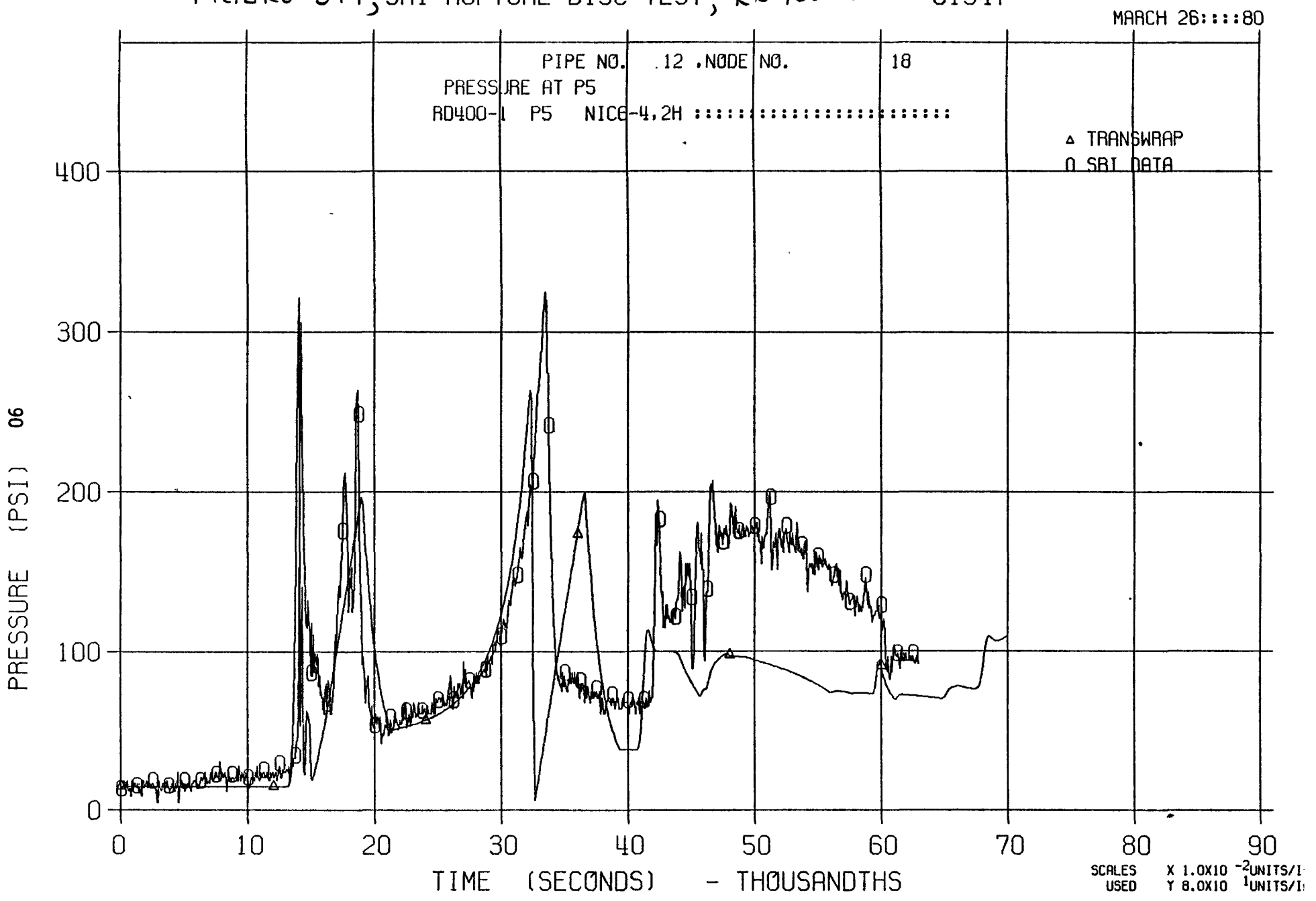

PL 5

FIGURE B18, SRI RUPTURE DISC TEST, RD400-1 8154T

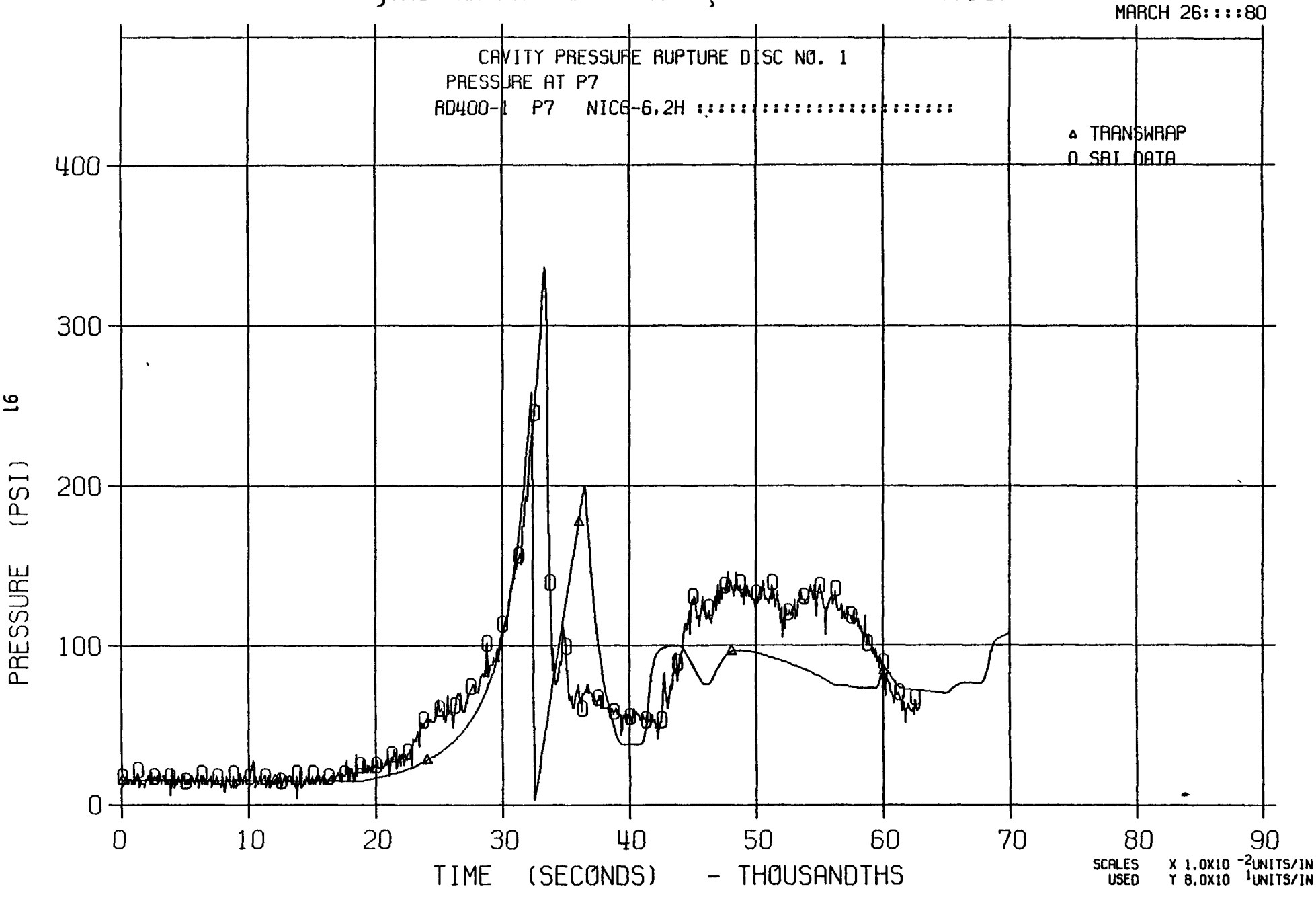

PL 6

FIGURE B19, SRI RUPTURE DISC TEST, RD 400-2 2089T

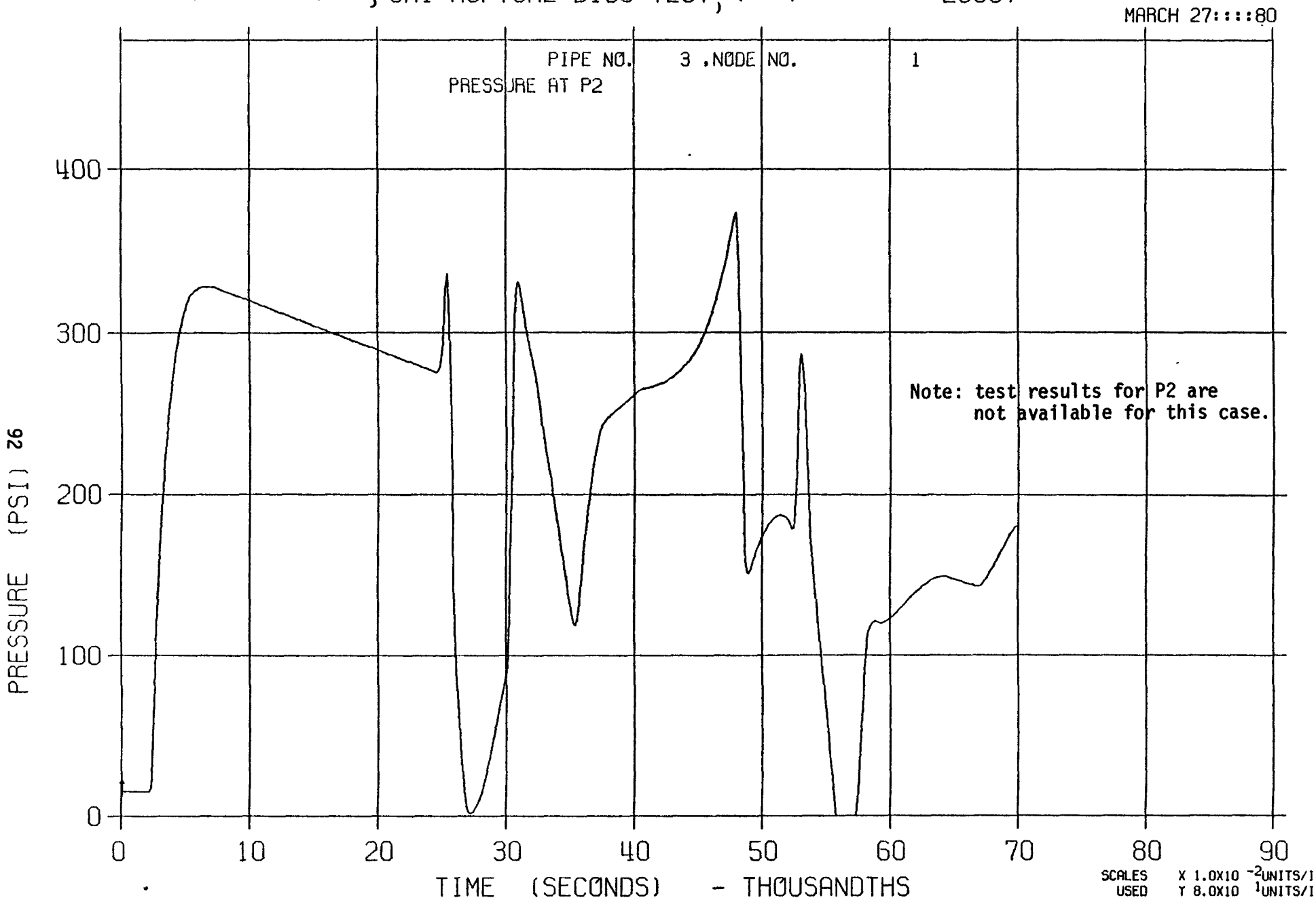

PL 2

FIGURE B20, SRI RUPTURE DISC TEST, RD 400-2 2089T

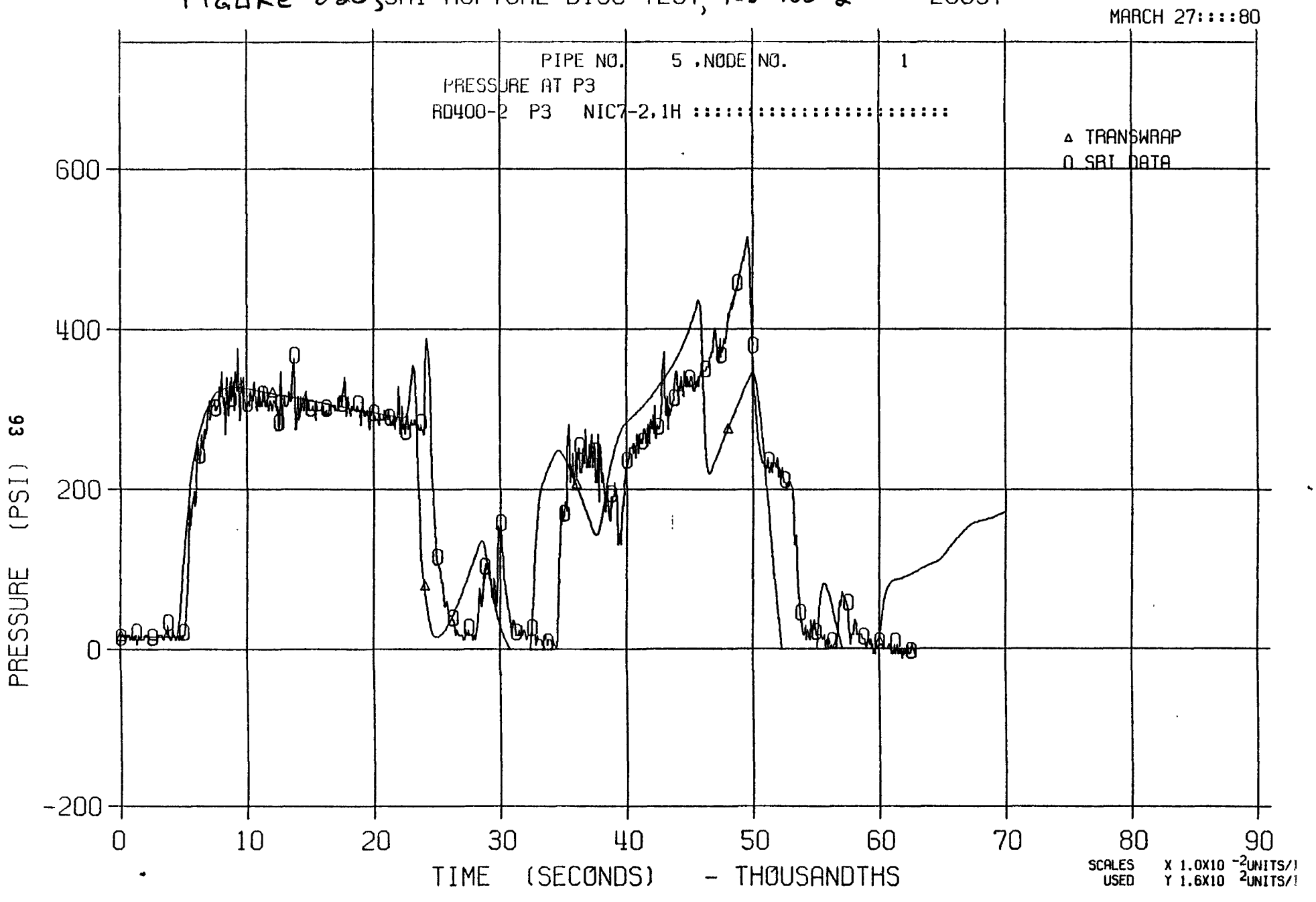

PL 3

FIGURE B21, SRI RUPTURE DISC TEST, RD400-2 2089T

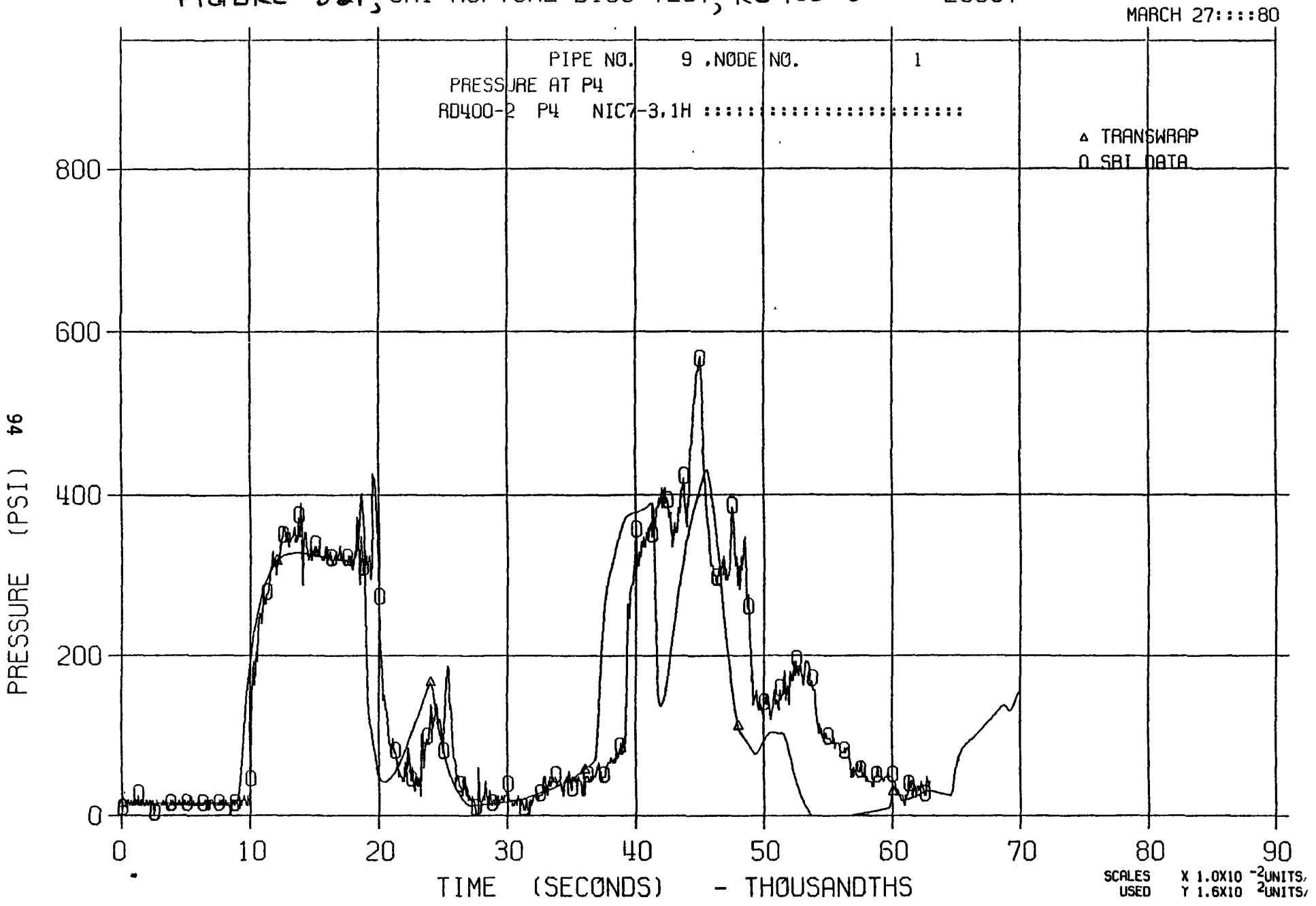

PL 4

FIGURE B22, SRI RUPTURE DISC TEST, RD 400-2 2089T

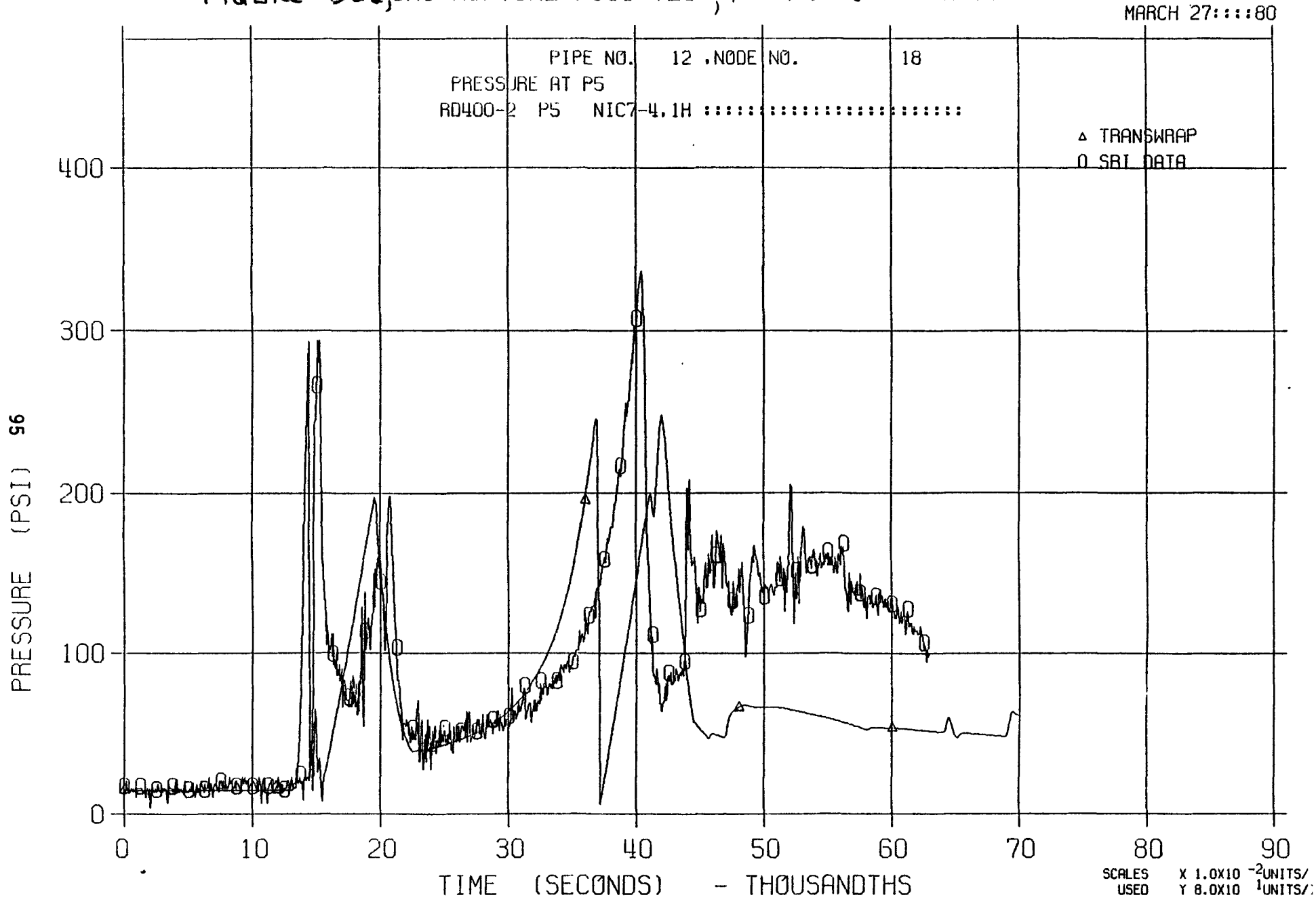

PL 5

FIGURE B23, SRI RUPTURE DISC TEST, RD 400-2 2089T

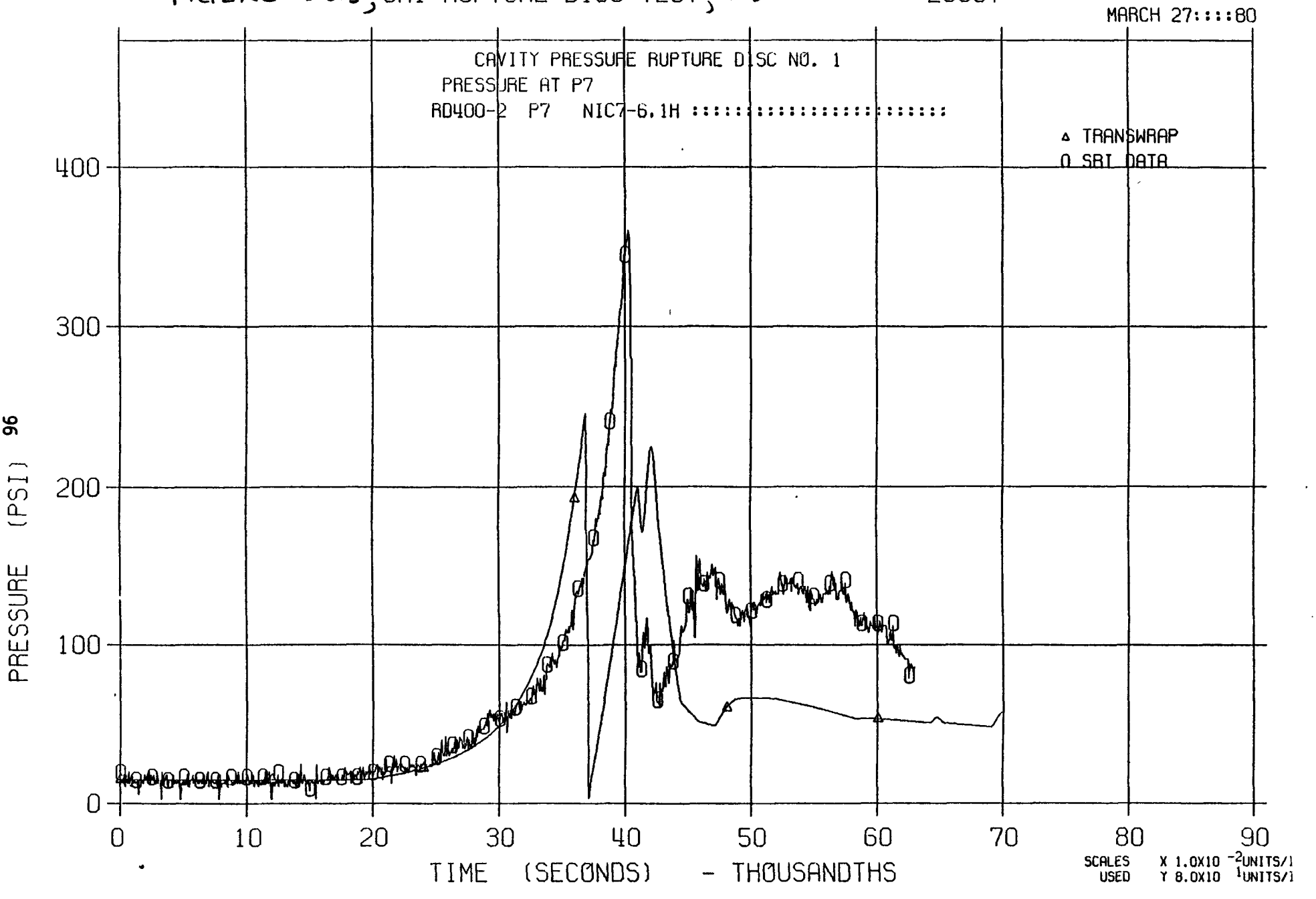

PL 6